The Aeroacoustics Response and Shear Layer Dynamics of Confined Cavities Subject to Low Mach Number Turbulent Flow

by

Marc Hanna

A thesis submitted to the School of Graduate and Postdoctoral Studies in partial fulfillment of the requirements for the degree of

Master of Applied Science in Mechanical Engineering

Faculty of Engineering and Applied Science

University of Ontario Institute of Technology (Ontario Tech University)

Oshawa, Ontario, Canada

April 2023

Thesis Examination Information

Submitted by: **Marc Hanna**

Master of Applied Science in **Mechanical Engineering**

The Aeroacoustics Response and Shear Layer Dynamics of Confined Cavities Subject to Low Mach Number Turbulent Flow

An oral defense of this thesis took place on April 12, 2023 in front of the following examining committee:

Examining Committee

Chair of Examining Committee	Dr. Zeinab El-Sayegh
Research Supervisor	Dr. Atef Mohany
Examining Committee Member	Dr. Martin Agelin-Chaab
Thesis Examiner	Dr. Moustafa El-Gindy

The above committee determined that the thesis is acceptable in form and content and that a satisfactory knowledge of the field covered by the thesis was demonstrated by the candidate during an oral examination. A signed copy of the Certificate of Approval is available from the School of Graduate and Postdoctoral Studies.

Abstract

Cavities exposed to low Mach number flow in various engineering applications are often liable for generating flow-excited acoustic oscillations, resulting in large acoustic amplitudes and vibrations. This compromises the safety and reliability of critical equipment due to a phenomenon attributed to interaction between the instability of the shear layer and the acoustic modes of a given system. This thesis experimentally investigates the aeroacoustics response of cylindrical cavities having aspect ratios of $h/L = 0.5$, 1, and 1.5, where h is the cavity depth and L is the shear layer impingement length, up to flow velocities of Mach 0.4. In view of the cavity confinement, the effects of the admission ratio w/W, where w is the cavity width and W is the duct width, on the aeroacoustics response and shear layer dynamics are also considered. The work extends the investigation to two-dimensional rectangular cavities and square cavities with similar aspect and admission ratios to the cylindrical cavities, as to establish the effect of the cavity shape on the resonance excitation frequencies and hydrodynamic modes of the system. Acoustic pressure measurements present Strouhal periodicities that agree well with values reported in literature. Cylindrical and square cavities with aspect ratio $h/L = 0.5$, however, exhibit unique behaviour due to the interference of the recirculation region within the cavity, ultimately modifying the symmetry of the shear layer. Particle image velocimetry (PIV) measurements present spatial characteristics of the shear layer dynamics, revealing improved flow modulation with increasing acoustic pressure, and significant asymmetry for shallow aspect ratios. The work presented in this thesis provides novel insight of the shear layer instability in confined cavities, and its effect on the flow-sound interaction mechanism.

Keywords: Aeroacoustics; Flow-excited acoustic resonance; Cavity flow; Cylindrical cavity; Shear layer instability

Acknowledgements

First and foremost, I would like to extend my gratitude to my supervisor and mentor, Professor Atef Mohany, for his unwavering support, expert guidance, and encouragement throughout this journey. His insights, feedback, and constructive criticism have been invaluable in shaping the direction and quality of this research. I am also grateful to Professor Martin Angelin-Chaab for his time and support, which was instrumental in refining the research and enriching my academic experience. I would like to express my sincere appreciation to the defence committee, Professor Zeinab El-Sayegh and Professor Moustafa El-Gindy, as well as the members of the Fluid-Structures and Noise Control Laboratory, who have created an inspiring and collaborative environment that has allowed me to grow as an engineer. I owe a special thanks to Dr. Mahmoud Shaaban, Dr. Omar Sadek, Dr. Moamen Abdelmwgoud, Dr. Mohammed Alziadeh, and my fellow researchers Rasha Noufal, Ali Saudy, Omar Sameh, Ahmed Shoukry, and Abdelrahman Alsaka for their immeasurable support and contributions to our research team. Their expertise, encouragement, and camaraderie have played an essential role in making this journey successful. Lastly, but certainly not with any less importance, I would like to express my sincere gratitude to my family and friends, who have always been a source of strength and support for me. I am deeply indebted to them for their unconditional love and encouragement throughout the years.

Psalm 91

Author's Declaration

I hereby declare that this thesis consists of original work of which I have authored. This is a true copy of the thesis, including any required final revisions, as accepted by my examiners.

I authorize the University of Ontario Institute of Technology (Ontario Tech University) to lend this thesis to other institutions or individuals for the purpose of scholarly research. I further authorize University of Ontario Institute of Technology (Ontario Tech University) to reproduce this thesis by photocopying or by other means, in total or in part, at the request of other institutions or individuals for the purpose of scholarly research. I understand that my thesis will be made electronically available to the public.

_____ Marc Hanna

Statement of Contributions

I hereby certify that I am the sole author of this thesis. I have used standard referencing practices to acknowledge ideas, research techniques, or other materials that belong to others. Furthermore, I hereby certify that I am the sole source of the creative works and/or inventive knowledge described in this thesis. The contents of chapters 2, 3, 4, and 5 have been co-authored and published with my Supervisor Dr. Atef Mohany.

Contents

List of Tables

List of Figures

Nomenclature

Symbol	Definition
St	Strouhal number
St_{peak}	Peak Strouhal number
c	Speed of sound in air
L	Cavity impingement length
D	Cavity diameter
r	Cavity radius
h	Cavity depth
H	Duct height
w	Cavity width
W	Duct width
$\mathrm{O}_{h/L}$	Cylindrical cavity notation ($D = 101.6mm$)
$\emptyset_{h/L}$	Cylindrical cavity notation ($D = 152.4mm$)
$\mathrm{R}_{h/L}$	Two-dimensional rectangular cavity notation
$\mathrm{S}_{h/L}$	Square cavity notation
U_∞	Free-stream flow velocity
u	Streamwise flow velocity component
M	Mach number
m_i	Hydrodynamic mode number
n_i	Acoustic mode number
$k = 0.57$	Average vortex convection speed
α	Open-pipe end-correction factor
γ	Phase delay constant
f_s	Shear layer oscillation frequency
f_{num}	Numerically estimated acoustic frequency

f_{onset}	Frequency at resonance onset
f_{peak}	Frequency at peak resonance
f_a	Theoretically estimated acoustic frequency
P	Acoustic pressure
P_{max}	Maximum acoustic pressure
P_{rms}	Root mean square acoustic pressure
M_i	Microphone sensor notation
$M_{\theta i}$	Shear layer impingement sensor notation
ρ	Density of air
a	Distance between cavity leading edge and duct inlet
θ	Boundary layer momentum thickness
Re	Reynolds number
C_p	Static pressure coefficient
SPL	Sound Pressure Level
PIV	Particle Image Velocimetry
$DEHS$	Di-Ethyl-Hexyl-Sebacat

Chapter 1

Introduction

1.1 Background & Literature Review

The self-excitation of acoustic oscillations and vibration has been recognized as a notable impedance to various engineering applications subject to low Mach number turbulent flow. The impact of self-induced dynamic loading on critical equipment has since fostered increasing research interest in recent decades to improve design guidelines, which subsequently requires a sounder understanding of the physical mechanisms responsible for such flow-induced vibrations. The presence of these adverse mechanisms are common amongst many industries and pose a severe threat to their safe operation, efficiency, and comfort. Flow over cavity geometries in particular have attracted significant attention and have been grounds for valuable research and development in automotive and aerospace applications. Initiatives have been taken in the automotive industry to better understand the pressure oscillations from separated flows past windows and sunroofs [34,51]. Such pressure fluctuations in vehicle cavities produce discomforting levels of noise to drivers and passengers, as well as reduced fuel economy for large freight carriers due to increased flow drag. Likewise, aerospace

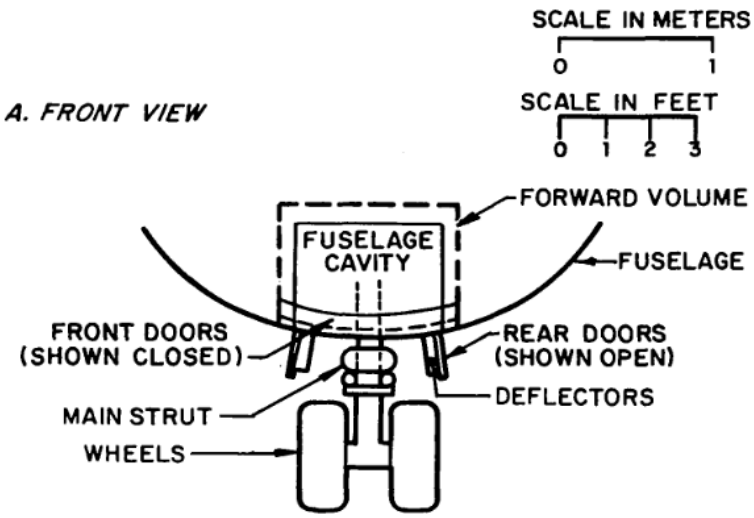

Figure 1.1: Boeing 727 nose landing gear [14].

applications have been investigated, such as the cavity flow over weapon bays in military aircraft due to their susceptibility of generating severe flow-oscillations and vibration [82, 90]. More recent developments have researched similar flow-induced noise and vibration for cavities formed by landing gear wheel wells, rocket motors, and jet engines, in pursuit of suppression techniques and innovative designs for technological advancements [24, 42, 44]. A simple schematic of the cavity formed by the landing gear of a Boeing 727 is shown in Fig. 1.1. Airport facilities are notorious for severe noise pollution from passenger jets, and hence require vast real-estate to construct, and more importantly, compromise the health and comfort of surrounding residents. Additionally, passenger jets must remain idle for a certain amount of time before take-off following another aircraft. While safety considerations related to wake turbulence are the primary reason for delays between aircraft takeoffs, noise abatement procedures are also a factor for large-scale airports. The flow oscillations associated with landing-gear cavities are responsible for up to 70% of airframe noise [65]. Therefore, addressing such noise pollution is of critical importance for aircraft manufacturers

in order to comply with more stringent regulations, and account for the concerns of surrounding communities.

With increasing energy demands, however, a more pertinent effort has been drawn to the energy sector regarding the cause and mitigation of flow-induced vibrations in applications such as combustion chambers [74], piping systems [16, 70, 83], as well as flow over cylinders and heat exchanger tube bundles [7, 11, 13]. Due to the geometric shapes and ever present fluid flow in nuclear power plant equipment, these systems provide inherent flow oscillations and favourable boundaries to excite acoustic standing waves, thus significantly increasing their vulnerability to flow induced oscillations. Numerous incidents have been documented outlining the excessive damage caused in

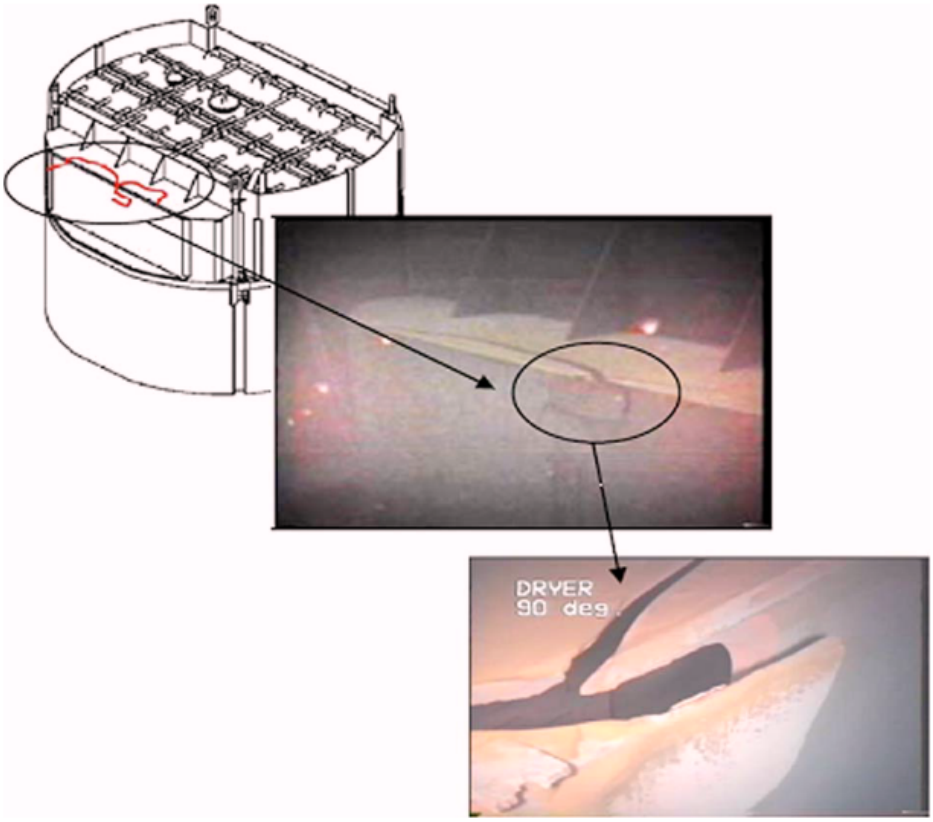

Figure 1.2: Steam dryer assembly of quad cities unit 2 (top left) and details of the acoustic fatigue failure on the outer hood [102].

boiling water reactors due to flow instabilities in main steam lines [23, 33, 95, 96]. Fig. 1.2 for example illustrates the acoustic fatigue in the Quad Cities unit 2 steam dryer due to intense flow-induced pulsations [102]. As nuclear energy composes 15% of Canada's electricity production, it is thus imperative to pursue further insight of such mechanisms and devise optimized design solutions, in order to safeguard facility assets and public welfare.

1.1.1 Self-Sustained Flow Oscillations

In cases where turbulent flow is travelling over rectangular shaped cavities, the geometric discontinuity provides the necessary condition to promote flow instabilities. The flow separation gives rise to an unstable shear layer which drives the self-sustained oscillations. These fluctuations in the flow generate acoustic pressure perturbations that amplify the initial instability of the shear layer, thus closing a feedback loop, as seen in Fig. 1.3. Flow-induced vibration in such cavity-like geometries are credited to the instability of the shear layer due to the flow separation, and has been well documented since early experimental campaigns on cavities, employing wall pressure measurements, hot-wire measurements, and schlieren observation [52, 80, 91]. These studies provided preliminary knowledge regarding flow instabilities for rectangular cavities at both low and transonic flow velocities.

Later work conducted by Rockwell and Naudascher [79] further categorized the instability mechanism into three categories, namely; fluid-dynamic, fluid-resonance, and fluid-elastic, each one reflecting the nature of the feedback mechanism. The fluid-dynamic feedback mechanism is a self-sustained form of oscillation where the flow separates at the upstream edge, creating a free shear layer over the cavity opening. The shear layer rolls into a vortical structure, which increases in size as it is convected downstream. The vortices result in pressure perturbations that amplify the initial

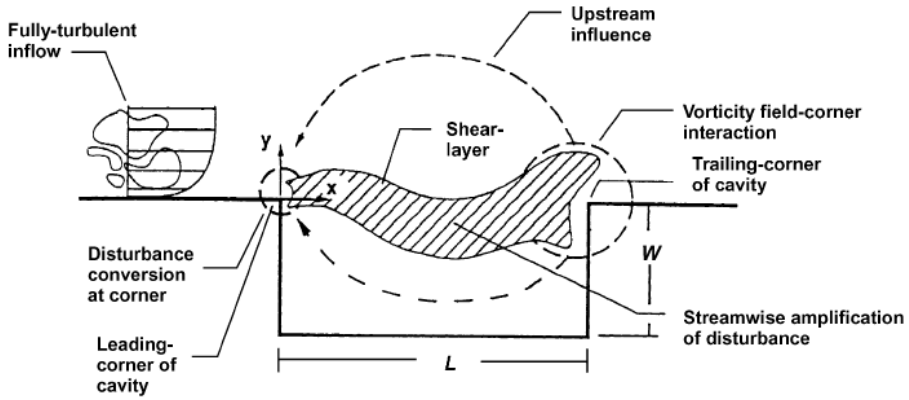

Figure 1.3: Principal elements of self-sustaining oscillation of turbulent flow past cavity associated with purely hydrodynamic effects [78].

instability at the upstream edge, thereby triggering the formation of another vortex and closing the feedback loop. It was later discovered that the behaviour of the shear layer, specifically the impingement, can be categorized depending on the clipping behaviour of the vortex core relative to the downstream edge of the cavity [76]. It was found that the vortex would exhibit either complete clipping into the cavity, partial clipping, partial escape, or complete escape downstream, as seen in Fig. 1.4. It was subsequently shown numerically using Direct Noise Computation that the impingement process seems to alternate between the previously mentioned categories [35]. In essence, the shear layer demonstrates a flapping motion, causing vortical structures to impinge on the downstream edge in a cyclic manner between the escape and clipping behaviour.

Rossiter [81] first proposed a semi-empirical formula to predict the dimensionless frequency of the flow oscillations over rectangular cavities, and is represented by the Strouhal number, St, as seen in Eq. 1.1, where a linear relationship exists between the frequency of the flow oscillations, f_s, the impingement length of the cavity, L, and the free-stream flow velocity, U_∞. Rossiter [81] explored the reliability of the formula for a large range of flow velocities, and suggested that the time required for

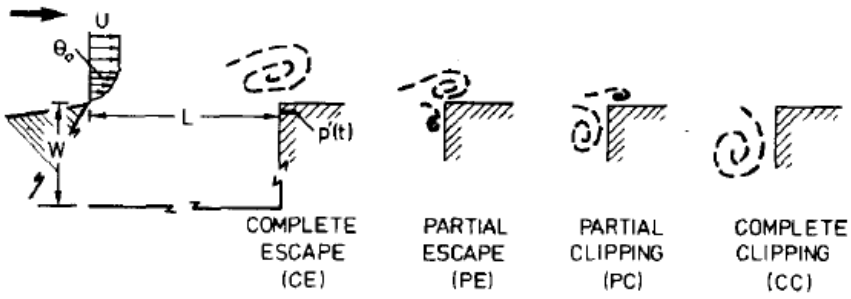

Figure 1.4: Cavity geometry and classes of possible vortex-edge interactions [76].

the vortices to travel downstream is L/U, while the time required for the acoustic pressure perturbation to return upstream is L/c, where c is the speed of sound. The frequency of the flow oscillations can thus be obtained by the summation of the two time-scales.

$$St = \frac{f_s L}{U_\infty} \simeq \frac{m_i - \gamma}{M + \frac{1}{k}} \tag{1.1}$$

Upon implementing empirical constants to fit the formula to the experimental data, the linear relationship can also be expressed in terms of the hydrodynamic mode number, m_i, the empirical constant for the phase delay between the downstream impingement and upstream feedback, γ, the Mach number, M, and the average convection speed of the vortices, $k = 0.57$. Throughout the years, authors have further demonstrated the accuracy of this formula, and have made analytical improvements as to appropriately fit Eq. 1.1 to experimental results [15, 41]. Future studies have demonstrated that the phase lag term is governed by the Mach number. At low flow velocities, the speed of sound is much greater than the free-stream velocity, therefore the acoustic pressure perturbations at the upstream edge occur almost instantaneously such that $\gamma = 0$, thus the phase delay is negligible [18, 29, 54]. As it can be seen in Eq. 1.1, the frequency of the shear layer instability is directly proportional to the flow velocity, where the corresponding Strouhal number signifies the shear layer hydrodynamic mode. Mathematically, this is a non-dimensional number representing

the frequency of the shear layer oscillations. In the physical sense, the hydrodynamic modes represent the number of vortices travelling over the cavity mouth during one flow cycle, where m_1 is the first hydrodynamic mode and has one vortex core travelling over the cavity.

As evidenced in literature, Eq. 1.1 serves as a viable semi-empirical formula to predict the Strouhal number of the flow oscillations, however, the physical interpretation of the formula is misleading. Although it provides relative accuracy, the notion that the impingement of the shear layer generates the flow tones in cavity-systems, contradicts with applications in which a similar mechanism appears, despite the absence of an impingement edge. This was emphasized by Tonon et al. [94], explaining the existence of similar flow-acoustic coupling in cylindrical pipes where the shear layer does not impinge on a uniform edge, such as two-dimensional cavities. The generation of velocity dependant flow-tones in cavity geometries are rather a product of a coupled interaction between the flow instability and the acoustic field. Powell [73] first established a generalized mathematical relationship between the vortex shedding and sound production, which was then generalized to estimate the time-averaged acoustic power [46–48]. The model developed by Howe [46] for the feedback loop involves the interaction between the unstable hydrodynamic flow field, and the acoustic field [30, 50].

The feedback mechanism discussed in this section is characterized as a self-sustained oscillation where the flow instability of the shear layer provides the necessary energy to generate acoustic tones, thereby further increasing the instability of the shear layer. The frequency of the instability in this case is mainly a function of the free-stream flow velocity and the length of the cavity opening.

1.1.2 Flow-Excited Acoustic Resonance

It has been established in the previous section that the instability of the shear layer transfers energy to the acoustic field which generates velocity dependent tones, thereby fostering a coupled interaction between the flow field and the acoustic field. Under certain conditions, cavity geometries exhibit acoustic modes at discrete frequencies which fall within the range of oscillation frequencies for the given operating flow velocities. In such circumstances, critical flow velocities exist where the associated oscillation frequency coincides with the acoustic mode of the system [61] Therefore, the shear layer oscillations excite the acoustic mode of the system, forming a distinct flow-acoustic coupling [88]. This is possible due to the favourable orientation of the velocity fluctuations with respect to the acoustic particle velocity. The pressure perturbations in this case promote the excitation of a standing acoustic wave [1]. As shown in Eq. 1.1, the frequency of the flow oscillations are proportional to the flow velocity, whereas the acoustic mode is mainly governed by the system's geometric shape. Consequently, the strong coupling between the flow field and the acoustic field ensues when both frequencies coincide, as shown in Fig. 1.5. During this coincidence, the flow oscillations and resonance frequency are said to be in a lock-in state. Subsequently, the aeroacoustics resonance is initiated at a discrete frequency and sustained for a finite range of flow velocities [87].

This coupled mechanism is therefore governed by an energy exchange process where the energy is periodically transferred between the flow field and the acoustic field. It was reported that the energy exchange process is attributed to a pressure differential across the source region due to the shear layer instability, which is in phase with the acoustic particle velocity [46, 47]. Therefore, the existence of an excitable acoustic mode provides positive feedback to the flow oscillations so long as the flow oscillations overcome the acoustic damping of the system. The coupled

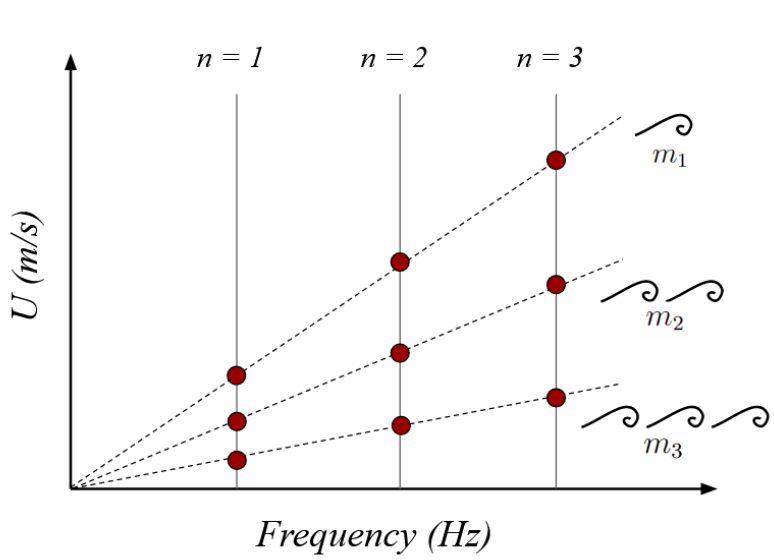

Figure 1.5: Schematic of the lock-in regions between the shear layer modes, m_i, and the acoustic modes, n_i.

interaction during resonance is much more pronounced, resulting in an amplification of the flow oscillations as well as the resonance tone [12]. Consequently, the strength of the acoustic field is liable for modulating and organizing the vortices in the shear layer [49, 98]. Additionally, the growth of the flow instabilities result in a significant increase in flow drag, negatively impacting the efficiency of the given system. This coupled feedback mechanism is called flow-excited acoustic resonance [63, 87].

As mentioned, there are two main aspects that are responsible for generating flow-acoustic coupling, namely; the flow field and the acoustic field. To that end, the resonance frequency of the system dictates the lock-in regions for the flow-excited resonance, which is dependent on the geometry of the cavity and surrounding boundaries. In general, the flow-excited acoustic resonance mechanism is prevalent amongst many engineering applications and is commonly used to refer to such instabilities. However, although the mechanisms responsible belong to the same category, i.e. fluid-resonance, details regarding the behaviour between the flow field and acoustic field

may differ. In fact, since a system's geometry governs the resonance acoustic mode, different geometric shapes generate distinct acoustic mode shapes, which in turn affect the topology of the shear layer. With the aim of developing insight to the flow-excited acoustic resonance in other cavity geometries, considerable research over the past few decades has committed to exploring various applications subject to similar effects due to the presence of turbulent flow. Such applications include cases where multiple cavities are present in a duct with various configurations, side branches in pipeline systems, cross-flow over cylinders and tube arrays, as well as circular axisymmetric cavities [2, 5, 6, 31, 37, 64, 78, 104]. The feedback mechanism explained in this section differs from that presented in Sec.1.1.1, in that the presence of an acoustic standing wave, which is geometry dependant, couples with the self-sustained flow oscillations, generating significantly higher amplitudes of acoustic pressure. Subsequently, the coupling demonstrates a more mutual energy exchange between the flow and acoustic field, evidenced in the enhanced organizing and modulation of the shear layer [49].

1.1.3 Rectangular Cavities

Acoustic Response

Given the nature of the coupled mechanism, it is fundamental to understand the behaviour of both; the fluid-dynamics and the acoustic field. With regard to the aforementioned studies, a common aspect amongst the investigations are that they were conducted on two-dimensional rectangular cavities. This is a crucial feature to be considered when evaluating the flow-acoustic coupling of cavities. The previously mentioned studies were geared towards certain industrial applications, explaining the rectangular cavity opening, however the two-dimensionality of the cavity also facilitated the analysis by neglecting three-dimensional characteristics. This was an

effective approach considering the lack of literature in this field only a few decades ago. The research and development that has since been made, in both literature and industry, has provided a better fundamental comprehension of the underlying physics responsible for the coupled phenomenon, allowing for progress to be made towards understanding more complex-shaped cavities.

In general, when referring to the geometric shape of rectangular cavities, it is proper convention to use their aspect ratio, h/L, which is the ratio between the cavity depth, h, and the impingement length, L. The dimensionless parameter allows for scaling of the results to a wide range of cavity cases. Additionally, the aspect ratio allows grouping of the cavities in either deep or shallow configurations. Deep cavities consist of depths larger than the impingement length, whereas shallow cavity depths are smaller than the impingement length. Much of the early literature has been conducted on rectangular cavities with shallow aspect ratios due to the nature of the applications considered. Cavities in the shallow regime typically induce broadband acoustic tones by virtue of the dynamic flow oscillations [4]. When the depth of the cavity becomes larger than the impingement length, it provides an acoustic depth mode, which would be in the direction orthogonal to the flow. This acoustic depth mode, if excited by the shear layer instabilities, will couple with the flow field and exhibit flow-excited acoustic resonance [27]. Plumblee et al. [72] highlighted this observation and suggested that the broadband noise generated in shallow cavities is due to the fluid-dynamic oscillations of the shear layer, and thus, increases proportionally with increasing flow velocities. In deep cavities, the acoustic depth mode promotes the flow-excited resonance mechanism, and this remains true in cases where the cavity is subject to external flow. However, it was later shown that shallow cavities may also excite acoustic standing waves if there is a confinement causing reflective boundaries [103]. Unlike the depth mode of deep cavities, where the acoustic mode is

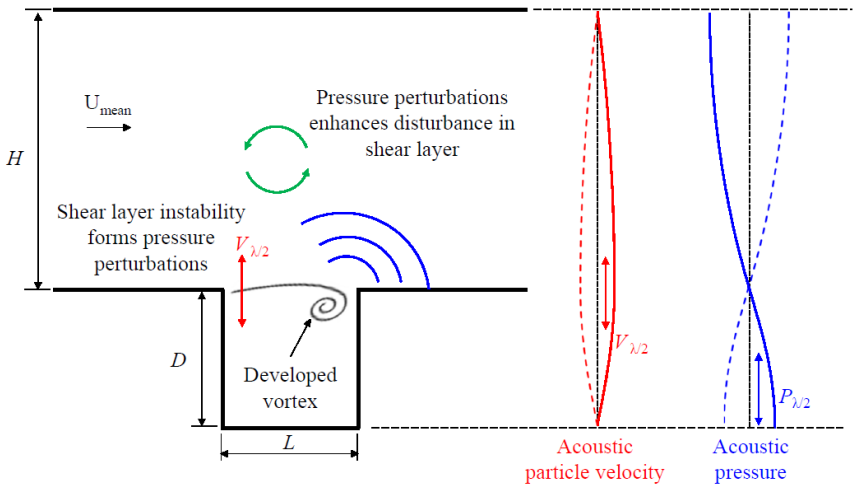

Figure 1.6: Illustration of the Fluid resonant feedback mechanism. Distribution of the acoustic particle velocity and pressure of the $(\frac{\lambda}{2})$ mode are shown schematically [1].

exclusively inside the cavity, the standing wave formed in shallow cavities subject to a reflective boundary spans the entire distance between this boundary and the cavity floor [1]. It was demonstrated that shallow cavities confined in a duct can excite a $1/2\lambda$ acoustic cross-mode where the cavity depth and duct height are the length scales used to predict the resonance frequency of this mode, as shown in Fig. 1.6. Hence, it is evident that the presence of a confinement significantly influences the feedback mechanism, and thus, the aeroacoustics behaviour of the system [11]. The acoustic mode is said to be a trapped acoustic mode since it is localized to a sub-set of the geometry, and is not sensitive to upstream and downstream acoustic boundary conditions.

Heller et al. [43] and Rossiter [81] observed flow-excited resonance in shallow ducted cavities subject to high Mach number flow and noted that the acoustic mode during resonance excitation can in-fact be the longitudinal acoustic mode of the duct, as well. In their investigations, a quality factor is given for the acoustic depth mode, and is defined as the ratio between the energy stored in the cavity and the energy

exchanged from the opening. The small quality factor for the shallow cavities in their studies explained the absence of the acoustic depth mode. Conversely, longitudinal modes of the main duct were observed to be coupled with the oscillations of the shear layer, which was accordingly modelled as a pseudo-piston propagating acoustic waves upstream and downstream [41]. The resonance frequencies for the longitudinal mode also agreed well with analytical results, which consisted of a stagnant fluid medium [93].

Hydrodynamic Behaviour

The aspect ratio is a crucial parameter as it accounts for the depth and impingement length of the cavity, which have the strongest influence on the flow-oscillations and acoustic modes [81, 102]. This philosophy implies the assumption that the cavities are two-dimensional in nature, where the shear layer topology is uniform in the spanwise direction. Therefore, a parameter to account for the width of the cavity would be irrelevant. Further investigations, however, have explored the effect of changing the cavity width and shown that the existence of friction boundaries on the sides of the cavity develop velocity gradients and become more prominent when reducing the width of the cavity relative to the impingement length [20, 77]. As a result, slight curvature in the spanwise direction of the cavity is observed. Small-scale, three-dimensional streams also emerge between consecutive vortex cores. Nevertheless, these small-scale, three-dimensional characteristics seem marginal in comparison to the overall two-dimensional topology of the shear layer. In addition, although the effect of the cavity width was explored, the same width was adopted to the duct confinement, therefore the effect of the cavity width relative to the width of an enclosure has not been explored. In regard to the shear layer dynamics, the linear relationship between the flow oscillations and flow velocity, as seen in Eq. 1.1, is normalized using

the impingement length to yield a non-dimensional frequency, known as the Strouhal number, St. This parameter represents a specific hydrodynamic mode, where m_1, m_2, and m_3 represent the first, second, and third hydrodynamic modes, respectively. The first hydrodynamic mode exhibits one vortex core in each flow cycle, where the number of vortex cores present in one flow cycle increases with higher order hydrodynamic modes. Literature regarding rectangular cavities, as those previously mentioned, report relatively similar Strouhal numbers of $\sim$ 0.5, 1, and 1.5, for m_1, m_2, and m_3, respectively. In comparison to axisymmetric cavities, where the geometry differs, Nakiboğlu et al. [64] provided a thorough numerical and experimental investigation on the effect of cavity depth on the Strouhal periodicities. Results demonstrated that for $h/L = 0.2$ - 0.5, the Strouhal number for m_1 continues to increase with increasing depth until a saturation point, where St is no longer affected by the depth for $h/L \geq 0.68$. Their experimental and numerical results described a linear relation between the reduction in cavity depths and St for aspect ratios less than 0.68, exemplifying the clear dependency of the shear layer dynamics on the aspect ratios of shallow cavities. No such dependency, however, appears in rectangular cavities, which further delineates the change in behaviour for other cavity geometries.

The observed linear relationship in the experiments of Nakiboğlu et al. [64] was described as a reduction in the convection speed of the vortex at the mouth of the cavity by virtue of the image vortex present at the floor of the cavity. This explanation, as illustrated in Fig. 1.7, considers strong effects due to the cavity floor in proximity of the mouth, such that increasing the depth of the cavity, minimizes the effects of the cavity floor on the shear layer dynamics. Evidently, the division of cavities into either shallow or deep configurations is beneficial due to the change in both the acoustic behaviour and the shear layer dynamics.

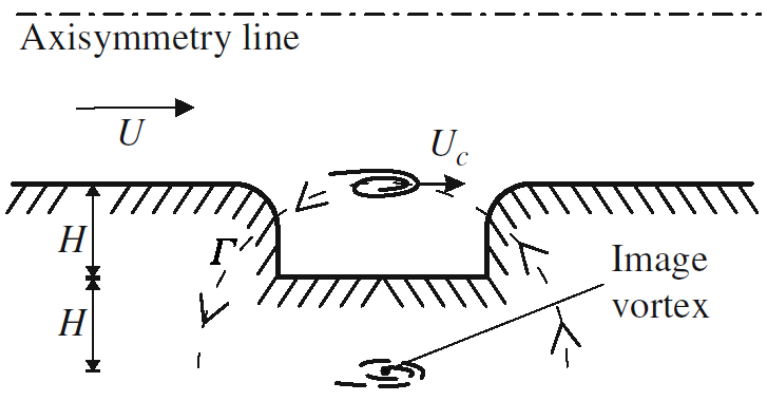

Figure 1.7: Schematic drawing of a concentrated vortex core at the cavity mouth and its image at the bottom of the cavity; arrows indicate the direction of circulation for the image vortex [64].

Convective Effects on the Resonance Frequency

It is understood that the acoustic mode of a cavity is geometry-dependent, and is thus associated with a static frequency value. Although these frequencies can be estimated with relative accuracy, feasible prediction methods assume a stagnant fluid medium, and thus no flow condition. The effect of increasing flow velocity on the resonance frequency has been reported by many authors for various cavity geometries [10]. Experiments by Shaaban and Mohany [89] demonstrated the resonance frequency to have a stronger dependence on the flow velocity for high Mach numbers. Such speeds introduce isentropic compressibility of the fluid medium, effectively reducing the speed of sound. This indicates the influence of convective effects on the resonance excitation and its role in accurately predicting the resonance frequency.

Theoretically, all hydrodynamic modes can successively excite the same acoustic mode, as seen in Fig. 1.5, however for the majority of applications, flow velocities typically exhibit up to the first three, as mentioned [102]. Investigations focused on the flow-excited resonance mechanism for various geometries, highlighted that as the

flow velocity is increased, the acoustic mode is successively excited by lower order hydrodynamic modes, and the amplitude of the acoustic resonance increases. The resonance amplitude is thus strongest when coupled with the first hydrodynamic mode, and is due to the increased momentum of the shear layer vortices [36, 104]. Resultantly, the increased resonance amplitude amplifies the oscillation of the shear layer and acts as an acoustical inertia, essentially introducing an added mass effect to the oscillation [37, 94, 103]. This was observed in their experiments, as the same acoustic mode was excited at slightly lower frequency values for every lower order hydrodynamic mode. The convection velocity was also seen to have an effect within the resonance range of flow velocities. It was shown that during lock-in, there is a slight, yet discernible increase in the resonance frequency attributed to the high acoustic pressure amplitudes during resonance excitation. Due to the strong pressure distribution during resonance, the shear layer oscillations changes from an added mass to an added stiffness effect [37, 102]. Ziada et al. [103] also suggested that the presence of a duct confinement surrounding the cavity reflects the sound generated by the dynamic flow oscillations. The sound reflected from the boundaries seems to promote the shear layer oscillations at lower Mach numbers, thereby explaining the slight deviation in Strouhal numbers when compared to similar cavities without any confinement.

Effect of Upstream Boundary Layer Characteristics

The boundary layer characteristics upstream from the cavity has also been reported to be an influential parameter on the flow-excited acoustic resonance. Sarohia [84], for example, discovered that the onset of oscillations can also be limited by the cavity length. It was found that there is a minimum aspect ratio, based on the thickness of the shear layer, that is required to induce flow-oscillations, as shown in Fig. 1.8.

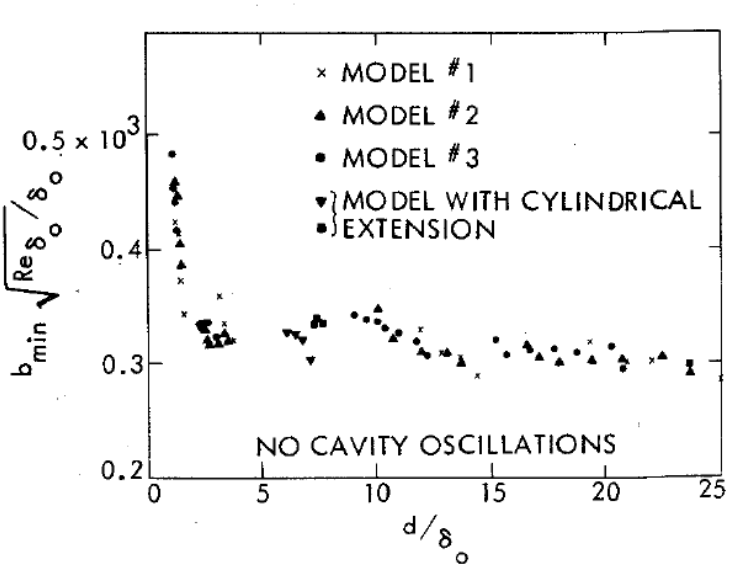

Figure 1.8: Region of cavity oscillation [84].

Nakiboğlu et al. [64] explored identical axisymmetric cavities in two separate configurations, where one configuration mounted the cavity near the duct inlet, and the other configuration mounted the cavity further downstream. This effectively explored effects of the momentum thickness of the shear layer on the onset of resonance excitation. It was found that the shear layer momentum thickness increases when increasing the upstream length from the inlet to the leading edge of the cavity. Due to the enlarged shear layer momentum thickness, the hydrodynamic amplification for higher order hydrodynamic modes are noticeably weaker and hinders the acoustic pressure perturbations from affecting the shear layer instability. Consequently, the higher order hydrodynamic modes in their investigation were not observed for the thicker momentum thickness of the downstream mounted cavity.

The approaching boundary layer is also a crucial feature when considering mitigation and suppression techniques. As the instability of the shear layer due to the cavity discontinuity is the source of the acoustic tone generation, numerous investigations have been made in developing both active and passive techniques to suppress

resonance excitation. Experiments in confined shallow rectangular cavities were conducted to assess the influence of varying the geometries of the upstream and downstream edges of the cavity to disrupt the shear layer [69]. Similar experimental studies were carried out to explore the effectiveness of spanwise control rods in suppressing the resonance excitation. It was found that implementing a control rod at the cavity leading edge would generate high-frequency vortices, impeding the flapping of the shear layer [1]. The effectiveness of this control technique significantly depends on a number of geometrics parameters, namely; the streamwise location of the rod with respect to the cavity leading edge, the gap between the rod and the wind tunnel wall, and the aspect ratio of the cavity. In general, passive techniques involve geometry modifications to disturb the shear layer formation and hence the coupling mechanism.

Active techniques can range from active spoilers or mass injection designs to ultimately modify the shear layer dynamics as to avoid coupling with the acoustic modes of the system. Both, active and passive control techniques have been further developed in later experiments demonstrating their capabilities in mitigating resonance excitation, and proposing universal criterion for optimal design parameters [53, 68, 88, 99]. Control techniques, however, have shown to be influenced by numerous parameters, thereby complicating the prediction of optimum design for suppressing resonance excitation. In addition, issues regarding flow-acoustic instabilities arise in industry applications, where design modifications for commissioned equipment is difficult to accomplish and not economically feasible. Suppression and mitigation methods are also likely to cause substantial pressure drop due to their intrusive nature on the flow-field [88]. Although such methods indicate promising results, there is much work yet to be made in further understanding the influence of various parameters on the optimal design for mitigating acoustic resonance. Subsequently, this requires a greater understanding of the fundamental physics responsible

for the coupled phenomenon. For this reason, the current work does not explore the effect of mitigation or suppression methods, but rather focuses on the improving the current state of knowledge regarding the fundamental interaction between the acoustic field and the shear layer instability of cavity flows.

1.1.4 Cylindrical Cavities

Acoustic Response

Cylindrical cavities are subject to similar flow-acoustic coupling mechanisms as the rectangular type, however, due to the inherent geometry of the cylindrical cavities, the acoustic modes excited take different form. The acoustic behaviour of cylinder pipes have been well understood and is thus utilized to estimate the resonance of cylindrical cavities since they are synonymous to a pipe with open-closed boundary conditions [37, 94]. Such geometries ideally yield $1/4\lambda$ acoustic mode shapes, where the acoustic pressure node is located at the open end of the pipe and the frequency is a function of the length of the pipe. Therefore, cylindrical cavities also excite depths modes similar to rectangular cavities and these acoustic modes are equally influenced by the convective effects as discussed in Sec.1.1.3. Numerical and experimental campaigns have provided valuable insight into the tone generation of flow over cylindrical cavities [38, 55, 60, 97]. Rayleigh [75] noted that the radiation from the open end of the cavity causes a discrepancy to the estimated values, to which he proposed end correction factors to account for the radiation. Two end correction factors were proposed, depending on whether the open end of the cavity is flanged or unflanged. Numerous future investigations have contributed to refining the value of these end corrections and even proposed expressions for the constants [22, 66, 67]. Nevertheless, the proposed modifications were not seen to have a significant impact

on estimating the resonance frequency of the cavity, and therefore the general approximation proposed by Rayleigh [75] still serves as a robust prediction method for the acoustic depth mode. It should be noted, however, that the cylindrical cavities mentioned here were subject to external flow, and hence, not confined by an enclosure, or the enclosure was much larger relative to the cavity. This is an important consideration as the confinement of a cavity by means of a duct is known to affect the acoustic modes of a system, which determines the system's liability to exciting an acoustic standing wave. As mentioned in Sec.1.1.3, Ziada et al. [103] conducted experiments on two-dimensional shallow rectangular cavities and demonstrated that the excited acoustic mode of the system is the transverse mode of the cavity-duct configuration. Such acoustic modes would not materialize without the presence of a duct or reflective boundary. Verdugo et al. [97] carried out similar measurements for cylindrical cavities in a duct, but the duct employed was much larger than the cavity. The velocity sweep revealed a "stepwise" evolution in the excited frequencies, leading up to the expected $1/4\lambda$ acoustic mode for cylindrical pipes. This differs from the discrete lock-in range behaviour typically reported in literature and was credited to the presence of the duct confinement, yet no further insight was given to the "stepwise" evolution of consecutively excited acoustic modes. Nevertheless, the experimental results of Verdugo et al. [97] presented valuable information regarding the three-dimensionality of the flow over cylindrical cavities by employing hot wire measurements at various locations in the cavity and wake region. It is thus evident that the aeroacoustics behaviour of cavities are greatly influenced by the presence of reflective boundaries in the near vicinity, and should be considered when addressing applications in confinements such as pipes and ducted systems.

Hydrodynamic behaviour

In the case of cylindrical cavities, similarly to the convention for rectangular cavities, they may be classified as deep or shallow depending on their aspect ratio, where the diameter of the cavity represents the impingement length. As outlined, dividing cavities into these two categories is beneficial due to potential changes in the flow behaviour when cavity depths become smaller than the impingement length. This categorization carries greater significance in cylindrical cavities. Accordingly, the cylindrical nature of the cavities provoke a number of differences in the acoustic and fluid-dynamic behaviour when compared to rectangular cavities. With regard to the flow behaviour, the aspect ratio of a cylindrical cavity is a fundamental parameter since, unlike the two-dimensional rectangular cavities, the flow for cylindrical cavities is seen to be highly three-dimensional. The early works of Hiwada et al. [45] explored the characteristics of flow patterns over cylindrical cavity openings for a range of shallow aspect ratios $h/L < 1$, providing some of the earliest research regarding such cavity-types. Gaudet and Winter [32] used oil-flow visualization techniques, showing interesting flow behaviour at the cavity walls. Through the experiments of Hiwada et al. [45], it was further revealed that for shallow cavities, the dynamics of the flow-field changes and is strongly dependent on the cavity depth. The work detailed asymmetric flow behaviour for a range of cavity aspect ratios by means of static pressure measurements on the interior walls of the cavity, where the asymmetry changes with varying depths. The static pressure measurements offer an appropriate representation of the static pressure distribution in the cavity, and hence the average flow field for all cases considered. Their findings were later confirmed by a number of studies on both, shallow and deep, cylindrical cavities [26, 56, 58]. The flow behaviour is characterized such that for $0.2 < h/L < 0.8$, the flow is seen to be asymmetric with respect to the streamwise direction, where the strongest asymmetry and levels of drag are reported

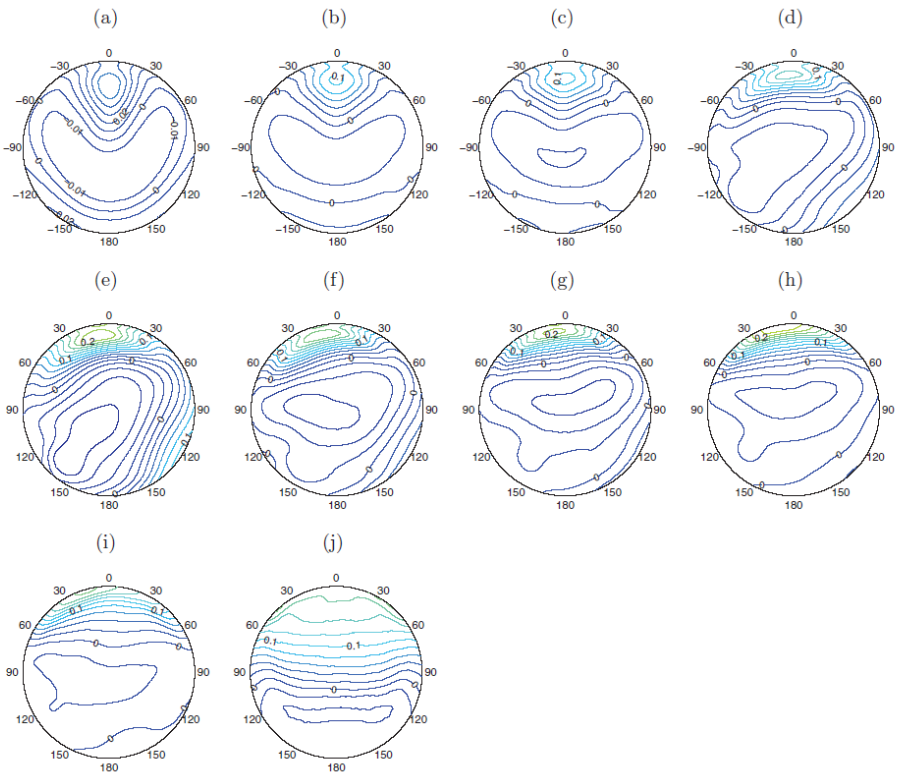

Figure 1.9: Static pressure coefficient (C_p) distribution on the cavity wall for aspect ratios between 0.1 and 1 [56].

for $h/L = 0.5$. The range of aspect ratios from $0.2 < h/L < 0.8$ is further divided into two categories based on their flow dynamics. For $0.2 < h/L < 0.4$, the asymmetric flow exhibits flapping behaviour with respect to the streamwise direction, while $0.4 < h/L < 0.8$ exhibit stable asymmetric flow. For cylindrical cavities with aspect ratios outside the range of 0.2 - 0.8, the flow is understood to be stable and symmetric. This illustrated in Fig. 1.9. Future studies have provided deeper insight into the asymmetric flow structure for shallow cylindrical cavities, showing that the asymmetry is not only relative to the streamwise direction of the flow, but also relative to the cavity plane [19, 39]. In other words, the shear layer in the spanwise direction is no longer parallel to the cavity opening. This is an important consideration when addressing acoustic tones generated by cylindrical cavities, particularly the shallow type. In

relation to the flow oscillations due to the shear layer instability, the semi-empirical formula proposed by Rossiter [81] has served useful and proven viable in predicting the non-dimensional frequency of the flow oscillations of cylindrical cavities as well. Authors throughout the years, as is the case with Howe [47], have made adjustments to Rossiter's formula on account of analytical improvements. This formula, however, has been developed using rectangular cavities where the impingement length of the cavity is uniform across the entire spanwise direction, hence the term *two-dimensional* cavity. Authors such as Czech et al. [21] and Mery et al. [59] have observed cylindrical cavities to exhibit similar Strouhal periodicity to those of rectangular cavities, which further demonstrates the significance of the impingement length in predicting the frequency of the flow oscillations. This is an interesting observation, considering the non-uniformity of circular cavities in comparison to the rectangular type. Their work further extended the approach proposed by Rossiter [81] to cylindrical cavities by employing effective length equations to account for the circular cavity opening. Although the proposed equations allow for a better fit of the experimental data using the semi-empirical formula, details of the shear layer's spatial characteristics and an explanation for the effective length equations are still unknown. Therefore, a more in-depth analysis of the flow patterns over the cavity opening is needed in order to provide a physical explanation for the use of effective length equations.

1.2 Motivation

The following research is motivated by the vulnerability of critical equipment in generating flow-acoustic coupled interactions. The dynamic oscillations of flow over cavities and their interaction with acoustic resonant modes have demonstrated the potential risk to the structural integrity of such mechanical systems and pose a safety hazard

to surrounding personnel. Comprehensive investigations and reviews exist regarding the aeroacoustics response of two-dimensional cavities subject to a wide range of flow velocities, however, literature concerning cylindrical cavities is far less. The complexity of cylindrical cavities introduces three-dimensional flow characteristics to the shear layer, thus conflicting with analytical methods developed assuming a uniform, two-dimensional impingement of the shear layer. Large discrepancies between the acoustic behaviour of confined and unconfined cavities suggest that the confinement promotes the reflection from the acoustic radiation of the cavity, thereby exciting trapped acoustic modes within the cavity and duct, whose characteristics are still unknown. Furthermore, in the case of confinements, no effort has been made regarding the diameter of the cavity in reference to the confinement. In addition, research reported for shallow cylindrical cavities outline the asymmetric flow that is initiated for such cavities and the dependency of this flow behaviour on the aspect ratio. However, no further explanation has been attributed to this observed dependency for shallow cylindrical cavities, nor is there enough evidence to firmly characterize the Strouhal periodicities. To this extent, the importance of the cavity aspect ratio on the flow-oscillations and aeroacoustics response is clear, though the aspect ratio does not consider the three-dimensionality of the cavity. Various shaped cavities may consist of the same cavity depth and impingement length, yet their dissimilarity in shape effectively generates a different acoustic response. On account of this, a thorough investigation on variously shaped cavities, which share the same aspect ratios and duct confinement, would serve as a comprehensive analysis of the aeroacoustics response for a wide range of applications subject to confined turbulent flow. A substantial portion responsible for flow-acoustic coupling is, of course, the cavity flow and shear layer dynamics. In spite of this, the complexity of experimentally measuring such small and complex physical quantities limit the knowledge in literature

regarding the flow patterns of the shear layer and its role in coupling with the acoustic field. However, accomplishing this would greatly serve existing research in providing interpretation to unexplained observations, as well as, contribute novel insight to the coupled phenomena.

1.3 Objectives

The objectives of this current research are as follows:

1. Experimentally characterize the aeroacoustics response of cylindrical cavities with various aspect ratios mounted to a rectangular duct.

2. Further explore the effects of the confinement on the aeroacoustics response of cylindrical cavities by investigating the admission ratio of the cavity-duct system.

3. Experimentally study the impingement behaviour of the shear layer for cylindrical cavities by directly measuring the dynamic pressure fluctuations on the downstream edge using pressure sensor probes.

4. Empirically explore the aeroaocustics response of two-dimensional rectangular cavities as well as square cavities in the same confinement. By effectively maintaining the aspect ratios, emphasis is placed on the effects of other geometric parameters, such as the admission ratio and the shape of the cavity opening.

5. Perform Particle Image Velocimetry (PIV) measurements on all cavity cases explored in order to visualize the shear layer topology in the spanwise plane, immediately atop the cavity opening, as well as its interaction with the acoustic noise production.

1.4 Thesis Outline

This thesis is organized into 6 chapters. The arrangement of the chapters are as follows:

- Chapter 1: This chapter consists of a general introduction regarding the self-sustained flow oscillations, as well as, the flow-excited acoustic resonance mechanism in cavity geometries. A detailed literature review on these mechanisms is discussed for both, rectangular and cylindrical cavities, respectively. This chapter also provides the outline and motivation behind the thesis, as well as, the objectives to accomplish throughout the investigation.

- Chapter 2: This chapter details the experimental methodology used to carry out the characterization of the aeroacoustics response, as well as the numerical methodology to predict the fundamental acoustic modes and corresponding acoustic pressure distribution for all cavity cases. This chapter also outlines the procedure employed to fulfill the PIV measurements to yield flow visualizations of the shear layer.

- Chapter 3: The content of this chapter is geared towards the first three objective, which present the aeroacoustics response of the cylindrical cavities, as well as the corresponding pressure distributions and Strouhal periodicities. Furthermore, detailed characteristics regarding the shear layer impingement behaviour for cylindrical cavities are presented.

- Chapter 4: The Aeroacoustics response of two-dimensional rectangular and square cavities are presented in comparison to the cylindrical cavities with similar aspect ratios. A detailed look into the peak Strouhal numbers during flow-excited resonance is also discussed.

- Chapter 5: Flow visualizations are demonstrated for the studied cavity cases in this thesis to illustrate the three-dimensional flow characteristics of the shear layer over the cavity opening and the influence of the acoustic amplification of the flow oscillations.

- Chapter 6: The final chapter summarizes the major findings throughout the investigation, discusses the novel contributions, as well as provides recommendations for future studies.

Chapter 2

Methodology

2.1 Wind Tunnel

The aeroacoustics measurements are performed on an open-loop wind tunnel, where the inner volume is shown in Fig. 2.1. The inner dimensions of the test section consists of height, $H = 127\ mm$, and width, $W = 254\ mm$. The airflow through the duct is generated via a centrifugal blower, which produces the necessary flow of air to free-stream flow velocities of up to 140 m/s, where the velocity sweeps are done in increments of $\sim 2.76\ m/s$. For all cavity configurations explored in this investigation, the distance between the inlet of the duct and the cavity section is maintained at 330 mm. In order to reduce the pressure drop and achieve stabilized flow over the cavity opening, a parabolic bell-mouth is installed at the inlet of the wind tunnel. The air then flows through a diffuser, increasing in the cross-sectional area with an inclusion angle of 14°. This inclusion angle ensures diffusion of the air flow downstream of the cavity, whilst avoiding flow separation from the diffuser walls. To support the main section of the wind tunnel, a heavy steel frame has been bolted directly to the facility's floor. The main section is firmly attached to the frame, with industrial rubber pads

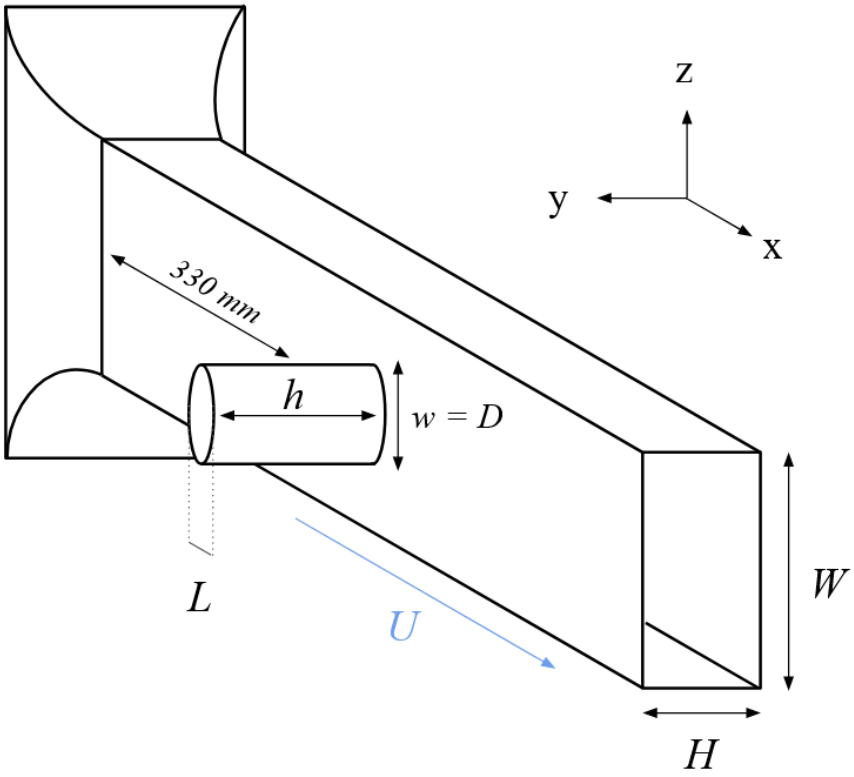

Figure 2.1: Schematic of the inner volume of the wind tunnel and cylindrical cavity configuration, including geometrical parameters.

in place to isolate it from any potential vibrations transmitted through the frame from the floor. To further limit any motion that might be introduced at higher flow velocities, steel cables connect the main test-section to the concrete wall, providing the necessary tension. These cables were initially installed for previous experiments involving sensitive measurements of the aerodynamic forces acting on cylinders in cross-flow, as described in Alziadeh and Mohany [9]. A flexible connection has been installed between the diffuser and fan blower to isolate the test-section from vibrations induced by the mechanical drive unit of the system. The mechanical drive unit itself is positioned atop 3/4 *in* rubber pads and has been fixed on an isolated concrete slab. The boundary layer characteristics upstream of a cavity have been reported to depend on certain geometrical parameters, as discussed in Sec.1.1.3, thereby influencing its

interaction with the acoustic field. The studies conducted by Sarohia [84] focused on relating the cavity aspect ratio to the thickness of the shear layer, detailing the minimum aspect ratio required to induce any sort of oscillation based on the thickness of the shear layer.

Nakiboğlu et al. [64] also demonstrated the influence of the shear layer momentum thickness on the Strouhal number, as well as the strength of the higher order hydrodynamic modes. However, the influenced imposed on the aeroacoustics response and shear layer dynamics of the cavity, by subtle changes in the upstream boundary layer profile are not as significant as the influence of the cavity aspect ratio. To this end, all cavities explored in this investigation consist of dimensions and a flow velocity range that guarantees flow oscillations, thus, the dependency proposed by Sarohia [84] is irrelevant for the current cases. Additionally, as the upstream distance from the duct inlet to the cavity section remains constant for all cases, the effect of the shear layer momentum thickness on the flow-acoustic coupling is not explored. The entire wind-tunnel apparatus employed in this investigation has been used in a number of successful studies involving cavity flow, see for example [1,3]. The characterization of the momentum thickness was done by means of hotwire measurements upstream of the cavity from 5-25 m/s. The low velocity range exists outside the resonant conditions of the system, as to ensure the acoustic amplitudes do not provoke vibration of the hotwire. It was found that the momentum thickness of the upstream boundary layer is inversely proportional to the flow velocity, thereby following a power law of $\theta/a \approx Re_a^{-0.2}$, where a denotes the upstream distance between the cavity leading edge and the inlet of the wind tunnel. [17]. The values for the shear layer momentum thickness can be seen in Fig. 2.2, and agree well with reported literature [5, 102].

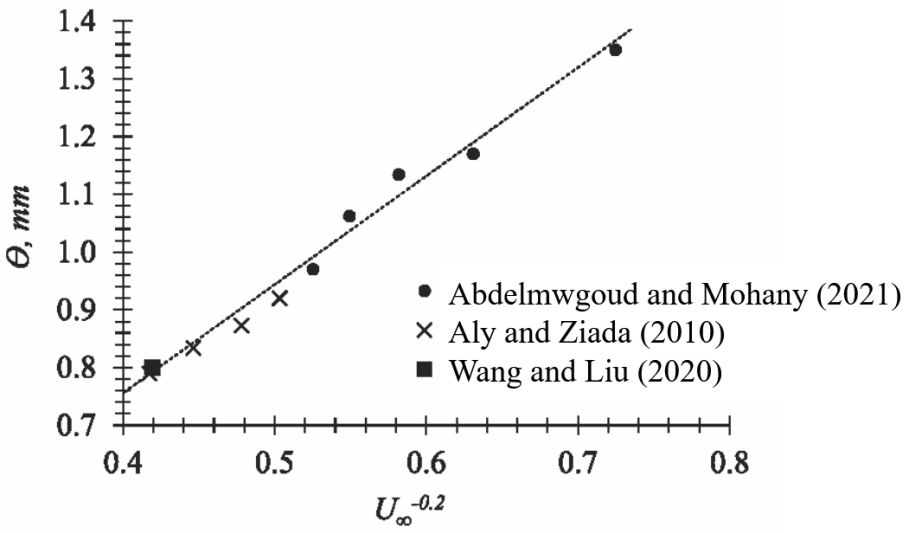

Figure 2.2: Boundary layer momentum thickness at the cavity leading edge [1].

2.2 Cylindrical Cavities

2.2.1 Cavity Configurations

The current work is geared towards uncovering details regarding the acoustics and flow-dynamics of cylindrical cavities subject to confined flow. Such cavities are not as common in literature in comparison to the rectangular type. Furthermore, the existing studies concerning cylindrical cavities involve external flow, and hence do not account for reflective boundaries in the vicinity of the cavity. As seen in Fig. 2.1, the cavities are mounted to the larger side of the wind tunnel, W, maintaining a flush surface on the inside of the test-section. By virtue of laser cutting tools, all edges in the cavity are sharp 90° corners. The diameter of the first cavity is $D = L = 101.6$ mm which corresponds to an admission ratio of $w/W = 0.4$. The admission ratio is introduced here as the ratio between the cavity width, w, and the duct width, W. For this cavity diameter, three aspect ratios ($h/L = 1.5$, 1, and 0.5) are investigated. To address the effect of changing the admission ratio on the aeroacoustics response,

the three aspect ratios are repeated for a second cavity diameter of $D = L = 152.4$ mm. The second diameter corresponds to an admission ratio of 0.6. For simplicity, a naming convention is assigned to refer to the cavity cases, where the smaller cavity diameter is referred to as $\mathrm{O}_{h/L}$, and the larger diameter as $\emptyset_{h/L}$. The subscript denotes the corresponding aspect ratio. A summary of the cavity cases can be seen in Table. 2.1.

Table 2.1: Geometrical parameters of the six cylindrical cavity cases.

$Cavity$	w/W	h/L		
$\mathrm{O}_{h/L}$	0.4	1.5	1	0.5
$\emptyset_{h/L}$	0.6	1.5	1	0.5

2.2.2 Instrumentation and Data Acquisition

The aeroacoustic measurements are achieved using dynamic pressure microphones at select locations throughout the cavity and duct configuration. The microphones are PCB model 377A12 with a nominal sensitivity of 25 mV/kPa, and have an outer diameter of 6.35 mm. Given that multiple microphones are used simultaneously during the experiments, the sensitivity of each individual microphone is calibrated using a G.R.A.S. 42AB pistonphone. This ensures that the sensitivity value for each microphone is adjusted to record the same signal and amplitude from a given source. The raw signal recorded by the microphones first passes through a PCB model 482C15 signal conditioner to improve the signal-to-noise ratio, then channelled to an NI 6218-BNC data acquisition card. All acoustic measurements are recorded over 60-second intervals at a sampling rate of 20 kHz. A much higher sampling rate relative to the frequency band of interest ensures that the measured signals are free of aliasing. Five total microphones are used to monitor the acoustic behaviour of the cavity-duct

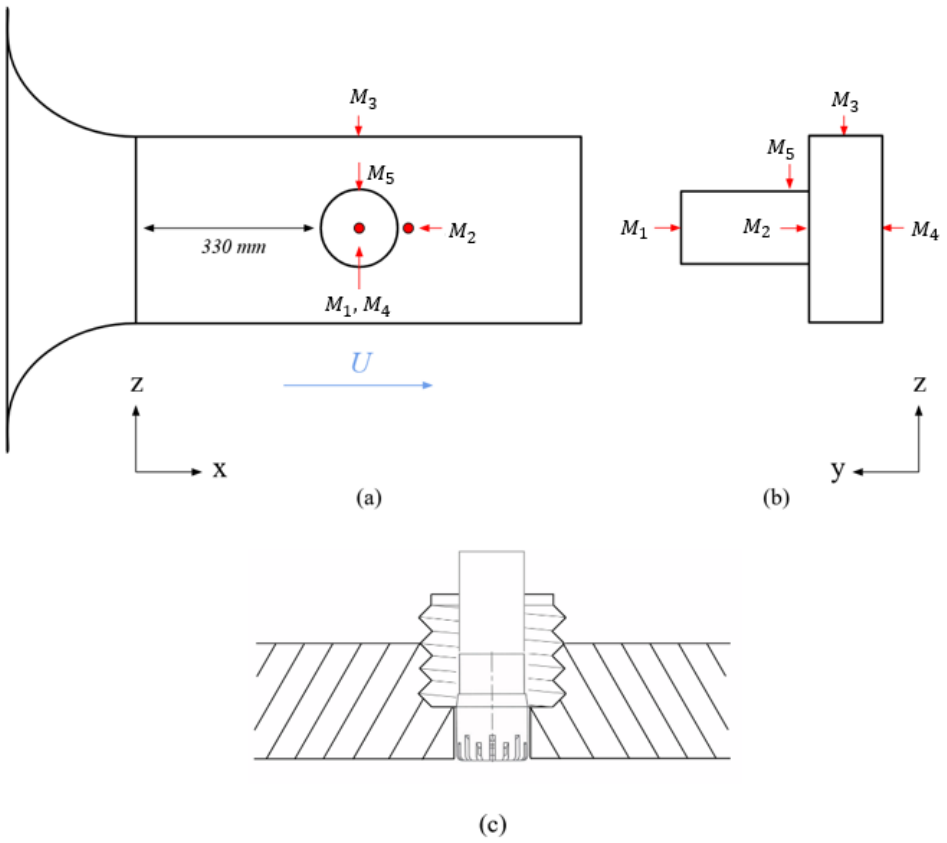

Figure 2.3: (a, b) Microphone locations for the acoustic pressure measurements and (c) installation of flush mounted microphone.

configuration. These microphones are labelled M_{1-5}. The first microphone M_1 is located at the centre of the cavity floor for all cases. This microphone is used as the main reference signal, since the highest acoustic pressure amplitudes for all transverse acoustic modes of interest occur at the floor of the cavity. Microphone M_2 is located in the centre of the spanwise dimension of the duct $W/2$ and is 6.35 mm downstream of the impingement edge. Microphone M_3 is placed at the top of the duct, centred at $H/2$, and aligned with the centre of the cavity. Microphone M_4 is placed on the opposite side of the duct, on the same axis as M_1. A fifth microphone M_5 is added at the top of the cavity such that it forms a plane with M_1, M_3, and M_4. The microphone configuration, as seen in Fig. 2.3, allows for investigation of the resonance frequencies

for confined cavities, as well as further insight into the acoustic pressure distribution during resonance excitation. All microphones employed are flush mounted to the inside of the cavity and duct walls in their respective locations, as shown in Fig. 2.3c.

2.2.3 Theoretical and Numerical Methodology

The acoustic resonance characteristics of a given system is a fundamental aspect in generating coupled flow-excited acoustic oscillations. The coupling occurs when the velocity dependant frequency of the shear layer oscillations coincide with natural acoustic modes of the system. These acoustic modes may be approximated with relatively good accuracy using theoretical calculations or numerical approach. This section outlines the estimation of the acoustic modes for the cylindrical cavities studied, using proposed theoretical equations, as well as numerical simulation. Although an analytical approach yields fair indication of the potentially excitable frequencies, these estimations are made assuming a stagnant fluid medium, thus no flow condition. Due to the convective effects on the resonance excitation, as discussed in Sec.1.1.3, it is expected that the experimentally measured values for the resonance frequencies will marginally deviate from the estimated values. The equation proposed by Rayleigh [75] provides a fair estimation for the acoustic depth mode of cylindrical cavities by implementing an end correction for the open-end of the cylinder. This can be seen in Eq. 2.1, where c is the speed of sound, h is the cavity depth, r is the cavity radius, and $\alpha = 0.8216$ is the end correction for infinite flange pipes.

$$f_{a1} = \frac{c(2n+1)}{4(h+\alpha r)} \qquad n = 0, 1, 2, ..., n \tag{2.1}$$

It is clear from this relationship that the acoustic pressure node of the $1/4\lambda$ acoustic mode is shifted outside the cavity by a distance that is a function of the cavity radius.

Furthermore, the effect of the radiation from the open-end is less significant as the depth of the cylinder increases relative to the radius. Therefore, Eq. 2.1 is used to estimate the acoustic depth modes for the given cylindrical cavities, and can also be used to estimate the higher order acoustic depth modes. Theoretical equations are viable options to estimate these resonance frequencies, however, this approach is highly dependent on the cavity aspect ratio and does not consider the presence of a confinement.

Accordingly, numerical acoustic models serve as a greater prediction tool for the acoustic behaviour by taking into account the duct confinement surrounding the cavity. This also provides grounds for comparison between the theoretical and numerical results. The numerical simulations are carried out using an acoustic finite element method provided in ANSYS suite to model the acoustic natural frequencies and corresponding pressure distribution of the system, within a stagnant fluid medium. These natural frequencies are calculated as the solutions to the Helmholtz equation shown in Eq. 2.2. The equation is governed by the acoustic pressure, p, as well as the wave number, $\left(\frac{\omega}{c}\right)$.

$$\nabla^2 p + \left(\frac{\omega}{c}\right)^2 p = 0 \tag{2.2}$$

The fluid domain consists of the same inner dimensions as the test-section of the wind tunnel, where the entire length of the duct in the streamwise direction is 762 mm and the cross-sectional area is 127 by 254 mm. The cavities inherit the same geometric features as shown in Table. 2.1 and are located at the centre of the large side of the duct, identical to the experimental apparatus. These dimensions are carefully selected in order to excite the natural frequencies within the given range of flow velocities. The properties of the fluid medium are calculated based on measured laboratory conditions, such as the room temperature and humidity percentage. Correspondingly,

the speed of sound is $c = 343\ m/s$ and the density of air is $\rho = 1.204\ kg/m^3$. The inlet and outlet of the test-section are treated as radiation boundaries to more accurately model the acoustic radiation propagating from the open ends of the duct, and effectively reduce the acoustic reflection from these boundaries. Using radiation boundaries over zero pressure boundaries for the open ends of the duct in the acoustic simulation, however, induces minimal change to the modelled pressure distribution of the transverse acoustic mode. This is because the resonance modes of interest involve only a sub-set of the cavity-duct system, referred to as trapped modes, and are not sensitive to boundary conditions [25, 94]. Linear elements are utilized with a maximum size of 6 mm as to ensure a sufficient amount of elements within one wavelength for the highest resonance frequency of interest. This was validated by conducting a mesh sensitivity analysis. Fig. 2.4 indicates that the estimated resonance frequency for the fundamental acoustic mode of the cavity-duct configuration is independent for mesh sizes exceeding $1{\times}10^5$ nodes.

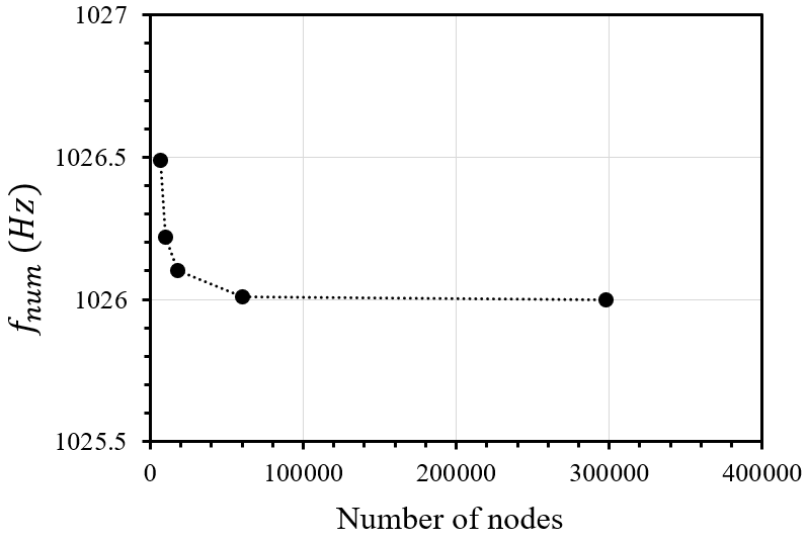

Figure 2.4: Effect of the number of mesh nodes on the fundamental acoustic mode for the highest frequency of interest.

2.3 Shear Layer Impingement Measurements

2.3.1 Cavity and Microphone Configuration

The instability of the shear layer over the cavity mouth is the driving mechanism for the flow-acoustic coupling. In the absence of acoustic resonance, the hydrodynamic modes dominate the frequency spectrum. In the physical sense, the hydrodynamic modes are representative of the number of vortex cores travelling over the cavity opening in a single flow-cycle, where the first hydrodynamic mode m_1 exhibits one vortex core. In the case of two-dimensional rectangular cavities, the hydrodynamic flow patterns are two-dimensional, thus the impingement of the shear layer on the downstream edge is relatively uniform across the entire span of the edge. The inherent three-dimensional flow patterns for cylindrical cavities eliminate the possibility of a uniform shear layer in the spanwise direction impinging on the downstream edge. Consequently, direct measurements on the downstream edge are conducted to reveal spectral content of the shear layer impingement. The cavities used for this investigation are the O_1 and $O_{1.5}$ cavities, as these aspect ratios generate symmetrical flow over the cavity mouth. The measurements are carried out using the microphone configuration shown in Fig. 2.5. A total of three microphones, namely; $M_{\theta 1}$, $M_{\theta 2}$, and $M_{\theta 3}$, are used for the measurements and are spaced 20° apart. Each measurement location consists of a 2 mm pressure tap which is machined though to protrude to the cavity trailing edge. A closer look at the installation of the microphone is shown on the right-hand side of Fig. 2.5.

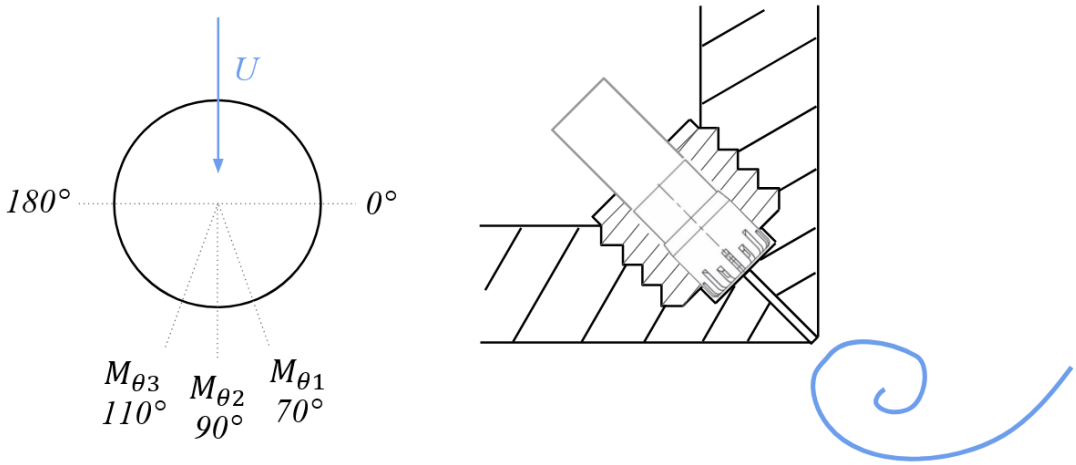

Figure 2.5: Microphone locations for acoustic pressure measurements of the shear layer impingement and installation of the microphone.

2.4 Rectangular and Square Cavities

2.4.1 Cavity Configurations

For this portion of the investigation, two-dimensional rectangular cavities and square cavities are employed to investigate the potential influence of the cavity shape on the aeroacoustics response of the cavity-duct configuration. This is motivated by the emphasis that is placed on the aspect ratio as a governing parameter, which does not take into consideration the three-dimensional shape of the cavity, nor its dimensions relative to the duct for confined cavities. On that account, it is of interest to explore cavities with various shapes, while maintaining the same cavity impingement length and depth. To accomplish this, as shown in Fig. 2.6, the $O_{1.5}$ and $O_{0.5}$ cavities are replicated into two-dimensional rectangular cavities and square cavities with the same aspect ratios. The flow patterns for cylindrical cavities with $0.2 < h/L < 0.8$, which are in the shallow cavity regime, are known to demonstrate increasing asymmetry in the flow relative to the stream-wise direction as the aspect ratio decreases. For this reason, the aspect ratio 0.5 is selected, as this aspect ratio is reported to have the

largest amount of flow asymmetry and cavity drag for cylindrical cavities. This asymmetric flow feature does not arise in two-dimensional rectangular cavities, however it is still unknown whether similar flow dynamics emerge in a square cavity with a similar aspect and admission ratio to the $O_{0.5}$ cavity. Subsequently, the aspect ratio

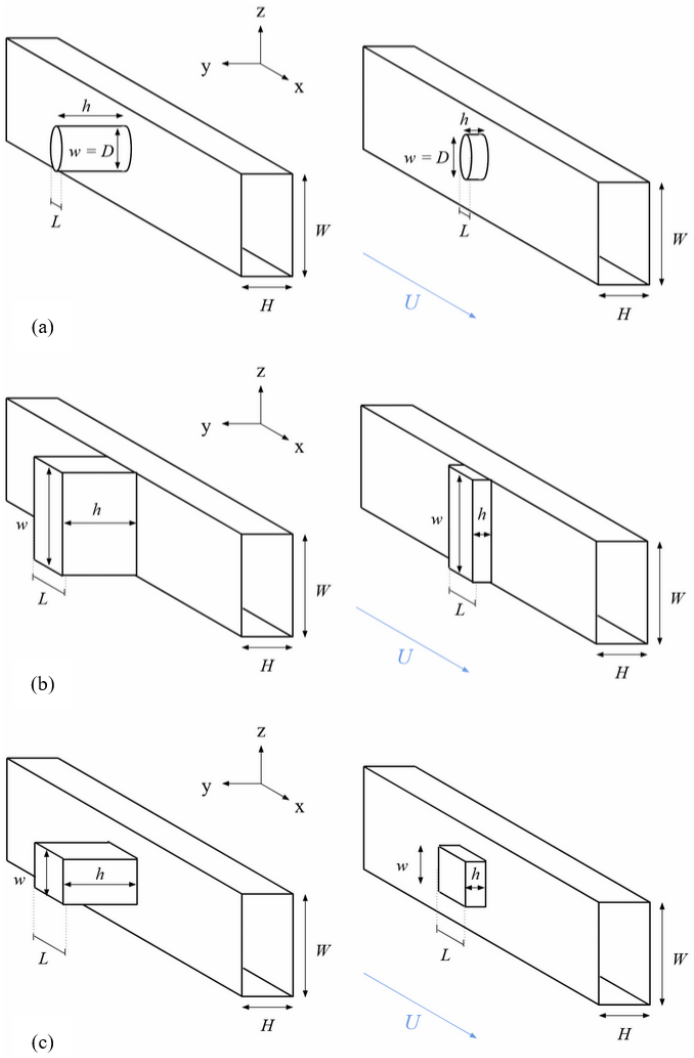

Figure 2.6: Aspect ratio $h/L = 1.5$ and 0.5 for a) cylindrical cavities, b) two-dimensional rectangular cavities, and c) square cavities.

of 1.5 is selected, as this case is known to completely excite the fundamental acoustic mode within the range of the studied flow velocities. This approach thus investigates

the influence of other geometric parameters on the flow-acoustic coupling, in addition to the aspect ratio. Following the same naming convention as the cylindrical cavities, the two-dimensional rectangular cavities will be labelled as $R_{h/L}$, and the square cavities as $S_{h/L}$. The rectangular and square cavities studied here are investigated using the same wind tunnel outlined in Sec.2.1, and bear the same microphone configuration as presented in Fig. 2.3.

2.4.2 Theoretical and Numerical Methodology

Prediction of the acoustic depth mode is rudimentary when evaluating the occurrence of flow-induced resonance. The resonance acoustic mode dictates the cut-on frequency which will interact with the oscillations of the shear layer. Therefore, an accurate prediction of these excitable acoustic modes should be a preliminary procedure to better understand such coupled mechanisms. Accordingly, a theoretical approach can be used, similar to the cylindrical cavities. To predict the acoustic mode of the cavity duct configuration, Ziada et al. [103] proposed an equation to approximate the acoustic mode by employing the mean height of the cavity-duct configuration, as seen in Eq. 2.3.

$$f_{a2} = \frac{nc}{2(H + 0.5h)} \qquad n = 1, 2, ..., n \tag{2.3}$$

This theoretical equation is viable for two-dimensional rectangular cavities when the aspect ratio is less than unity and the cavity is reasonably confined. However, this approach was only utilized on shallow cavities mounted in a duct. On the other hand, the behaviour of two-dimensional rectangular cavities with depths much larger than the impingement length demonstrate acoustic depth modes trapped within the cavity similar to deep cylindrical cavities [28]. Therefore, the applicability of Eq. 2.3

for two-dimensional rectangular cavities with aspect ratios slightly larger than one is still unknown. In general, the acoustic mode shapes for cylindrical pipes are much simpler to predict than rectangular or square shapes, thus analytical equations are much simpler to derive and use in such situations. Moreover, since the characteristics of the acoustic mode for the $S_{h/L}$ cavities also pose uncertainties and are not common in literature, the numerical simulation and experimental results will serve as a greater prediction tool and provide a reference when addressing the reliability of Eq. 2.3 against various geometrically shaped cavities. The numerical simulation model and procedure employed here is identical to that outlined in Sec.2.2.3, with exception to the cavity shapes.

2.5 Techniques of Particle Image Velocimetry

Fig. 2.7 shows the experimental set-up used for flow visualization measurements. The campaign is carried out using an EverGreen PIV system accompanied by a double-pulse Nd: YAG laser. The laser is used to provide the necessary illumination for capturing instances of the flow. The laser beam produces a wavelength of 531 nm at a maximum frequency and peak power of 15 Hz and 200 mJ, respectively. In conjunction with the laser, a double frame 12-bit Charged-Coupled Device (CCD) camera with a resolution of 2752 X 2200 pixels is used to effectively capture the flow field. The camera is equipped with a Nikon AF Nikkor 50 mm f/1.8D lens. This lens provides high optical quality, low distortion, and a large aperture, which is necessary to capture high-quality images while minimizing noise. The total distance between the camera and the measurement plane is 500 mm. The camera was calibrated in order to convert pixel coordinates into physical units. This was accomplished using a precision ruler with clear marker points as a calibration target, placed exactly

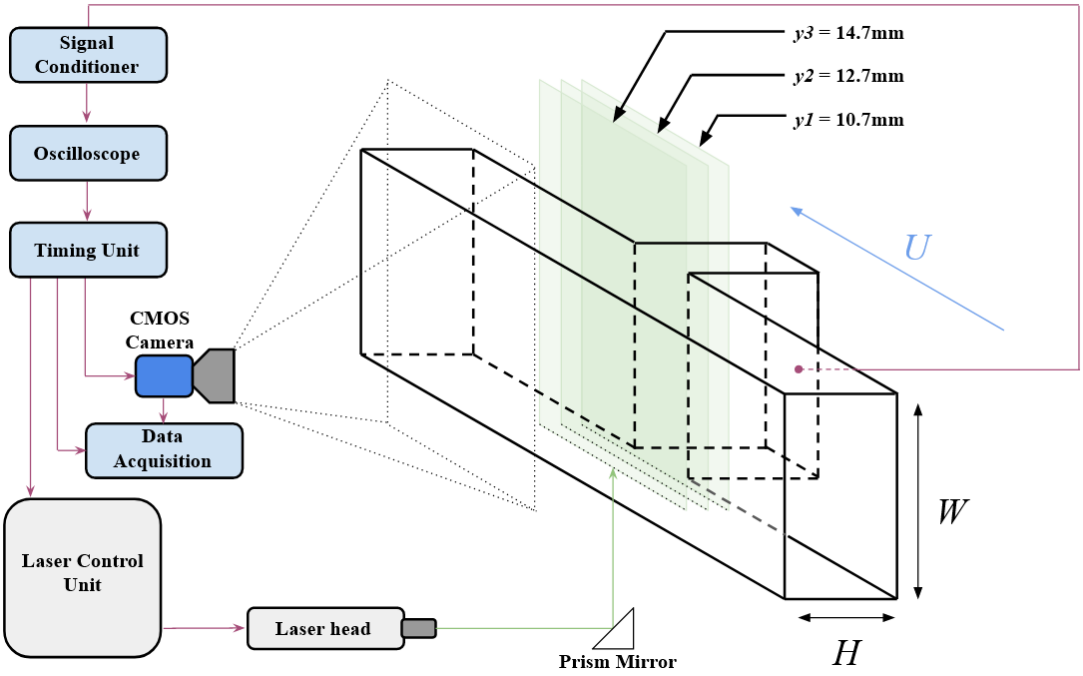

Figure 2.7: Schematic illustration of the experimental setup for the PIV system, including the three spanwise measurement plane locations for the laser sheet.

on the measurement plane of interest. The side of the duct, opposite of the cavity plane, consists of an acrylic window to effectively allow a field of view for the camera. The testing environment is seeded with liquid DEHS using an aerosol generator. The maximum particle size for this seeding medium is of 1 μm which guarantees a uniform distribution of the seeding particles in the flow field. The seeding particles are thus illuminated by the laser, rendering clear discrete particles in the captured images, which is pivotal for accurate velocity vector calculations. The purpose of the flow visualizations are to analyze the shear layer's behaviour for a wide range of flow velocities by means of time-averaged and phase-locked PIV measurements. Since the fundamental acoustic mode for each cavity case presents an acoustic pressure anti-node at the cavity floor, the signal from microphone M_1, flush mounted to the centre of the cavity floor, is used to trigger the laser pulses. The laser timing unit controls the laser pulses and image acquisition such that they occur simultaneously to capture

image pairs at predetermined instances in the acoustic pressure cycle using a method described by Mohany et al. [62]. This allows for snapshots of the flow corresponding to different phases of the acoustic pressure cycle. In the current study, 250 image pairs are captured at eight evenly distributed phases of the acoustic pressure cycle for a total of 2000 pairs. The main focus of the phase-locked measurements is to explore the spanwise shape and concentration of the shear layer vortices. Four phases, however, are presented for brevity as to exhibit these characteristics adequately, without compromising critical information regarding the coupled-interaction. In the shallow cavity cases where resonance excitation is absent, average flow characteristics are captured with 2000 random image pairs. The images are preprocessed using DaVis 10.0 software by subtracting the maximum image intensity with a filter size of 3 pixels, effectively reducing noise and spurious reflections. The vector fields are computed using an iterative multi-pass cross-correlation technique [85]. An initial window size of 32 by 32 pixels is used for the initial interrogation window, followed by four passes at a final interrogation window size of 16 by 16 pixels, both having 50% overlap. By applying a universal outlier detection technique, as described by Westerweel and Scarano [100], the vector fields are post-processed to further remove spurious vectors. The final vector field has a minimum spatial resolution of $0.015L$ by $0.015L$. Following the method described by Sciacchitano and Wieneke [86], the maximum uncertainty of the statistical quantities for the instantaneous streamwise and spanwise velocity vectors do not exceed 3% with a 95% confidence interval (refer to Appendix A). The mean velocity components are then extracted from the velocity vectors to reconstruct the phase-averaged velocity contour in the streamwise direction during a flow cycle. In absence of acoustic resonance, the time-averaged velocity contours are plotted. Fig. 2.7 also presents the location of the laser sheet, effectively showing the measurement planes for the flow visualization. The laser sheet is parallel to the plane of the cavity

opening, and is located 10.7 mm away from this surface. This measurement plane offers a view of the spanwise shape of the shear layer along the cavity width. Measurements with the laser sheet positioned at further distances, specifically; 12.7 mm and 14.7 mm, provide additional information on the velocity components of the shear layer at evenly spaced planes in the y direction. This effectively provides an inclusive understanding of the spatial characteristics of the shear layer in the spanwise plane as it travels over the cavity mouth.

Chapter 3

Aeroacoustics Response of Cylindrical Cavities

3.1 Prediction of Acoustic Resonance Modes

The results from the analytical predictions of the cylindrical cavities are provided in Table. 3.1, along with the experimental results for comparison. The theoretically calculated values and the numerical results are shown under the columns, f_{a1} and f_{num}, respectively. Accordingly, Eq. 2.1 is utilized to estimate the resonance frequency of the cavities. The experimental results are shown in red, where f_{onset} represents the measured frequency at the onset of resonance, and f_{peak} is the frequency at peak acoustic amplitudes. The experimental results are discussed to greater lengths in the following section, but are included in Table. 3.1 as to compare them to the predicted frequencies. Fig. 3.1 presents the normalized acoustic pressure distribution P/P_{max} at the given resonance frequency for cylindrical cavities. A section cut is made in the centre of the streamwise direction to analyze the acoustic pressure distribution between the cavity and duct.

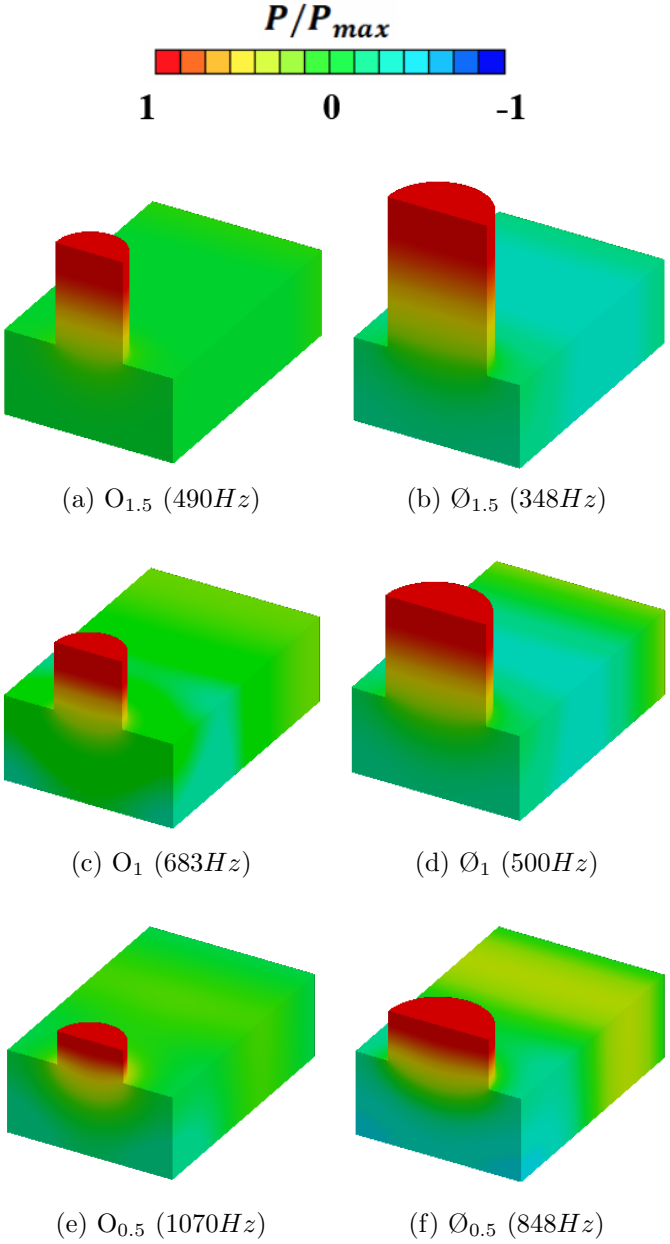

(a) $O_{1.5}$ ($490Hz$) (b) $Ø_{1.5}$ ($348Hz$)

(c) O_1 ($683Hz$) (d) $Ø_1$ ($500Hz$)

(e) $O_{0.5}$ ($1070Hz$) (f) $Ø_{0.5}$ ($848Hz$)

Figure 3.1: Dimensionless acoustic pressure distribution from numerical model for the $O_{h/L}$ cavities a), c), e) and the $Ø_{h/L}$ cavities b), d), f).

It is evident from Table. 3.1 that the numerical approach serves as a better prediction tool to estimate the resonance frequencies. The improved accuracy of the numerical approach in predicting f_{peak} is due to the fact that the numerical simulation includes the boundaries of the duct as well models the acoustic radiation from the duct inlet and outlet. The discrepancy to the theoretical values is especially clear for the $\emptyset_{0.5}$ when comparing f_{a1} and f_{peak}. This deviation of $\sim 31\%$ is attributed to the fact that the reflective boundaries of the duct in combination with the shallow cavity depth promotes the interaction between the cavity and the duct, as seen in Fig. 3.1f. This interaction demonstrates significant reflection from the duct wall, opposite of the cavity, where the normalized pressure is 40% of the maximum value observed on the cavity floor. Accordingly, a $1/2\lambda$ acoustic mode shape represents the acoustic pressure distribution, instead of the expected $1/4\lambda$ for cylindrical cavities. It should be noted that the excitation of this mode for $\emptyset_{0.5}$ is more prominent than $O_{0.5}$, where the normalized pressure on the opposite side of the cavity in Fig. 3.1e is only 10% of the maximum value. This is owing to the admission ratio of the geometries. The larger diameter of the $\emptyset_{0.5}$ cavity increases relative to the duct width, thereby improving the interaction between the cavity and duct. As a result, a $1/2\lambda$

Table 3.1: Theoretical and numerical results for the resonance acoustic modes of the cylindrical cavities.

			$f(Hz)$			
$Cavity$	w/W	h/L	f_{a1}	f_{num}	f_{onset}	f_{peak}
$O_{h/L}$	0.4	1.5	442	490 $(1/4\lambda)$	468	510
		1	598	683 $(1/4\lambda)$	613	671
		0.5	927	1070 $(1/4\lambda)$	-	1050
$\emptyset_{h/L}$	0.6	1.5	295	348 $(1/4\lambda)$	312	330
		1	399	500 $(1/4\lambda)$	464	466
		0.5	618	848 $(1/2\lambda)$	-	840

acoustic mode is materialized, such that the system behaves more as two-dimensional rectangular cavity, strictly speaking about the acoustic response. A general observation can be made regarding the numerical results for the $\emptyset_{h/L}$ cavities. The larger diameter of the cavity relative to the duct width appears to improve the radiation into the duct. This is observed in the duct portion of the $\emptyset_{h/L}$ cavities in Fig. 3.1, where acoustic pressure is seen to be distributed within the duct. Comparing this to the smaller admission ratio, the $\mathrm{O}_{h/L}$ cavities do not demonstrate such radiation due to the acoustic mode entrapment. Therefore, the acoustic pressure within the duct for the $\mathrm{O}_{h/L}$ cavities are nearly zero. Furthermore, it is clear from the prediction methods, that the numerical simulations provide a more reliable solution in predicting potentially excitable acoustic modes, delineating the fact that the presence of reflective boundaries have a considerable effect on accurately predicting the resonance frequencies of ducted cavities.

3.2 Aeroacoustics Response

3.2.1 Deep Cavities

Fig. 3.2 presents the aeroacoustics response of the $\mathrm{O}_{h/L}$ and $\emptyset_{h/L}$ cavities with aspect ratios of 1.5 and 1, respectively. The plots depict the experimental normalized acoustic pressure $P_{rms}/\rho c U_\infty$ as a function of the free-stream flow velocity. The peak frequency of the generated tone at each flow velocity is plotted against the right, vertical axis. The acoustic pressure measurements reported here are extracted from microphone M_1, at the floor of the cavity, which recorded the highest amplitudes of acoustic pressure in each cavity case. The plots are also accompanied by diagonal lines representing the shear layer hydrodynamic modes. As previously discussed, the hydrodynamic modes, or shear layer modes, represent the number of vortex cores

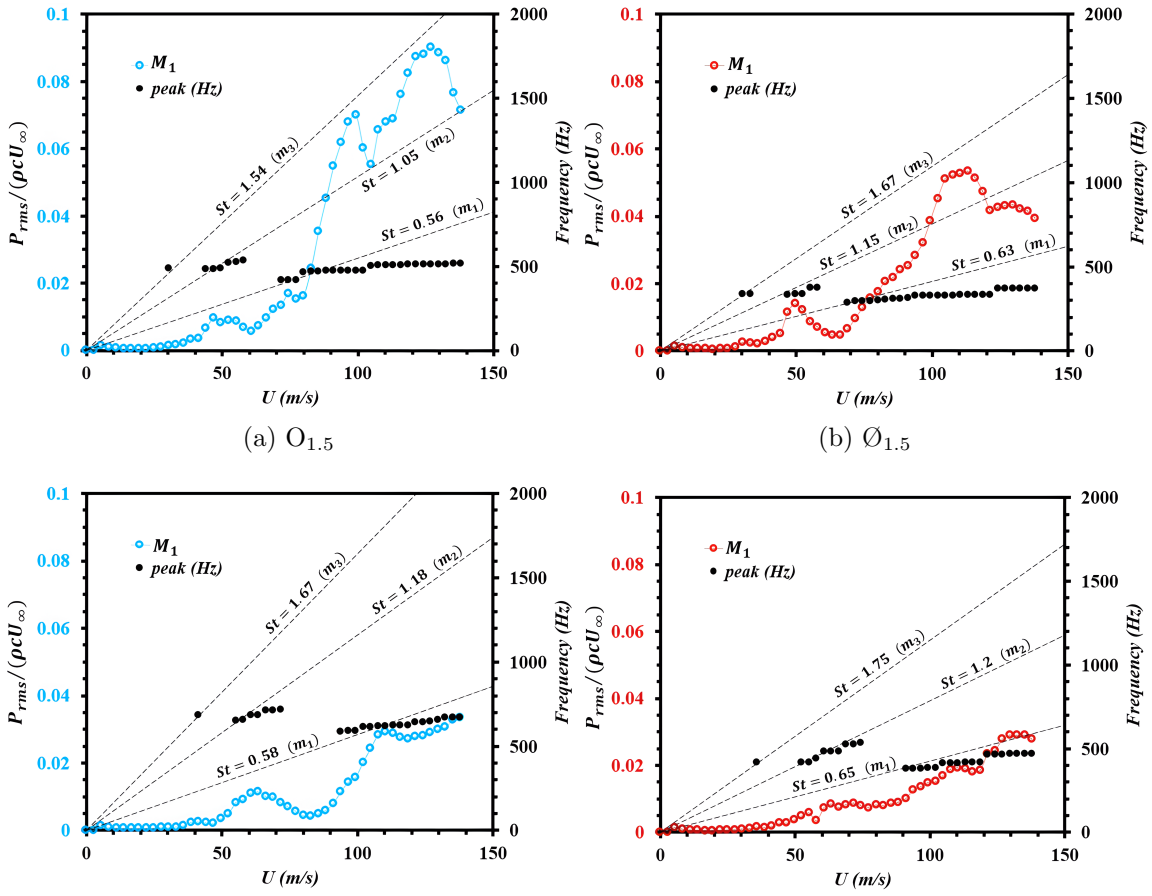

(a) $O_{1.5}$ (b) $\emptyset_{1.5}$

(c) O_1 (d) $\emptyset_1$

Figure 3.2: Normalized acoustic pressure $P_{rms}/(\rho c U_\infty)$ as a function of the mean flow U_∞ of the $O_{h/L}$ and $\emptyset_{h/L}$ cavities with $h/L = 1.5$ and 1. The diagonal lines represent the global Strouhal numbers of the shear layer modes.

travelling across the open mouth of the cavity. The linear relationship between the frequency of the shear layer oscillations, f_s, and free-stream flow velocity, U_∞, is the Strouhal number, St, which corresponds to the slope of the diagonal lines in Fig. 3.2. Each diagonal line represents a hydrodynamic mode, and is hence associated with a Strouhal number. The values for the Strouhal numbers are estimated by first identifying the frequency of the shear layer oscillations for a specific flow velocity. This is then repeated for each measured flow velocity in a given range, before resonance excitation. The frequencies are used to calculate the corresponding Strouhal numbers, and are

then averaged over all flow velocities measured. Evidently, in Fig. 3.2, a significant increase in the normalized acoustic pressure occurs when the velocity dependent shear layer oscillations coincide with the fundamental acoustic mode of the cavity-duct configuration. For all cavity cases shown in Fig. 3.2, the first three hydrodynamic modes, m_3, m_2, and m_1 are observed in decreasing order as the flow velocity increases. It is clear that the amplitude of the acoustic resonance becomes significantly stronger for decreasing hydrodynamic modes. This is apparent at higher flow velocities, where the first hydrodynamic mode m_1 is seen to coincide with the resonance field, resulting in a large discrete lock-in range and a significant increase in the normalized acoustic pressure. The literature concerning the Strouhal periodicities for rectangular cavities are comprehensive and are typically reported occurring around 0.5, 1, and 1.5 for m_1, m_2, and m_3, respectively [1, 103]. It has been found that cylindrical cavities $h/L \geq 1$ also exhibit similar Strouhal numbers with exception to slight variations [57, 71, 97]. Such variations are attributed to the change in the geometric shape of the cavity opening, however, the relatively unaltered Strouhal numbers further outlines their dependency on the impingement length of the cavity. Accordingly, the four cases shown in Fig. 3.2 have $h/L \geq 1$ and indeed agree with Strouhal numbers reported in literature. These values can be seen in Fig. 4.4 and will be further discussed in a later section. The $O_{1.5}$ cavity is shown in Fig. 3.2a, and also depicts the strongest resonance case of all four cases in Fig. 3.2. In accordance with the literature, the first three hydrodynamic modes consecutively excite the fundamental acoustic mode. Yet, further scrutiny of the lock-in range, excited by m_1, reveals interesting behaviour regarding the frequency of excitation. The frequency during the lock-in range appears to be sustained close to the predicted mode for a range of flow velocities, before it suddenly jumps to a higher frequency. The sudden frequency switch is associated with two distinct peaks in the acoustic pressure spectrum. The convective effects on the

resonance is seen to influence the resonance frequency as the flow velocity increases. Ziada et al. [103], for example, detailed the that the lock-in frequency slightly increases during resonance due to the maximum shear layer oscillations changing from an added mass effect to an added stiffness effect. In this particular event, there would be a distinct pressure peak for the flow velocities within the lock-in range. On the other hand, Fig. 3.2a demonstrates the presence of two pressure peaks that appear to be associated with two distinct frequencies. This behaviour differs from the typical observations reported in literature for rectangular and cylindrical cavities, suggesting that the presence of the duct, and hence the acoustic reflection, affects the resonance behaviour of the system. When comparing to the same aspect ratio for $\emptyset_{1.5}$, Fig. 3.2b, a similar behaviour is observed with the presence of a double peak for two distinct frequencies. Although the cavities in Fig. 3.2a and 3.2b share the same aspect ratio, a significant decrease in the normalized acoustic pressure is noticed. The ratio between the cavity depth and diameter is maintained for both cavities, however both parameters are larger for the $\emptyset_{1.5}$ cavity. It is thus interesting to note that the deeper cavity generates nearly half the normalized acoustic pressure when compared to the $O_{1.5}$ cavity. The larger depth promotes a lower resonance frequency that should be easier to excite for the studied flow velocities. This, however, is not the case, and suggests that the larger diameter of the $\emptyset_{1.5}$ cavity increases the acoustic radiation from the cavity to the surrounding environment, thereby further increasing the acoustic reflection from the surrounding boundaries. This reinforces the consideration of the αr term in Eq. 2.1 where the effects of the cavity radius must be considered when the dimensions of the depth and radius are relatively close. Fig. 3.2c and 3.2d illustrate the O_1 and $\emptyset_1$ cavities. Upon first inspection of the cavities with aspect ratio of 1, the normalized acoustic pressure is significantly lower than those with aspect ratio of 1.5. This is credited to the fact that the shallower cavities consist of smaller depths,

and hence, higher resonance frequencies and higher acoustic radiation. These higher frequencies are inherently excited at higher flow velocities, since the hydrodynamic modes remain the same. As a result, the coincidence occurs closer to the end of the velocity range studied, and therefore does not capture the entire lock-in range. In addition, the cavities with aspect ratio of 1 shown in Fig. 3.2c and 3.2d, increase the effect of the cavity radius on the acoustic resonance frequency and amplitude due to the radiation, further explaining the reduction in normalized pressure for the cavities of this aspect ratio. A similar increase in the frequencies during the lock-in period is in-fact discernible in all cavity cases shown in Fig. 3.2. The frequencies in the lock-in range appear to be increasing in a step-like manner when excited by the first hydrodynamic mode. These step-like increases in the resonance frequencies seem to become less apparent as the cavity depth becomes larger. For the aspect ratios of 1.5, despite the sudden frequency switch, the lock-in range appears much more discrete than the cavities with aspect ratio of 1. Experiments conducted by Verdugo et al. [97] on a cylindrical cavity with aspect ratio of 1.357 reported a "stepwise" increase in resonance frequencies during the lock-in period, similar to those observed in Fig. 3.2. In their investigation, the step-wise behaviour of the frequencies was attributed to the confinement of the cavity, yet the confinement used was reasonably large relative to the cavity, and no further explanation was given to this step-wise behaviour. Investigations regarding cylindrical cavities, in the absence of a confinement, report a uniform increase in the frequencies during the lock-in period as opposed to a step-like increase [58]. This therefore suggests that the confinement imposes an effect on the acoustic field of the system and promotes the excitation of consecutive frequencies in a step-like manner. Furthermore, increasing the cavity depth relative to the diameter enhances the potential of exciting the $1/4\lambda$ acoustic depth mode, and thus reduces the significance of the radiation from the cavity due to the entrapment of the acoustic

mode. The plots shown in Fig. 3.3 correspond to the same cavity cases in Fig. 3.2. This figure presents the maximum sound pressure level (SPL) measured from the cavity floor, for the given range of flow velocities. The red vertical dashed lines are used to represent the velocity at which the acoustic pressure begins to increase due to the corresponding hydrodynamic coupling. Fig. 3.3a shows the sound pressure level for the $O_{1.5}$ cavity, where the amplitude begins to increase at $U_\infty \sim 75$ m/s, owing to the first hydrodynamic mode. When analyzing the lower velocity range, the second hydrodynamic mode is also visible at $\sim 45\ m/s$. When comparing this cavity to O_1 in Fig. 3.3c, the onset of the acoustic resonance due to m_1 occurs at a higher flow velocity of $U_\infty \sim 93$ m/s, and the higher order hydrodynamic modes are also shifted to higher flow velocities. This delay in the flow velocity at the onset of resonance is attributed to the reduction in cavity depth. The $O_{h/L}$ cavities share the same diameter, therefore the reduction in cavity depth, whilst maintaining the cavity diameter, increases the frequency of the acoustic mode. The velocity dependant oscillations of the shear layer, however, are not affected since the impingement length of the cavity remains the same. Consequently, the velocity must be further increased in order for the hydrodynamic mode to coincide with the acoustic mode of the cavity. The same trend is observed between Fig. 3.3b and 3.3d for the $Ø_{h/L}$ cavities, where the reduction in cavity depth results in a $\sim 20\%$ increase in the flow velocity at the onset of resonance excitation. Moreover, comparing the same aspect ratio between Fig. 3.3a and 3.3b shows that the velocity at the onset of resonance is unaffected. This is attributed to the same aspect ratio shared between the two cavities. The increase in cavity depth for the $Ø_{1.5}$ cavity reduces the frequency of the acoustic mode, however, since the cavity diameter is increased proportionally, the frequency of the shear layer oscillations are also reduced. Resultantly, the steeper progression of the velocity dependent shear layer oscillations, interact with an acoustic mode at a lower

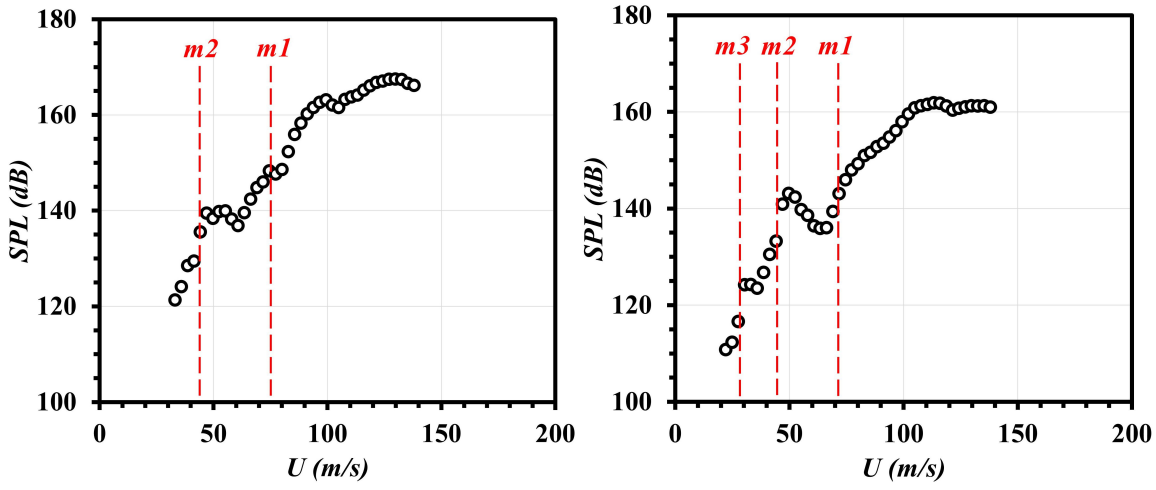

(a) $O_{1.5}$

(b) $\emptyset_{1.5}$

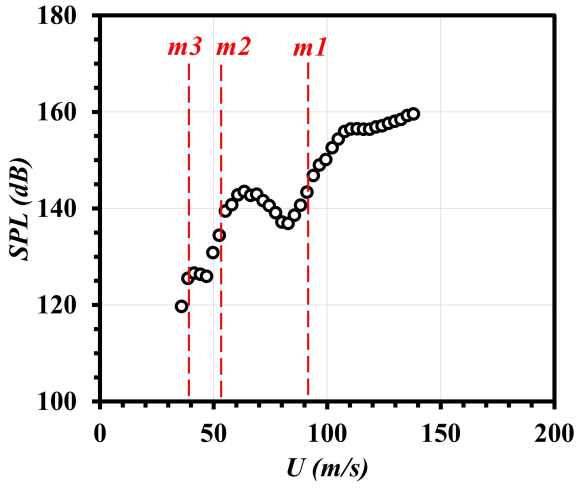

(c) O_1

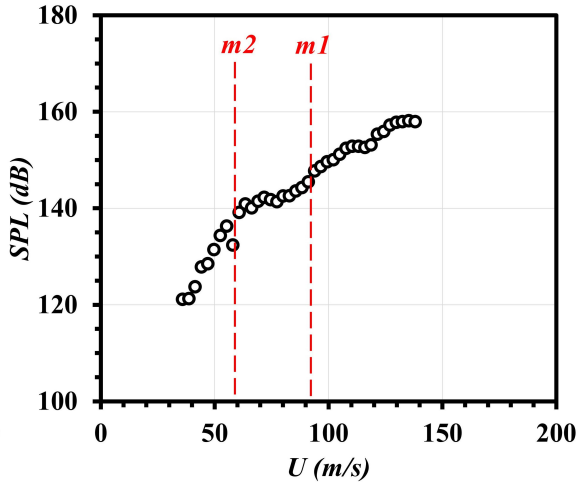

(d) $\emptyset_1$

Figure 3.3: The free-stream flow velocity U_∞ at the onset of resonance for the $O_{h/L}$ and $\emptyset_{h/L}$ cavities with $h/L = 1.5$ and 1. The vertical lines represent the shear layer mode responsible for the increase in sound pressure level (SPL).

cut-on frequency, effectively maintaining the same Strouhal number. Accordingly, the flow velocity at the onset of resonance is maintained. Comparison of Fig. 3.3c and 3.3d demonstrate the same trend where the onset flow velocity remains unchanged due to retaining the same aspect ratio.

3.2.2 Shallow Cavities

The aeroacoustics response for the $O_{0.5}$ and $Ø_{0.5}$ cavities are shown in Fig. 3.4. The reason for presenting the shallow cylindrical cases independently are two-fold. Firstly, both cases lacked strong acoustic resonance due to the high cut-on frequency introduced by the shallow depth, and are therefore presented as waterfall plots. Secondly, the behaviour of shallow cylindrical cavities differ considerably from their deeper counterpart and are thus presented separately to discuss the details. The waterfall plots combine the frequency spectrum at each flow velocity, and the colour map represents the sound pressure level in dB/Hz. For the $O_{0.5}$ cavity shown in Fig. 3.4a, a weak but distinct tone appears at $\sim 1050\ Hz$, which is $\sim 1.9\%$ lower than the numerically predicted value. The $Ø_{0.5}$ cavity shown in Fig. 3.4b exhibits a more broadband tone at $\sim 840\ Hz$. This case was also well predicted by the numerical model, but not by the theoretical calculation using Eq. 2.1. As seen in Fig. 3.1f, the normalized pressure distribution for this case in particular demonstrates a $1/2\lambda$ acoustic mode shape trapped between the cavity floor and the opposite wall of the duct. The larger admission ratio for this cavity case improves the interaction between the cavity and duct, thereby promoting an acoustic standing wave which begins to resemble that of a two-dimensional rectangular cavity. Evidently, the numerical simulation accounts for the duct boundaries, providing a much more accurate representation of the acoustic pressure distribution, as opposed to the theoretical approach which neglects any reflective surfaces outside the cavity. The diagonal lines in Fig. 3.4 again represent

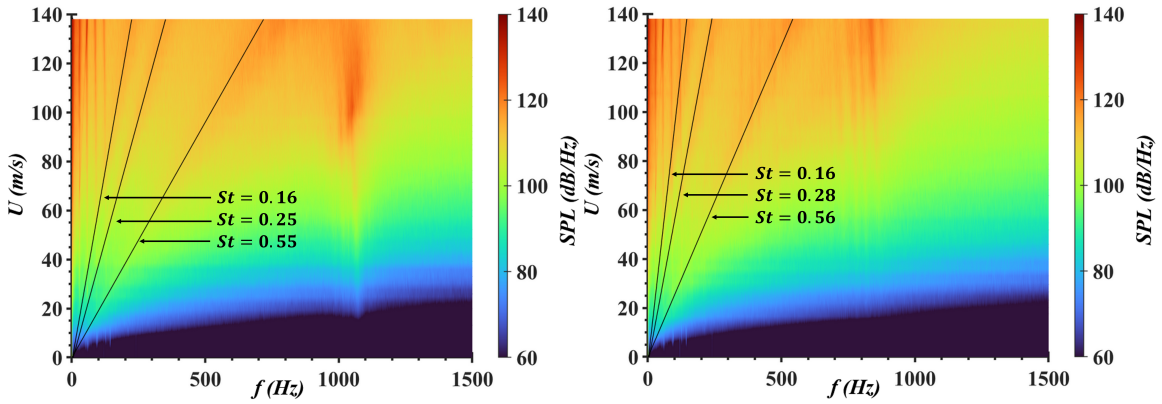

(a) $O_{0.5}$ (b) $\emptyset_{0.5}$

Figure 3.4: The Sound Pressure Level as a function of the mean flow U_∞ of the $O_{0.5}$ and $\emptyset_{0.5}$ cavities. The diagonal lines represent the global Strouhal numbers for the shear layer modes.

the Strouhal periodicities for the lowest three hydrodynamic modes. In both shallow cavities, resonance is not initiated as in the deeper cases, however the acoustic modes are discernible as a weak interaction excited by a hydrodynamic mode of $St \sim 0.55$. This Strouhal number is similar to the value obtained for m_1 in the deeper cylindrical cavities previously discussed, as well as reported values in literature. Nevertheless, the waterfall plots also exhibit velocity dependent tones generated at significantly lower frequencies. In both Fig. 3.4a and 3.4b, evidence of two-lower order hydrodynamic modes at $St \sim 0.16$ and 0.25 are observed.

These values greatly deviate from the anticipated values reported in literature, as well as the deeper cavities in the previous section. It is important to mention that the presence of these lower order hydrodynamic modes in both shallow cavities indicates a strong influence of the aspect ratio on the hydrodynamic modes for shallow cylindrical cavities. The hydrodynamic modes of the shear layer represent the sound generated by the flow oscillations over the cavity, and do not depend on the acoustic modes of the system. The flow tones produced for the shallow cavities in Fig. 3.4 therefore signify

substantial change in the flow pattern, compared to deeper cylindrical cavities, and is responsible for the deviations in the measured Strouhal numbers [40]. Furthermore, literature concerning shallow cylindrical cavities outline asymmetric flow behaviour for cavities with aspect ratios $0.2 < h/L < 0.8$, where the highest levels of flow drag and asymmetry are reported for the current case of $h/L = 0.5$. This is a crucial aspect that warrants consideration when addressing the low Strouhal numbers for the shallow cylindrical cavities, since shallow two-dimensional rectangular cavities do not develop any flow asymmetry in the streamwise direction, nor do they exhibit such changes in the Strouhal numbers. This hence supports the notion that shallow cylindrical cavities modify the flow structure, which in turn plays a significant role in the generated aeroacoustic noise.

3.2.3 Acoustic Pressure Distribution

Fig. 3.5 provides further detail regarding the acoustic pressure distribution during the lock-in range. The $O_{1.5}$ cavity is used to demonstrate changes in the acoustic pressure as the flow velocity is increased, since this cavity presents the strongest resonance case of those studied in this investigation. The dimensionless pressure fluctuations P_{rms}/P_{max} are plotted using M_1, M_3, M_4, and M_5 as shown in Fig. 2.3. These four sensors form a cross-sectional plane down the centre of the cavity and duct configuration. Fig. 3.5a, 3.5b, and 3.5c demonstrate the pressure distribution at three distinct regions within the lock-in range, highlighted in green on the spectral plots. Near the start of the lock-in range, in Fig. 3.5a, the $1/4\lambda$ acoustic depth mode of the cavity is not fully materialized, and as the velocity increases, the nodal point of the acoustic mode shifts closer towards the cavity mouth. This can be seen in Fig. 3.5a, where the normalized acoustic pressure in the duct decreases with increasing flow velocity. The second region continues to exhibit a shift in the nodal point of

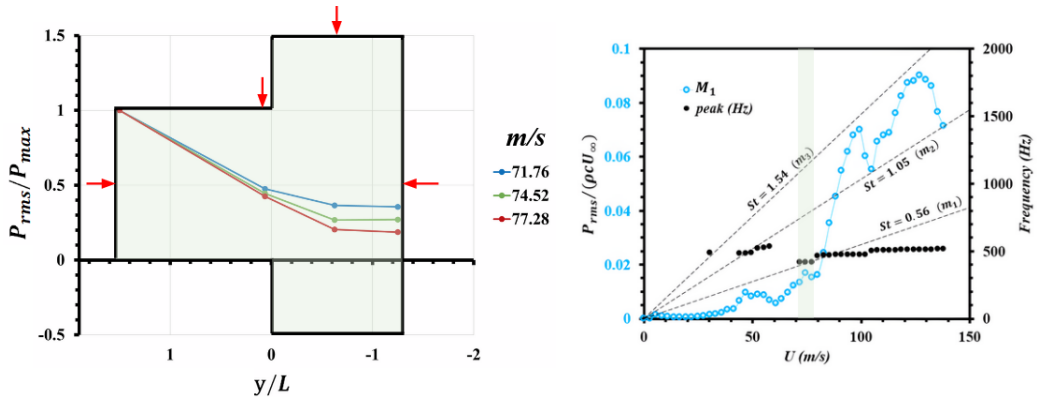

(a) 72 - 77 m/s

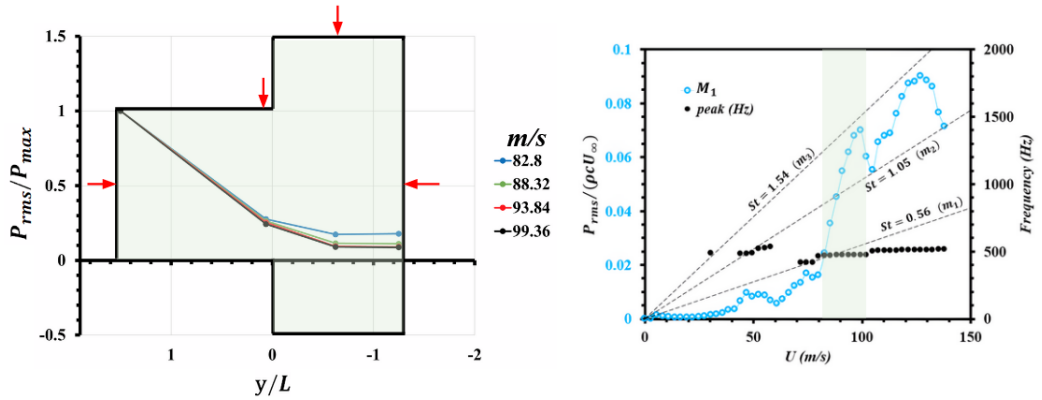

(b) 83 - 99 m/s

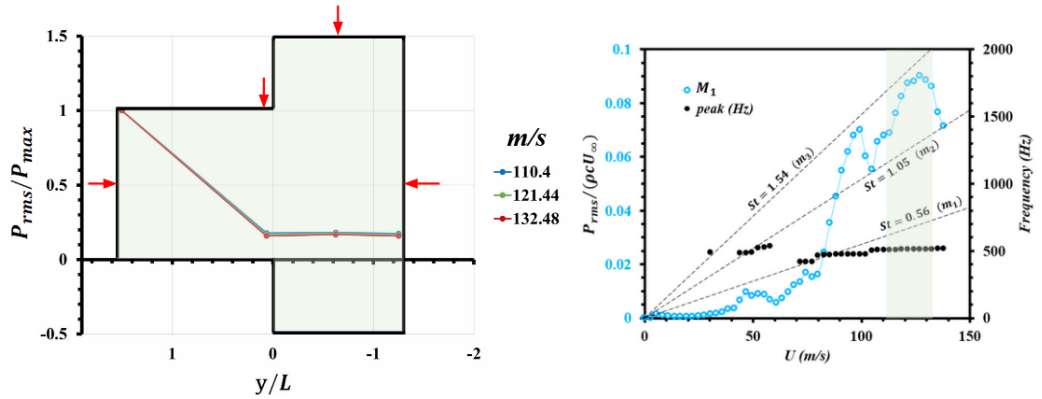

(c) 110 - 133 m/s

Figure 3.5: Normalized acoustic pressure P_{rms}/P_{max} distribution for the $O_{1.5}$ cavity at the given velocity ranges.

the mode shape, although, begins to converge near the point of maximum amplitude.

In the third region, the acoustic resonance is the strongest and the acoustic pressure

distribution no longer presents any changes in the mode shape until the flow velocities exceed the lock-in range. Additionally, all the microphones, except for M_1 in the cavity, show minimal pressure fluctuations in the duct while the $1/4\lambda$ acoustic mode is completely trapped within the cavity. The progression of the acoustic pressure distribution during resonance excitation provides valuable insight into the acoustic mode shape, thereby validating the numerical results, and demonstrating the added stiffness effect observed during resonance lock-in.

3.3 Dynamics of the Shear Layer Impingement

The current section focuses on the shear layer behaviour of cylindrical cavities. Specifically, the $O_{1.5}$ and O_1 cavities are used in this portion of the study to gain further understanding of the dynamic fluctuations on the downstream edge of a cylindrical cavity. This section is motivated by the fact that cylindrical cavities do not have a constant cavity length as the rectangular or square cavities, and it would thus be of interest to analyze the dynamic fluctuations on the trailing edge in the absence of acoustic resonance. Greater detail regarding the shear layer flow topology will be covered in a later section by means of PIV measurements. For the two cylindrical cavities examined in this section, the microphone configuration shown in Fig. 2.5 is adopted, where three evenly spaced microphones are mounted to pressure taps on the cavity trailing edge. Experiments conducted by Verdugo et al. [97] utilized hotwire measurements in different spanwise and streamwise locations, just above the cavity opening. The streamwise profiles of the velocity fluctuations in their work showed the relative size and three-dimensionality of the shear layer over cylindrical cavities, as well as the growth of the shear layer as it progresses downstream. Similar findings were reported by means of static pressure measurements on the inner cavity walls, for

an aspect ratio of 1 [55]. The mean flow is shown to be symmetrical with respect to the streamwise plane. The three-dimensionality of the flow is observed as a localized high pressure zone at the centre of the cavity downstream edge and floor, due to the shear layer impingement and recirculation zone within the cavity. The following measurements are geared towards better understanding the impingement behaviour of cylindrical cavities. Fig. 3.6 and 3.8 present the fluctuating acoustic pressure as a function of the Strouhal number for four consecutive flow velocities for $h/L = 1$ and 1.5, respectively. The dynamic pressure signals in these two figures are measured using $M_{\theta 2}$, as seen in Fig. 2.5, located at the very downstream, centre portion of the cavity edge. The spectral data was used here to first identify the hydrodynamic modes of the shear layer, showing a clear progression of the shear layer oscillations, in both cases, around the anticipated values of $St \sim 0.5$, 1, and 1.5. Fig. 3.7, for an aspect ratio of 1.5, demonstrates the spectral content for all three microphones simultaneously at 27.6, 30.4, and 33.1 m/s, respectively. The peaks of three shear layer modes in Fig. 3.7 can be identified and tracked for these flow velocities, where the third hydrodynamic mode m_3 is seen to amplify as it approaches the acoustic cut-on frequency of the cavity. Scrutinizing the signals at each flow velocity shows that the frequency of the dynamic pressure fluctuations remain the same, irrespective of the radial location on the cavity downstream edge. However, this can only be said for the current configuration, where the microphones span a total of 40° on the downstream edge. A more pronounced feature is the deviation in the amplitudes between the sensors. $M_{\theta 1}$ and $M_{\theta 3}$ are both spaced evenly from the centre stream-wise direction and reveal a notable similarity in both spectral profiles. Although the frequency characteristics of $M_{\theta 2}$ agree with the other two sensors, the amplitude is significantly lower. Fig. 3.9 presents the same three velocities, but for the cavity aspect ratio of 1. Unlike the deeper cavity, this case presents similarities in both the frequency and

pressure amplitude profiles for all three sensor locations on the cavity downstream edge. Comparison between the $O_{1.5}$ and O_1 cavities here suggests that the depth plays a role in the flow topology, such that the reduced cavity depth interacts with the recirculating region in the cavity. Consequently, the trajectory of the shear layer and impingement locations on the downstream edge are directly impacted by this geometric perturbation.

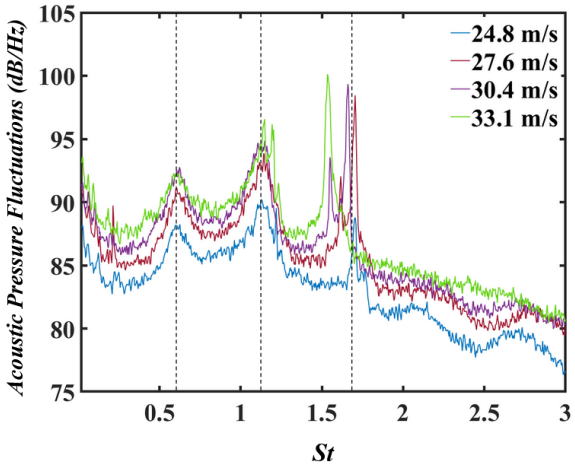

Figure 3.6: Fluctuating acoustic pressure at four consecutive flow velocities for the $O_{1.5}$ cavity. Linear progression of the hydrodynamic modes are seen as relatively constant values for St.

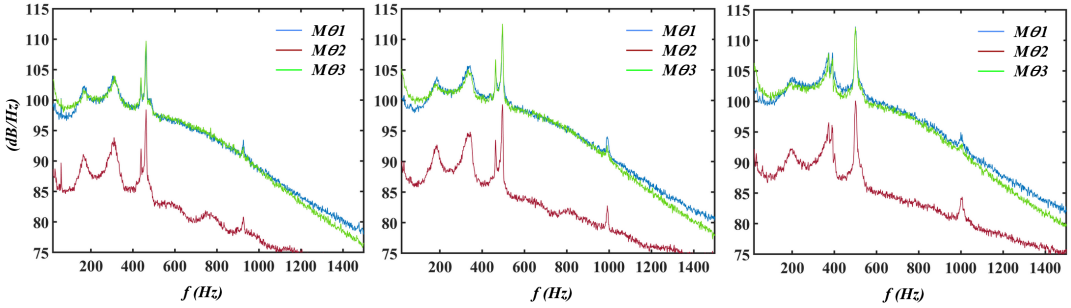

(a) 27.6 m/s (b) 30.4 m/s (c) 33.1 m/s

Figure 3.7: Fluctuating acoustic pressure from three pressure probes ($M_{\theta 1}$, $M_{\theta 2}$, $M_{\theta 3}$) at the cavity trailing edge for the $O_{1.5}$ cavity. The measurements are shown for three consecutive flow velocities.

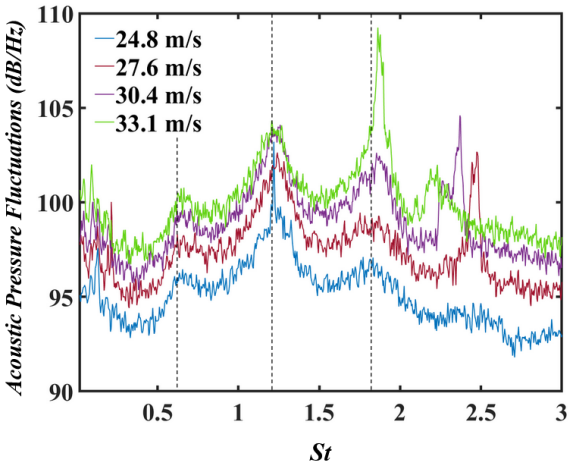

Figure 3.8: Fluctuating acoustic pressure at four consecutive flow velocities for the O_1 cavity. Linear progression of the hydrodynamic modes are seen as relatively constant values for St.

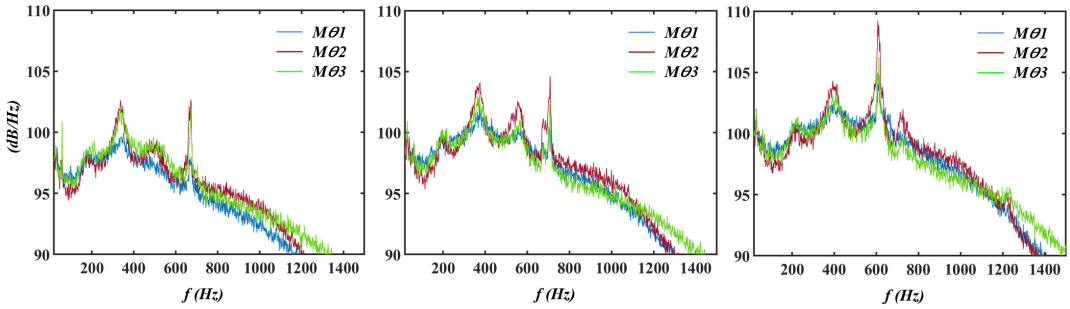

(a) 27.6 m/s (b) 30.4 m/s (c) 33.1 m/s

Figure 3.9: Fluctuating acoustic pressure from three pressure probes ($M_{\theta 1}$, $M_{\theta 2}$, $M_{\theta 3}$) at the cavity trailing edge for the O_1 cavity. The measurements are shown for three consecutive flow velocities.

3.4 Chapter Summary

3.4.1 Aeroacoustics Response

In this section, the aeroaocustics response of cylindrical cavities with $h/L = 0.5$, 1, and 1.5 are presented for flow velocities of up to Mach 0.4. The numerical simulations provided much more accurate predictions for the resonance acoustic modes in all cav-

ity cases, attributed to appropriately modelling the duct confinement and radiation boundaries. Strouhal numbers for cylindrical cavities of $h/L \geq 1$ exhibit hydrodynamic modes at the typical values reported in literature. Though the hydrodynamic modes appear less affected by the aspect and admission ratios, a large decrease in normalized acoustic pressure is observed due to the increase in acoustic radiation for larger admission ratios or shallower aspect ratios, effectively hindering the entrapment of a trapped acoustic mode in the cavity. Intermittent increases in the excited frequencies emerge in a step-like pattern before the lock-in range and is attributed to the presence of the duct confinement and the reflection of the surrounding boundaries.

The pressure distribution in the cavity-duct configuration at increasing flow velocities demonstrates a change in the acoustic mode shape due to the convection velocity. The pressure distribution appears to become increasingly trapped at higher flow velocities, explaining the compressibility effect responsible for the increase in frequency during resonance lock-in.

The shallow cylindrical cavities exhibit significant deviations in the hydrodynamic modes in comparison to their deeper counter-parts. Although these lower Strouhal numbers may be attributed to the asymmetric flow reported in literature for such cavities, flow visualizations will be presented in a later section discussing the flow topology and its effect on the generated low velocity dependant tones.

Moreover, the numerical and experimental results represent excitation of the cavity at the anticipated fundamental acoustic mode, with exception to the $\emptyset_{0.5}$ cavity. This change in the acoustic behaviour for this particular cavity is credited to the admission ratio of the cavity, where the numerical model displays a $1/2\lambda$ acoustic mode due to the larger diameter relative to the confinement. The larger diameter in combination with the duct geometry promotes the interaction between the two domains, therefore, materializing a trapped mode which is a function of the cavity depth and duct height,

rather than an acoustic mode, exclusively trapped in the cylindrical cavity.

3.4.2 Shear Layer Impingement

In the current section, measurements of the shear layer impingement on the downstream edge of the cavity are presented for the $O_{1.5}$ and O_1 cavities. The Strouhal periodicity at consecutive flow velocities in both cases confirm the hydrodynamic modes of the cavities, in good agreement with reported literature. The spectral content of all microphones at consecutive flow velocities presents interesting behaviour regarding both the frequencies of the three hydrodynamic modes and their relative amplitude. Despite the separate locations for the microphones along the cavity radius, both cases demonstrate impingement frequencies at the same values. This is an interesting observation considering the three-dimensional shape of the cavity, suggesting that the shear layer is subject to velocity fluctuations affecting the spanwise shape of the shear layer, such that the impingement appears simultaneously on the downstream edge. Therefore, no change in the impingement frequencies are measured amongst the microphones. A larger discrepancy is seen regarding the amplitudes of the acoustic pressure of both cylindrical cases. Evidently, the aspect ratio of 1 exhibits virtually identical pressure spectrums despite the microphone locations, whilst the aspect ratio of 1.5 shows a large decrease in the amplitude measured at the centre of the downstream edge. The considerable decrease in the pressure at this particular pressure tap is attributed to the impingement location of the shear layer, which occurs below the trailing edge. As the depth is reduced to an aspect ratio of $h/L \leq 1$, the cavity floor becomes increasingly intrusive to the three-dimensional recirculation region at the cavity opening. Resultantly, the shifted recirculation region affects the trajectory and impingement of the shear layer relative to the centre of the trailing edge. Ultimately, the location of the impingement is influenced by cavity depths

within the range of $1 \geq h/L \geq 1.5$, thereby influencing the fluctuation amplitudes measured from $M_{\theta 2}$, and exhibiting the three-dimensionality of the shear layer.

Chapter 4

Aeroacoustics Response of Two-Dimensional Rectangular and Square Cavities

4.1 Prediction of Acoustic Resonance Modes

A similar tabulation, as that seen in Table. 3.1 for cylindrical cavities, is shown here in Table. 4.1 for the $R_{h/L}$ and $S_{h/L}$ cavities. The theoretical natural frequency f_{a2} is calculated using Eq. 2.3 for the cases studied in this chapter. This theoretical formula considers the mean height, $H+0.5h$, of the cavity-duct configuration, however, it does not account for the cavity width in reference to the duct width. Therefore, since the cavity depth and duct height are the same in both the $R_{h/L}$ and $S_{h/L}$ cavities, the theoretical results yield the same value for both cavity shapes. Thus, the numerical simulation allows for a more reliable prediction of the acoustic modes by appropriately modelling the duct confinement boundaries. When comparing the predicted values to the experimentally measured frequencies, f_{peak}, it is clear that the experimental

Table 4.1: Theoretical and numerical results for the resonance acoustic modes of the rectangular and square cavities.

			$f(Hz)$			
$Cavity$	w/W	h/L	f_{a2}	f_{num}	f_{onset}	f_{peak}
$R_{h/L}$	1	1.5	844	504 (1/2λ)	477	528
		0.5	1125	1062 (1/2λ)	-	1080
$S_{h/L}$	0.4	1.5	844	492 (1/4λ)	474	479
		0.5	1125	1065 (1/4λ)	-	1033

results deviate considerably from the calculated values, signifying the effects of the reflective and radiative boundaries, as well as the admission ratio of the cavity. The numerical model is evidently far superior in predicting the acoustic modes, where the results from the pressure distribution are shown in Fig. 4.1. The resonance frequency of both $R_{h/L}$ cavities are well estimated by the numerical model, and do in fact excite the 1/2λ acoustic cross-mode with the cavity-duct configuration. However, a much larger discrepancy is seen between f_{a2} and f_{num} for $R_{1.5}$, despite exciting the 1/2λ acoustic mode. This is attributed to the cavity depth, since Eq. 2.3 is developed for shallow cavities. Consequently, the calculated frequency using Eq. 2.3 depends on the mean height of the cavity and duct configuration. On the other hand, the experimental result reveals that the 1/2λ acoustic mode materializes, though it becomes a function of the actual length of the cavity depth and duct height, rather than the mean height proposed in literature [103]. This explains the reduced value of f_{peak} experimentally measured for the $R_{1.5}$ cavity. Regarding the $S_{h/L}$ cavities, the theoretical approach no longer appears to be valid. The numerical results, instead, demonstrate a 1/4λ acoustic mode shape for both cavities and agrees well with the experimentally measured values. Despite sharing the same aspect ratio as the $R_{h/L}$ cavities, the resonance behaviour for the $S_{h/L}$ cavities are observed to exhibit acoustic

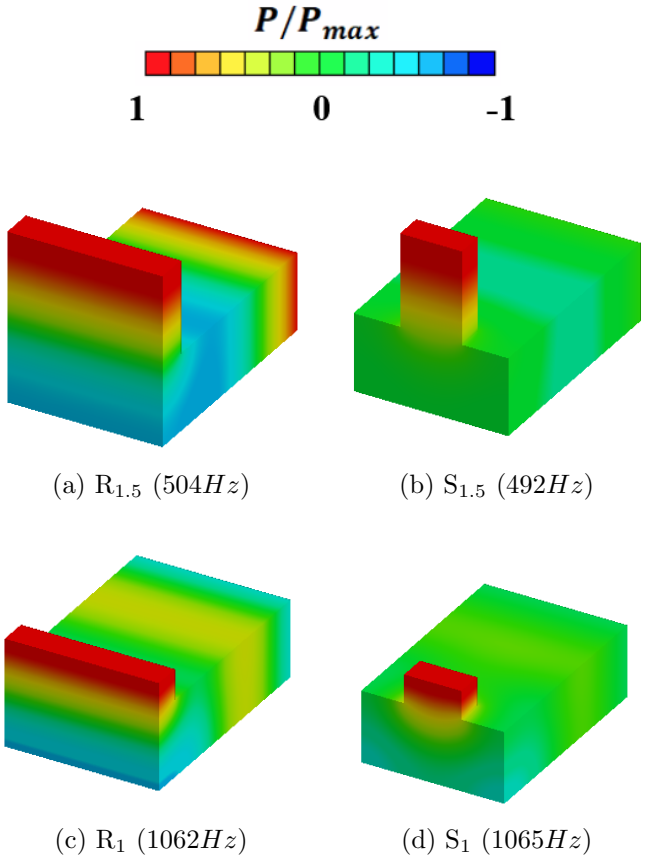

(a) $R_{1.5}$ ($504Hz$) (b) $S_{1.5}$ ($492Hz$)

(c) R_1 ($1062Hz$) (d) S_1 ($1065Hz$)

Figure 4.1: Dimensionless acoustic pressure distribution from numerical model for the $R_{h/L}$ cavities a), c), and the $S_{h/L}$ cavities b), d).

behaviour similar to the cylindrical cavities with matching aspect ratios and admission ratios, though the acoustic pressure generated is much higher for cylindrical cavities.

4.2 Aeroacoustics Response

4.2.1 Deep Cavities

In this section, the $R_{h/L}$ and $S_{h/L}$ cavities are experimentally investigated for the same range of flow velocities studied in Sec.3.4.1. As mentioned, both cavity geometries in this chapter consist of the same impingement length and depth as the $O_{1.5}$ and

$O_{0.5}$ cavities, hence $L = D$. The aeroacoustics response for both deeper cases are presented in Fig. 4.2. The $R_{1.5}$ cavity, shown in Fig. 4.2a, reveals intriguing behaviour for the lock-in frequencies excited by m_1. The first hydrodynamic mode generates a sustained oscillation at $\sim 390\ Hz$ for a range of flow velocities. This frequency falls below the numerically obtained cut-on frequency of 504 Hz and resembles a similar "stepwise" increase in the lock-in frequencies prior to resonance excitation [97]. The cause of this step-like increase for the frequencies in their investigation was attributed to the reflection imposed by the confinement of the cavity. Similarly, this premature excitation has also been noted to occur due to the acoustic reflection caused by the duct walls in the nearby vicinity of the cavity [103]. In fact, the frequency spectrum for the cylindrical cases studied show a resemblance where the resonance is not initiated immediately but rather gradually, creating steps in the frequency response. The quality of the resonance lock-in and acoustic amplitude is thus greatly affected by the shape of the cavity.

The frequency in Fig. 4.2a suddenly switches to the resonance frequency, in good agreement with the numerical value. For this cavity case in particular, however, the acoustic amplitude is not amplified despite a sustained oscillation at the predicted acoustic mode. This is a consequence of the higher order acoustic mode being excited by the second hydrodynamic mode m_2. This feature, which is only witnessed in this specific cavity case, suggests an interesting characteristic where the second hydrodynamic mode has enough energy to provoke the excitation of the higher order acoustic resonance mode. This is attributed to the fact that two-dimensional cavities present a far more uniform shear layer in spanwise direction in comparison to the cylindrical and square shapes. In addition, this cavity case provides favourable dimensions to excite a higher acoustic mode, and as a result, two potential lock-in ranges are observed. Subsequently, the switching between the two acoustic modes causes a de-

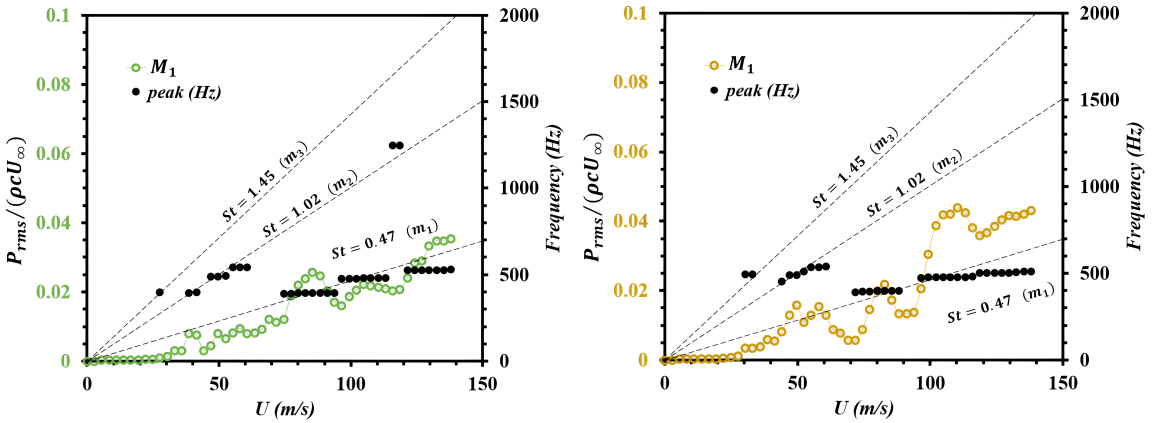

(a) $R_{1.5}$ (b) $S_{1.5}$

Figure 4.2: Normalized acoustic pressure $P_{rms}/(\rho c U_\infty)$ as a function of the mean flow U_∞ of the $R_{1.5}$ and $S_{1.5}$ cavities. The diagonal lines represent the global Strouhal numbers of the shear layer modes.

structive interference, explaining the reduced acoustic pressure at this range of flow velocities. The $S_{1.5}$ cavity shown in Fig. 4.2b demonstrates a similar response to its cylindrical counterpart, where the frequency of the acoustic mode appears synonymous to the $1/4\lambda$ acoustic mode, and is duly modelled by the numerical simulation as presented in Fig. 4.1b. The reduction in the acoustic pressure, however, is attributed to the square shape of the cavity, which is less favourable than the cylindrical cavity in exciting such modes.

4.2.2 Shallow Cavities

The $R_{0.5}$ and $S_{0.5}$ cavities are shown in Fig. 4.3. Unlike the shallow cylindrical cavities, the low velocity dependent tones are not present in these shallow cases. As expected, the hydrodynamic modes of the shear layer do not exhibit significant deviations from their deeper counterpart, and thus remain a function of the cavity impingement length. Furthermore, the anticipated $1/2\lambda$ acoustic mode for the $R_{0.5}$ cavity is materialized as it is excited by m_2, justifying the relatively weak and broad-

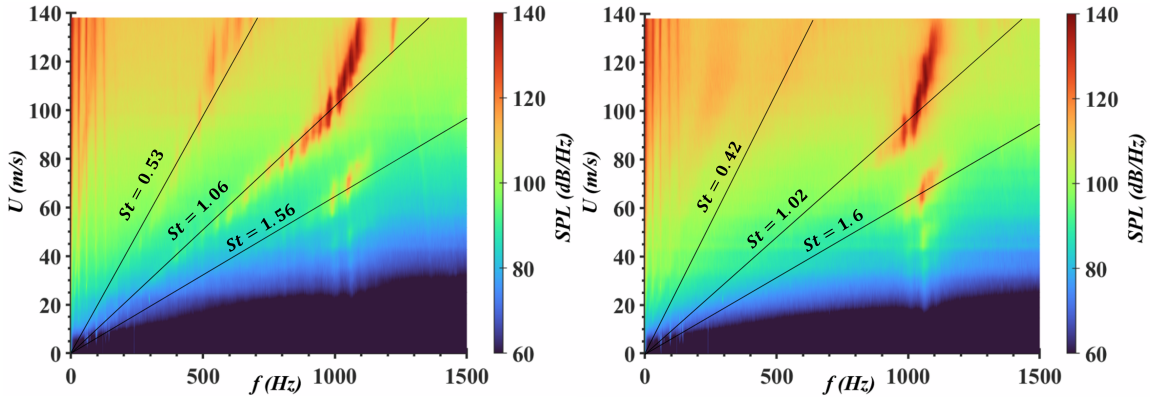

(a) $R_{0.5}$ (b) $S_{0.5}$

Figure 4.3: The Sound Pressure Level as a function of the mean flow U_∞ of the $R_{0.5}$ and $S_{0.5}$ cavities. The diagonal lines represent the global Strouhal numbers for the shear layer modes.

band lock-in range. In spite of this, the $S_{0.5}$ cavity in Fig. 4.3b presents hydrodynamic modes at the same values as its deeper cavity, however, broadband low velocity dependent tones seem to also emerge at $St \sim 0.24$, similar to the shallow cylindrical cavities. The presence of this lower shear layer mode for the $S_{0.5}$ cavity is a result of sharing the same aspect and admission ratio as the $O_{0.5}$ cavity. From a geometrical perspective, the $O_{0.5}$ and $S_{0.5}$ cavities consist of the same cavity depth, length, and width. The only distinction is the shape of the cavity opening. The presence of this lower order hydrodynamic mode in both, the shallow cylindrical and square cavities, indicates a resemblance in the flow dynamics and acoustic behaviour of the two cavities due to the maintained geometric parameters. This proposition is substantiated by the absence of such tones in the shallow two-dimensional rectangular cavity shown in Fig. 4.3a, where the progression of the shear layer oscillations are relatively unaffected by the reduction in cavity depth and should not exhibit three-dimensional flow characteristics. Therefore, the finite width relative to the duct width induces changes in the flow pattern, but it is not as severe as that seen for shallow cylindrical cavities.

4.3 Strouhal Periodicity

The Strouhal numbers, discussed thus far, represent the global Strouhal numbers, as they represent the linear progression of f_s with increasing flow velocity, in absence of acoustic resonance excitation. As such, detecting the progression of this frequency must be done before resonance excitation, typically below 30 m/s. For the measurements within this velocity range, the frequency of the shear layer oscillations for the detectable hydrodynamic modes are obtained and used to compute their Strouhal numbers. This is repeated for all measured flow velocities within this range. The Strouhal numbers obtained from each measurement below 30 m/s are then averaged accordingly with their hydrodynamic modes to yield estimated values for the global Strouhal numbers. These values can be seen in Fig. 4.4 which are plotted as a function of the aspect ratio. Fig. 4.4 provides a summary for the global Strouhal numbers of all the cavities studied in this investigation. The Strouhal numbers in Fig. 4.4 are not affected by the resonance characteristics of the cavity as they are obtained before resonance excitation, and are thus only a function of the cavities' aspect ratio and free-stream flow velocity. The $O_{1.5}$ cavity shows a slight but discernible increase in St when reducing the depth to an aspect ratio of 1. Whereas, a further reduction in cavity depth to an aspect ratio of 0.5 causes a significant deviation in the velocity dependent tones. The same trend can be seen for the $Ø_{h/L}$ cavities, though the Strouhal numbers for the larger admission ratio are shifted to slightly higher values. Since the $O_{h/L}$ and $Ø_{h/L}$ cavities share the same aspect ratio, the slight deviation in the Strouhal numbers for the $Ø_{h/L}$ cavities is attributed to the larger diameter and its relation to the duct width. In addition, the presence of a confinement causes the sound generation by the shear layer to be reflected [103]. This reflection promotes the shear layer oscillations at lower Mach numbers, effectively increasing the Strouhal

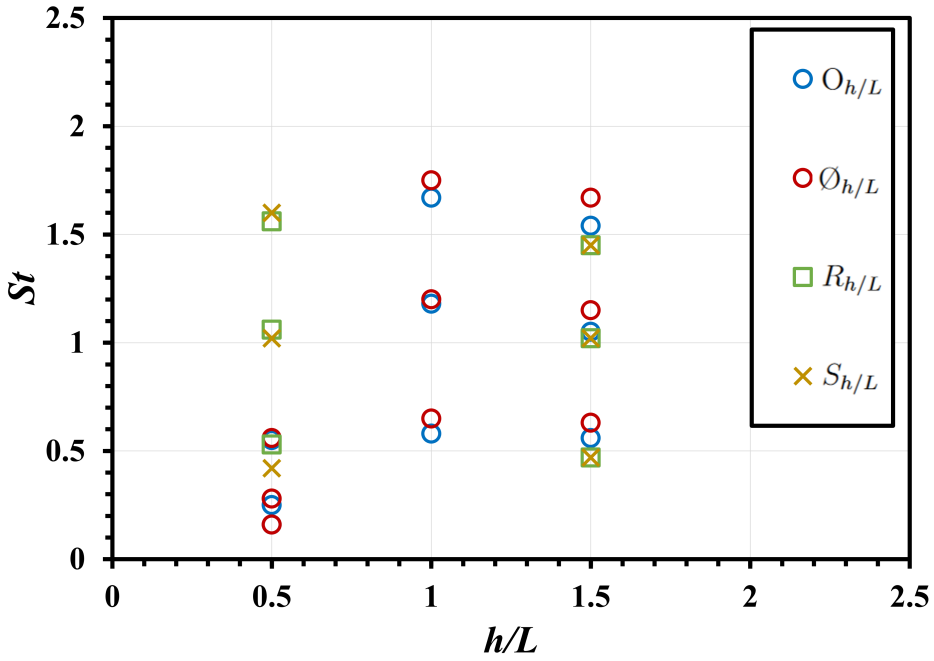

Figure 4.4: Experimentally obtained global Strouhal numbers, St, obtained before resonance excitation as a function of the cavity aspect ratio.

number. Though the $Ø_{h/L}$ cavities are still confined, their larger diameter relative to $O_{h/L}$ influences the sound radiation from the cavity, and hence the reflection from the surrounding boundaries. The substantial deviation in Strouhal numbers, observed for shallow cylindrical cavities, is attributed to the change in flow dynamics reported for this geometry. The $R_{h/L}$ and $S_{h/L}$ cavities appear to be much less affected by the aspect ratio, with exception to the $S_{0.5}$. This case particularly revealed similar attributes to both, the two-dimensional rectangular cavities and the cylindrical cavities. As seen in Fig. 4.3b for the $S_{0.5}$ cavity, three hydrodynamic modes are present in the response around the typical Strouhal numbers of 0.5, 1, and 1.5, thus resembling the hydrodynamic behaviour of two-dimensional rectangular cavities. However, a lower order hydrodynamic mode emerges, similar to the lower order mode observed in the shallow cylindrical cavities. This resemblance suggests that the maintained geometric parameters amongst the $S_{h/L}$ and $O_{h/L}$ cavities, induces similarities in the flow dy-

namics as well as the aeroacoustics response, despite having different cavity-shaped mouths. A second definition for the Strouhal number, St_{peak}, is used and represents the Strouhal numbers during resonance excitation. The peak Strouhal numbers are calculated similarly to the global Strouhal numbers, but using the frequency during peak resonance excitation. The resonance frequency dominates the spectrum, obscuring the frequency of the shear layer oscillations. From the Strouhal relationship, it is evident that since the dominant frequency during resonance lock-in is no longer increasing with increasing flow velocity, the Strouhal numbers will drop, which effectively represents the lock-in range. As this behaviour differs from the definition of the global Strouhal numbers, the peak Strouhal numbers are presented and briefly discussed for the resonance range. Fig. 4.5 depicts the relationship between the Strouhal numbers at peak frequencies, St_{peak}, the Mach number, M, and the normalized acoustic pressure at the corresponding peak Strouhal numbers. With regard to St_{peak} for the given range of Mach numbers, the experimental data evidently segregates into two groups, where the cavities with $h/L = 1$ initiate the excitation at higher Mach numbers. This was outlined in Fig. 3.3, where the excitation at higher Mach numbers were attributed to the increase in the acoustic cut-on frequency by reducing the cavity depth. The remaining cavities, however, share the same aspect ratio and similar acoustic cut-on frequency. Therefore, any change in cavity length affecting the shear layer oscillations is accompanied by a change in cavity depth affecting the resonance frequency, effectively maintaining the onset flow velocity. The normalized pressure at the peak Strouhal numbers clearly shows the strength of the resonance for each case. All cavities of aspect ratio 1.5, excited resonance near the cut-on frequency, yet the resonance is noticeably stronger for the cylindrical cases since this geometry greatly promotes the excitation of a trapped acoustic mode. Additionally, the $O_{1.5}$ cavity produces the highest levels of acoustic pressure, as the smaller diameter would

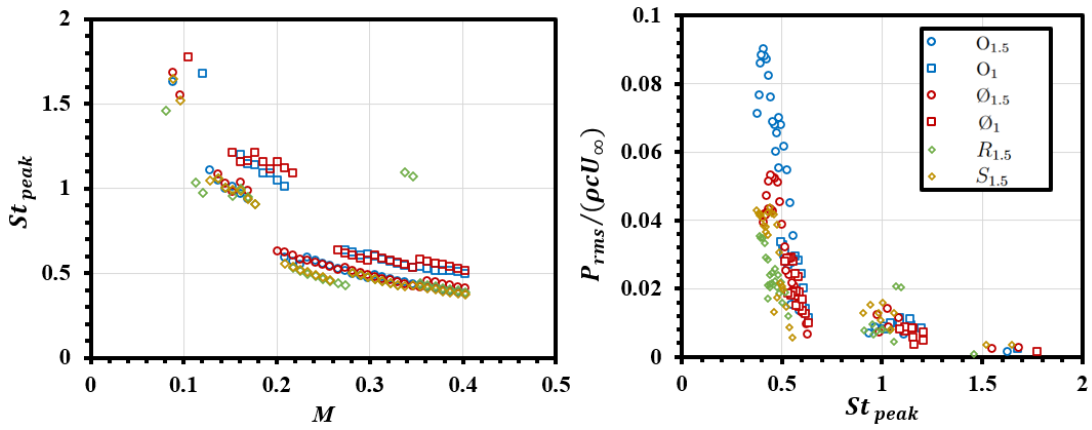

Figure 4.5: The peak Strouhal numbers, St_{peak}, as a function of the Mach number (left) and the normalized acoustic pressure at corresponding peak Strouhal numbers (right) during resonance excitation.

limit the acoustic radiation to the duct in comparison to a larger cavity diameter of $Ø_{1.5}$. Furthermore, the values of St_{peak} corresponding to the strongest level of acoustic pressure, seem to collapse well at a value of ~ 0.44 for all cavities of aspect ratio 1.5. The cavities with an aspect ratio of 1 present maximum amplitudes at slightly higher Strouhal numbers than the deeper cavities. Although Nakiboğlu et al. [64] examined the aeroacoustic power generated for axisymmetric cavities, a similar trend regarding the peak Strouhal numbers for various cavity depths was reported. For their investigated range of $0.2 \leq h/L \leq 1.175$, reducing the cavity depth, decreases the peak Strouhal numbers. However, in their investigation, the peak Strouhal numbers remain relatively independent for aspect ratios larger than 0.675, with exception to subtle discrepancies. This is a similar trend to that seen in Fig. 4.5 where the reduced depths for the aspect ratios of 1, resulted in a slight shift to higher peak Strouhal numbers. However, this shift is negligible, and the values are therefore independent of the cavity depth. Their experimental and numerical results also described a linear relation between the reduction in cavity depths and peak Strouhal numbers for aspect ratios less than 0.675, exemplifying the clear dependency of the aspect

ratio on the onset of resonance excitation for shallow cavities. The observed linear relationship was described as a reduction in the convection speed of the vortex at the mouth of the cavity by virtue of the image vortex present at the floor of the cavity. This explanation considers strong effects due to the cavity floor in proximity of the mouth, such that increasing the depth minimizes the effects of the floor, explaining the relatively independent values obtained for all the cases presented in Fig. 4.5. A significant reduction in the global Strouhal numbers for the shallow cylindrical cavities studied also appear to be due to a strong dependence on the aspect ratio, as seen in Fig. 4.4. Though, the values reported by Nakiboğlu et al. [64] for shallow cavities do not decrease as much as those studied here, and are performed on a different cavity configuration, the proposition of an interaction with the cavity floor that causes a reduction in vortex convection speed is a viable suggestion. This would agree well with the asymmetry reported for cylindrical cavities with an aspect ratio of 0.5, where a substantial change in the flow behaviour could greatly affect the aerodynamic noise generated from shallow cavities. Further detail regarding the flow topology of the shear layer will be discussed in the following chapter as to compliment the aeroacoustics response measurements.

4.4 Chapter Summary

The results put forward in this section present the aeroacoustics response of the two-dimensional rectangular and square cavities. The resonance excitation for the $R_{1.5}$ cavity exhibits a standing acoustic mode shape as anticipated, however, the frequency is much lower than the theoretically calculated value, as the standing acoustic wave for this aspect ratio is a function of the cavity depth and duct height, as opposed to the mean height proposed in literature. Both $R_{h/L}$ cavities demonstrated the largest

amounts of reflection from the duct, depicting standing acoustic waves consisting of the entire cavity depth and duct height rather than an acoustic mode trapped exclusively in the duct. The presence of acoustic mode switching occurred between the fundamental and higher order acoustic modes for the $R_{1.5}$ cavity, by virtue of the first and second hydrodynamic modes. The second hydrodynamic mode in this case contains sufficient energy to excite a higher order acoustic mode, resulting in a destructive interference between the two acoustic modes, where neither frequency is adequately sustained. The $S_{h/L}$ cavities, however, presented similar acoustic behaviour to the cylindrical $O_{h/L}$ cavities with the same non-dimensional geometric parameters, where the acoustic mode is trapped within the cavity. This is credited to the fact that the $O_{h/L}$ and $S_{h/L}$ cavities share the same aspect and admission ratio, though the normalized acoustic pressure for the $S_{1.5}$ is far lower than the cylindrical counter-part, due to the unfavourable square shape in comparison to the cylindrical case. Moreover, the $R_{0.5}$ cavity demonstrates hydrodynamic modes near the typical values and is negligibly affected by the aspect ratio. The $S_{0.5}$ cavity also yields a similar behaviour, with the exception of a weak broadband, lower order hydrodynamic mode. The emergence of this hydrodynamic mode resembles those seen in shallow cylindrical cavities, suggesting that the maintained aspect and admission ratio amongst the $S_{0.5}$ and $O_{0.5}$ cavities induce similar flow dynamics, and hence, mutual characteristics in the aeroacoustics response. A detailed look at the peak Strouhal numbers summarizes the effect of the Mach number, geometric parameters, and normalized acoustic pressure for each case, agreeing well with reported trends in literature.

Chapter 5

Flow Visualization

5.1 PIV Results

This section focuses on the shear layer topology for the cavities presented in Fig. 2.6, as to complement the aeroacoustics response with flow visualizations at select free-stream velocities. The measurements are conducted for a range of flow velocities, where average flow profiles are shown for off-resonance conditions, and phased-locked imagery is used during acoustic resonance. The laser sheet is parallel to the cavity plane, and is located 10.7 mm away, as shown in Fig. 2.7. This is referred to as location y_1, such that y_2 and y_3 refer to 12.7 and 14.7 mm, respectively. Many thorough investigations such as Yamouni et al. [101] have conducted analysis on rectangular cavities while assuming two-dimensional flow over the cavity mouth. Numerical investigations such as Sun et al. [92] explored the flow dynamics over the width of such cavities, further proving the relative two-dimensionality of the shear layer. In view of this, the measurements are first presented for the deep and shallow, two-dimensional rectangular cavity, as this is understood to exhibit highly coherent vortex formation with relatively weak three-dimensional effects in the spanwise direction. However,

both aforementioned studies consisted of numerical studies on shallow cavities, while the following are direct experimental results regarding measurement planes and cavities not yet explored.

5.1.1 Two-Dimensional Rectangular Cavities

Fig. 5.1 illustrates phase-locked PIV measurements for the $R_{1.5}$ cavity at $U_\infty = 81\ m/s$, where the flow cycle is shown at four evenly spaced phases. The contour plots represent the phase-averaged normalized velocity fluctuations in the streamwise direction, $\frac{\langle u \rangle}{U_\infty}$. This selected flow velocity is near the onset of excitation, where the acoustic tone of the cavity depth mode begins to amplify. Resultantly, the acoustic amplification begins to modulate the shear layer into a coherent vortex. This flow velocity is associated with the first hydrodynamic mode, hence the presence of only one vortex core in the flow cycle. The flow structure at this velocity already exhibits a strong spanwise coherence early in the lock-in range, despite the weak resonance amplitude, which delineates the influence of the acoustic field on the flow patterns of the shear layer. At the beginning of the flow cycle, the shear layer rolls into the cavity, and the near-wake region is formed at the upstream edge. The vortex core proceeds to roll up as it moves towards the downstream edge. As the core rolls up, the intensity of the velocity fluctuations near the centre of the core are observed passing through the laser sheet before being severed at the impingement edge. A portion of the vortex is swept into the cavity, thereby amplifying the recirculation zone. These set of events in the flow cycle can be related to the formulation proposed by Howe [46, 47], which describes the instantaneous acoustic power generated by a compact vortex in a fluid volume, V, and can be expressed as shown in Eq. 5.1.

$$\Pi = -\rho \int_V \langle (\vec{\omega} \times \vec{u}) \cdot \vec{v} \rangle \, dV \tag{5.1}$$

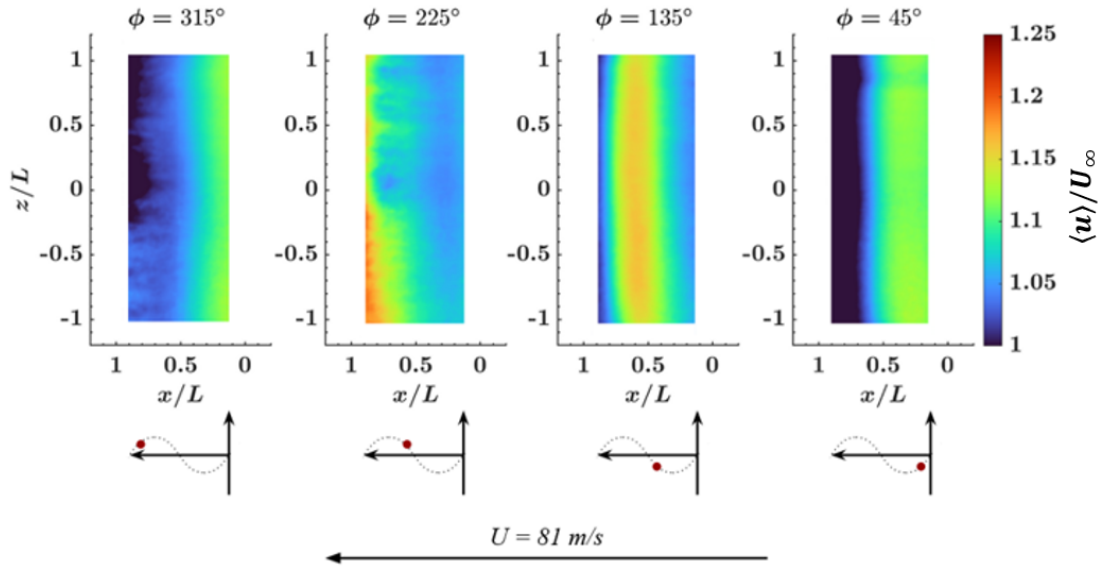

Figure 5.1: The normalized phase-averaged streamwise velocity contours at 81 m/s for the $R_{1.5}$ cavity. The results are obtained from phase-locked measurements with the acoustic pressure cycle.

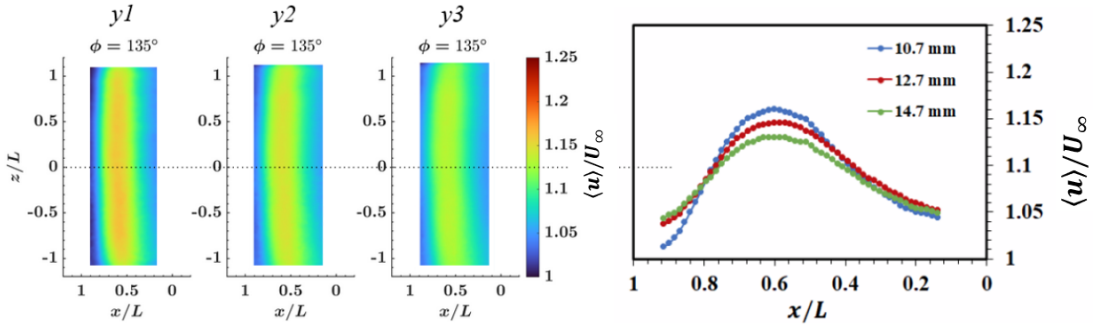

Figure 5.2: The normalized phase-averaged streamwise velocity contours of the $\phi = 135°$ phase mark in the flow cycle at different measurement planes (y_1, y_2, y_3). The results reflect the case shown in Fig. 5.1.

In the above expression, ρ represents the fluid density, ω is the vorticity field, u is the flow velocity field, and v represents the acoustic particle velocity. From this expression, the energy is transferred from the flow field to the acoustic field by virtue of the Magnus force $\rho(\vec{\omega} \times \vec{u})$ [8]. The resonance is self-sustained if the integral in Eq. 5.1 is positive over an acoustic cycle. Considering the phase-averaged measurements in Fig. 5.1, the shear layer first rolls into the cavity at the leading edge, which

is proportional to the motion of the acoustic particle velocity. As the shear layer rolls back up towards the downstream edge, the acoustic particle velocity vector would be in the opposite direction [102]. The development of the vortex core thereby signifies the production of acoustic power over an acoustic pressure cycle. A slight but discernible curvature is also notable at the extremities of the vortex core, which is a product of the viscous forces near the side walls of the cavity-duct configuration. Fig. 5.2 directs the attention to the $\phi = 135°$ mark in the flow cycle. The velocity fluctuations are shown for y_1, y_2, and y_3, respectively. One will notice the decrease in the velocity fluctuations as the laser sheet is moved away from the cavity mouth by a distance of $0.04L$. The figure in the right, plots the velocity fluctuation across the stream-wise opening of the cavity, where the data points are extracted at the centre of the cavity at $z/L = 0$. The normalized velocity fluctuations of at each laser sheet location is plotted, showing a peak fluctuation centred around $x/L = 0.6$ for all three laser sheets. Additionally, the velocity fluctuations in this case decrease linearly with increasing distance from the cavity mouth.

Fig. 5.3 portrays the flows cycle at $U_\infty = 130\ m/s$ during the strongest occurrence of acoustic resonance for this cavity case. The flow pattern at this velocity depicts a similar set of events as $U_\infty = 81\ m/s$, however, a few key differences can be emphasized. More notably, the curvature of the vortex near the walls seems to be less apparent as the flow velocity is increased, and the acoustic pressure generated is strongest. Furthermore, the vortex core appears to be shifted according to the acoustic pressure cycle. This is evident in Fig. 5.4 where at the specific instance of $\phi = 135°$, the intense velocity fluctuations from the vortex core are slightly further downstream compared to the same instance in the flow at $U_\infty = 81\ m/s$. At this high flow velocity, the flow-acoustic coupling is the strongest, further enhancing the flow modulation process of the shear layer. The velocity trace at $z = 0$ shows much

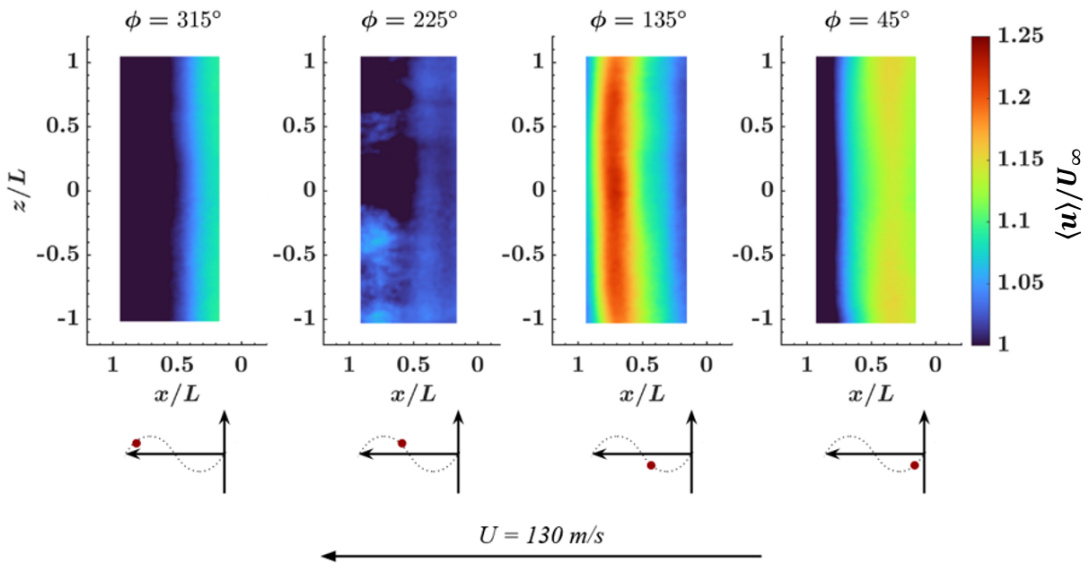

Figure 5.3: The normalized phase-averaged streamwise velocity contours at 130 m/s for the $R_{1.5}$ cavity. The results are obtained from phase-locked measurements with the acoustic pressure cycle.

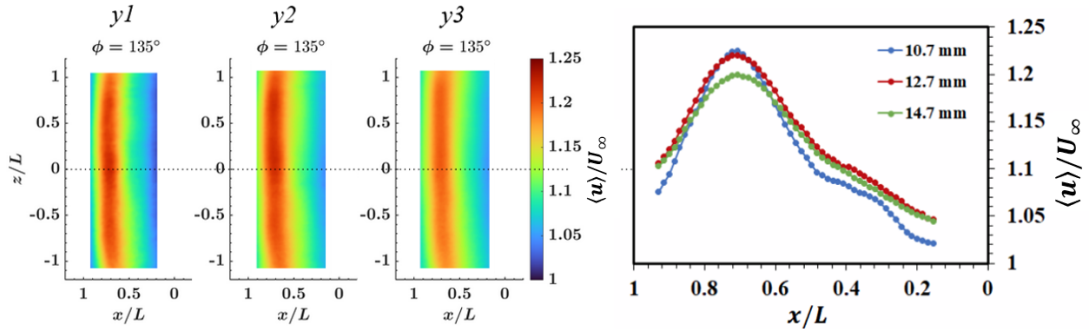

Figure 5.4: The normalized phase-averaged streamwise velocity contours of the $\phi = 135°$ phase mark in the flow cycle at different measurement planes (y_1, y_2, y_3). The results reflect the case shown in Fig. 5.3.

larger amplitudes in the velocity fluctuations centred around $x/L = 0.75$, which is further downstream than that seen at $U_\infty = 81\ m/s$. Evidently, as the flow velocity increases, such that acoustic pressure becomes stronger during the lock-in range, the shear layer thereby also oscillates at maximum amplitudes and are further organized due to the enhanced modulation introduced by the resonance amplitude. This strong coupling, as well as the high flow-velocity, renders the lower curvature near the walls

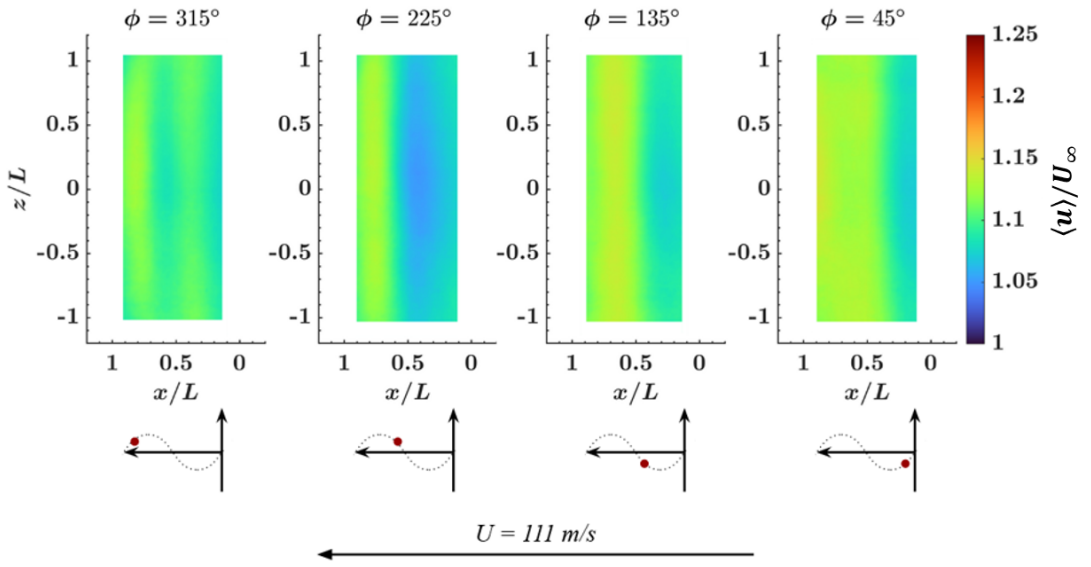

Figure 5.5: The normalized phase-averaged streamwise velocity contours at 111 m/s for the $R_{1.5}$ cavity. The results are obtained from phase-locked measurements with the acoustic pressure cycle, using laser plane y_3.

and enhances the overall spanwise coherence of the vortex core. Fig. 5.5 illustrates the flow cycle at $U_\infty = 111$ m/s, which was associated with a peculiar mode switch in the aeroacoustics response. At this flow velocity, the fundamental acoustic mode of the cavity was excited by the first hydrodynamic mode, while the higher order acoustic depth mode was intermittently excited by the second hydrodynamic mode. This caused a randomized mode switching between the two acoustic modes, resulting in an destructive interference where both resonance modes are moderately excited. Fig. 5.5 demonstrates the existence of the two vortex cores in the shear layer by account of the second hydrodynamic mode. However, in other stages of the flow cycle, the cores seem to merge, causing an uneven spacing to the formation of the following vortex core. Nevertheless, it is still unclear whether the two vortex cores originate from the same instance of flow separation, then split into two cores. Consequently, the flow cycle shown in Fig. 5.5 is presented for the laser location, y_3 since closer laser sheet planes proved challenging in distinguishing the existence of the second hy-

drodynamic mode. Fig. 5.6 outlines the flow cycle for the shallow $R_{0.5}$ cavity at U_∞ = 114 m/s. This cavity case exhibits moderate amplitudes at the $1/2\lambda$ cross mode of the cavity-duct configuration, excited by the second hydrodynamic mode. The presence of two, evenly spaced, vortex cores are apparent in this case. Despite this, the spanwise coherence of the vortex core seems to fall off significantly. The velocity pattern shows a more uneven distribution of the velocity fluctuations. This can be attributed to the lack of acoustic resonance in this cavity case. The cut-on frequency of the cavity-duct configuration is only excited by the second hydrodynamic mode, generating moderate broad-band amplitudes. This lack of resonance excitation hinders the modulation process of the shear layer, therefore resulting in a more random spanwise flow profile. The incoming boundary layer is thus more sensitive to any perturbations that can potentially be introduced upstream of the cavity.

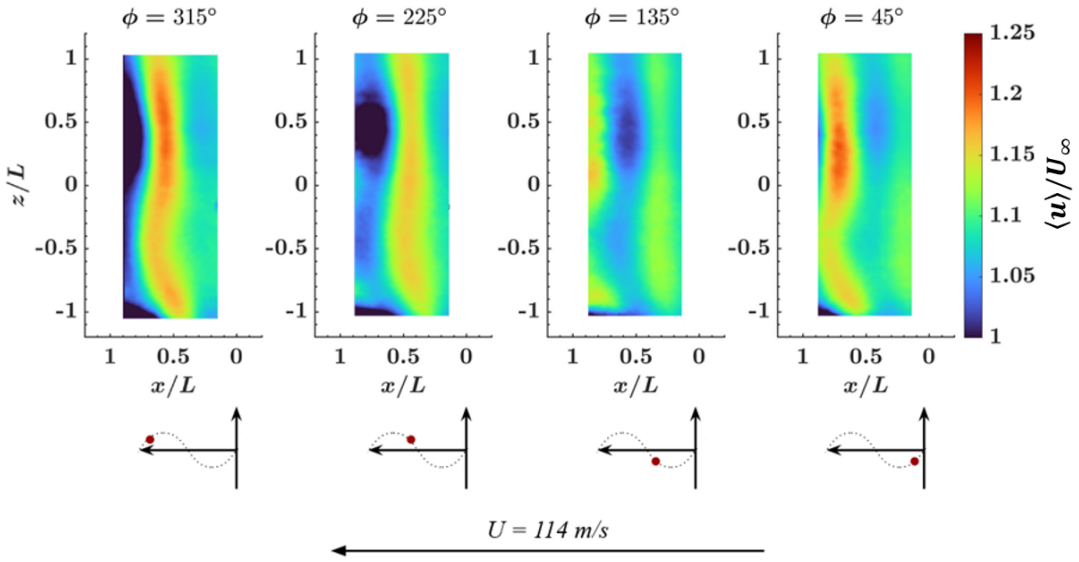

Figure 5.6: The normalized phase-averaged streamwise velocity contours at 114 m/s for the $R_{0.5}$ cavity.

5.1.2 Cylindrical Cavities

Fig. 5.7 presents the phase-locked measurements for the cylindrical cavity, $O_{1.5}$. The figure demonstrates four phases in the flow cycle for three flow velocities, where each flow velocity illustrates a different hydrodynamic mode. At $U_\infty = 31\ m/s$, the third hydrodynamic mode is depicted in the shear layer. In this flow cycle, three vortices are seen travelling over the cavity opening, which is more apparent at later instances in the flow cycle. This particular flow velocity is synonymous to the spectral data shown in Fig. 3.7b, where a significant deviation in the sound pressure level is observed for microphone $M_{\theta 2}$, at the centre of the downstream edge, in comparison to the other two microphones. All the flow velocities in this cylindrical case present a symmetrical, three-dimensional flow profile, seen as a crescent-like curvature in the spanwise direction, though the characteristics of the curvature change with increasing resonance amplitudes. The general profile of the curvature agrees well with static pressure contours reported in literature, which is attributed to the three-dimensional recirculation zone concentrated along the centre stream-wise direction at $z/L = 0$. This suggests that the matching frequencies seen in Fig. 3.7 and 3.9 are due to an almost simultaneous impingement for this localized region of the downstream edge. Despite the matching frequencies, the discrepancy in amplitudes observed in Fig. 3.7 for $h/L = 1.5$ proposes that the recirculation zone in the cavity is larger for the deeper case, thus the shear layer impingement profile on the downstream edge would be affected by this recirculation. As a result, lower amplitudes of dynamic pressure are measured at the centre of the downstream edge. Unlike the two-dimensional rectangular cavity, the shear layer does not necessarily roll as far into the cavity, but rather forward, due to the delayed separation occurring symmetrically along the cavity edge, retaining the initial separation. This effectively causes localized velocity fluctuations near the centre of the vortex at $z/L = 0$, generating the three-dimensional recirculation region

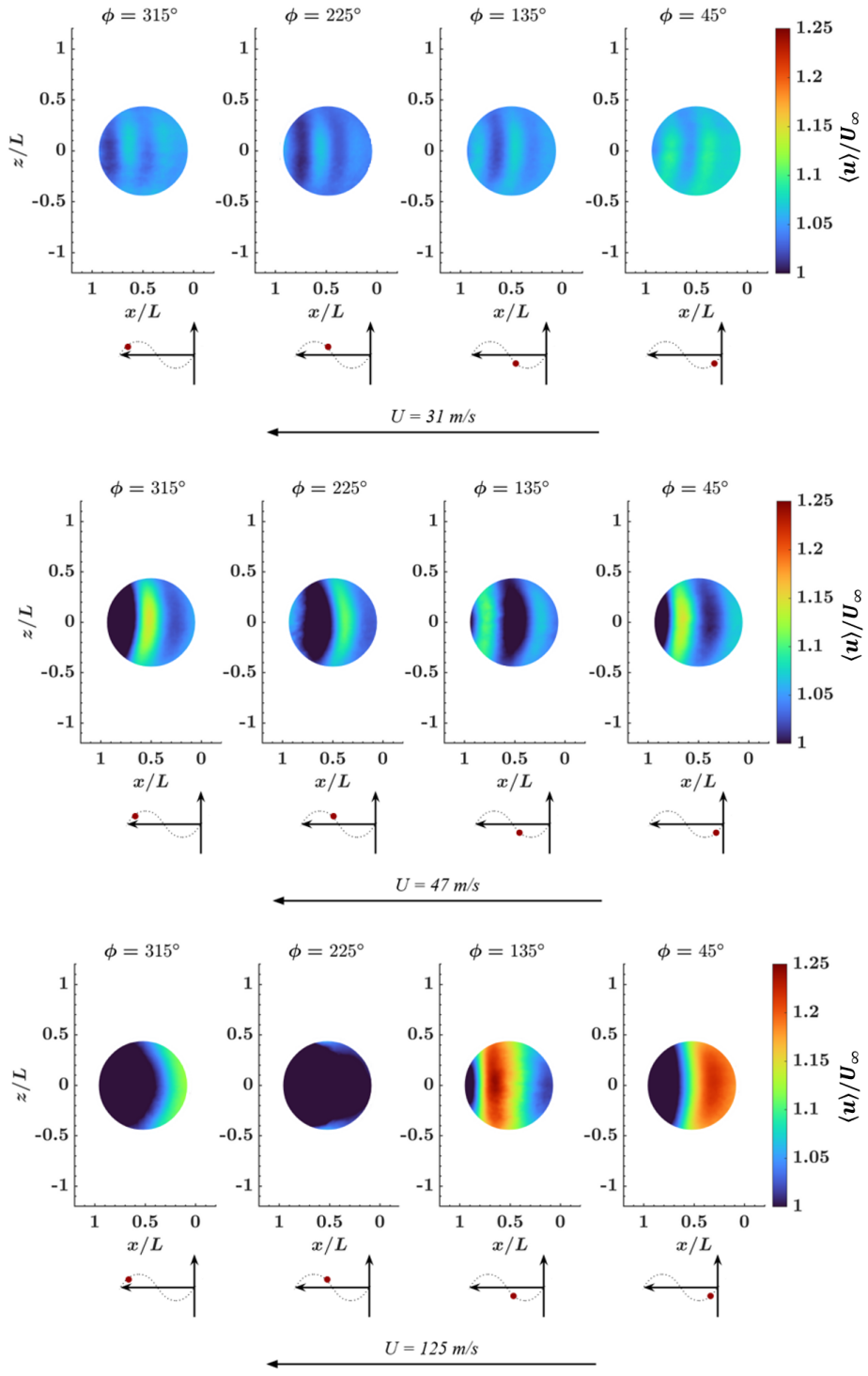

Figure 5.7: The normalized phase-averaged streamwise velocity contours at a) 31 m/s, b) 47 m/s, and c) 125 m/s for the $O_{1.5}$ cavity.

in the cavity. The vortex then travels forward towards the downstream edge. For the low flow velocities, as the vortices move downstream, the curvature remains relatively consistent. However, at $U_\infty = 125\ m/s$, the modulation from the acoustic resonance organizes the first hydrodynamic mode, increasing the velocity fluctuations at $z/L = 0$ as to overcome the curvature. Another interesting aspect to note is that the shear layer oscillations occur in the mixing region between the cavity volume and the mean flow in the duct. Therefore, during the flow cycle a portion of the shear layer is still present in the cavity and convected downstream, hence, it must be subject to a change in velocity due to the cylindrical walls of the cavity. The lower portion of the shear layer which manages to travel upwards to escape the cavity is accelerating due to the reduction in cavity size, which would further explain the three-dimensionality of shear flows over cylindrical cavities. Fig. 5.8 depicts the normalized time-averaged velocity fluctuations in the streamwise direction, $\bar{u}/U_\infty$, for the $O_{0.5}$ cavity. The average flow characteristics are presented due to the lack of acoustic resonance for this cavity case. The average contour plots evidently demonstrate the asymmetry in the flow with respect to the stream-wise direction. Since the early studies of Hiwada et al. [45], it has been well established that cylindrical cavities with $h/L = 0.5$ exhibit stable, asymmetric flow. The asymmetry is the highest at this aspect ratio, hence, the increased cavity drag. The direction of the stable asymmetry can also switch to the opposite side, where the orientation selection is random and can be changed by introducing upstream flow perturbations. The asymmetry reported for this aspect ratio is caused by interference of the recirculation zone, typically unaffected in deeper aspect ratios. Reducing the cavity depth for the same diameter would in essence alter the shape of the recirculation zone in the cavity. This would induce significant velocity fluctuations in the spanwise direction, thereby increasing the three-dimensionality of the recirculation zone. The direction of this three-dimensionality is random, yet

stable. The average flow seems to travel asymmetrically across the cavity towards z/L = -0.5, while recirculating a diagonal vortex cone beneath the shear layer, where the centre of the core escapes the cavity towards $z/L = 0.5$. The asymmetry of the recirculation zone is thus relative to both, the streamwise direction and the spanwise plane of the cavity opening. This proposition resembles the vortex tube suggested by Dybenko and Savory [26]. It is interesting to note that no change in flow orientation or flow profile is observed when comparing $U_\infty = 31\ m/s$ and $105\ m/s$, with exception to a steeper velocity gradient.

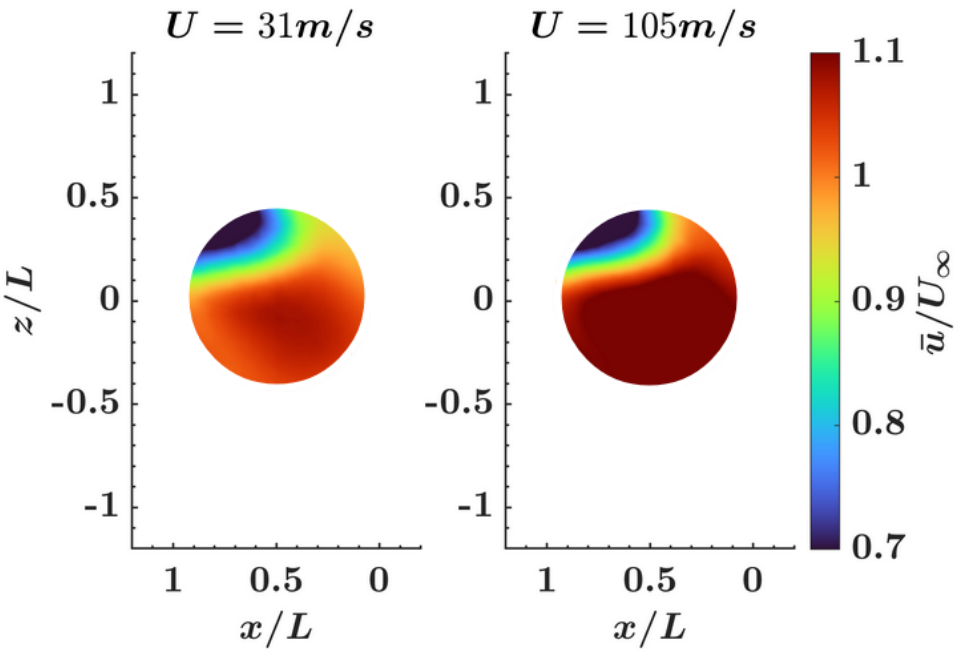

Figure 5.8: The normalized time-averaged streamwise velocity contours at 31 m/s and 105 m/s for the $O_{0.5}$ cavity.

5.1.3 Square Cavities

Fig. 5.9 presents the $S_{1.5}$ cavity. For this cavity case, a premature excitation of the acoustic depth mode materializes at $U_\infty = 81\ m/s$, similar to the cylindrical cavity with the same aspect ratio. This cavity case in particular exhibits similarities to

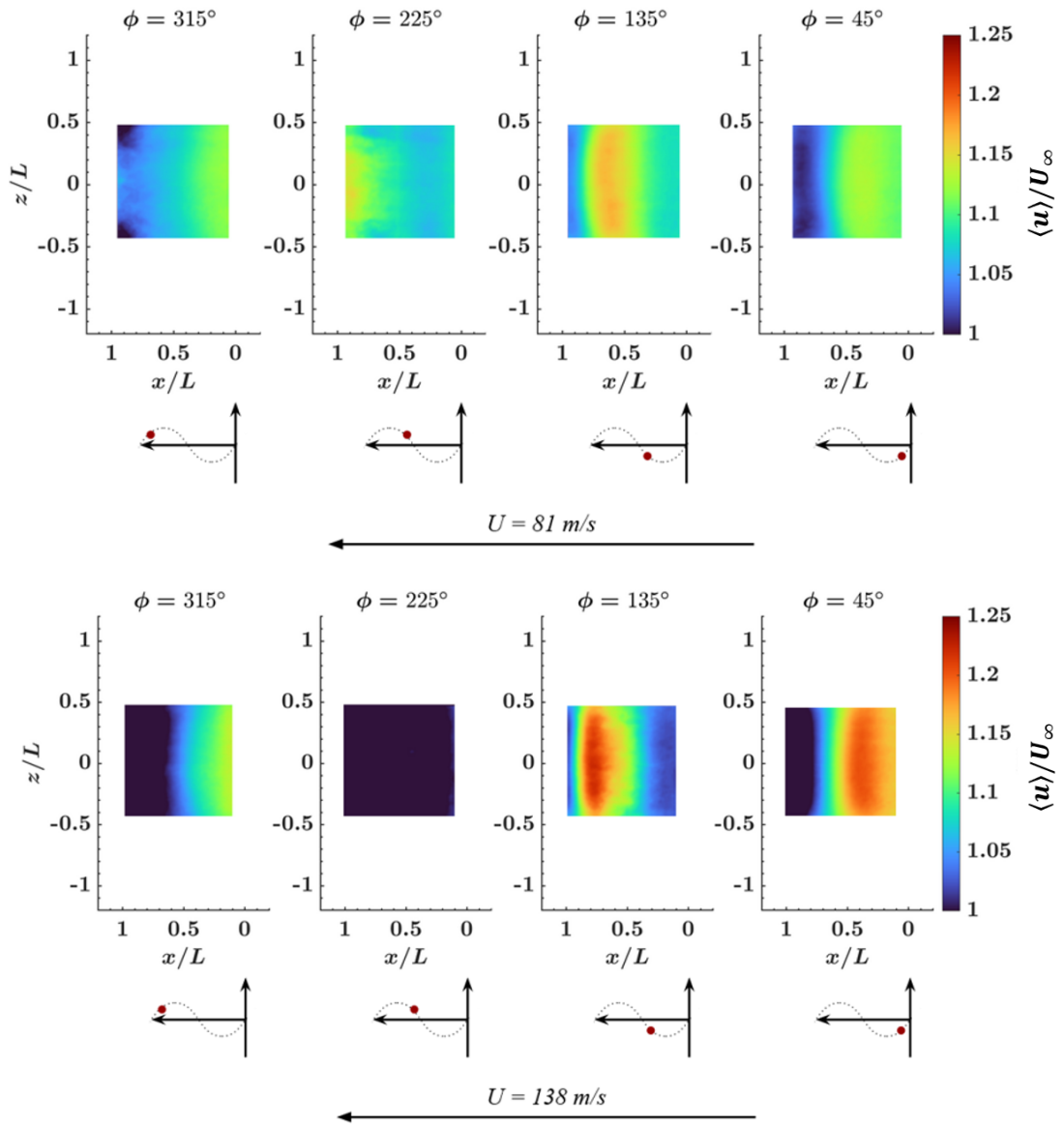

Figure 5.9: The normalized phase-averaged streamwise velocity contours at a) 81 m/s and b) 138 m/s for the $S_{1.5}$ cavity.

both the two-dimensional and the cylindrical cavities. The shear layer for the first hydrodynamic mode rolls into the cavity and is swept up towards the downstream edge, analogous to the $R_{1.5}$ cavity. As the vortex impinges, however, the wake of the vortex reveals a slight quasi two-dimensional pattern due to the finite spanwise length of the cavity downstream edge. At a higher flow velocity, the shear layer

is further modulated by the resonance, generating a more concentrated vortex with a strong spanwise coherence. However, the quasi two-dimensional pattern in the vortex wake is more apparent. Moreover, the influence of the high flow velocity and strong acoustic modulation promotes the shedding of discrete vortices, as opposed to the weaker resonance range at a lower flow velocity, where the upstream shear layer appears more continuous. Fig. 5.10 provides the four phase flow cycle for the $S_{0.5}$ cavity. This case presented a relatively broadband tone with moderate amplitudes, excited by the second hydrodynamic mode. Accordingly, at $U_\infty = 97\ m/s$, two vortices are seen travelling over the cavity mouth. In contrast to the deeper $S_{1.5}$ cavity, these vortex cores exhibit more curvature and cavity drag. This resembles the flow cycle of the shallow $R_{0.5}$ cavity in Fig. 5.6, ergo, the lack of acoustic resonance hinders the modulation process of the flow, reducing the spanwise coherence of the shear layer. Nevertheless, it should be noted that the aeroacoustics response of the shallow $S_{0.5}$ cavity in Fig. 4.3b also generated velocity-dependent tones for $St \sim 0.24$, resembling the shallow cylindrical cavities. This feature was not observed in

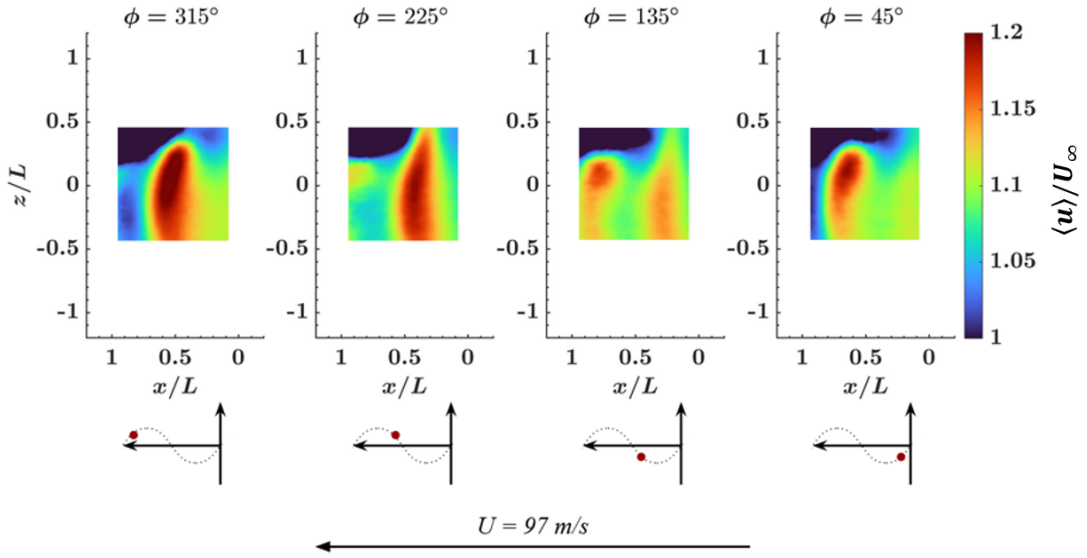

Figure 5.10: The normalized phase-averaged streamwise velocity contours at 97 m/s for the $S_{0.5}$ cavity.

Fig. 4.3a for the aeroacoustics response of the $R_{0.5}$ cavity. Further assessment of Fig. 5.10 shows a consistent recirculation region for the entire flow cycle. This flow feature is comparable to the shallow $O_{0.5}$ cavity in Fig. 5.8, where the asymmetry of the recirculation zone in the cavity is affected by the shallow floor. As a result, a portion of the recirculation region escapes the cavity, creating the asymmetric flow profile seen in both the $O_{0.5}$ and $S_{0.5}$ cavities. This is an interesting resemblance between the two cases when considering the aeroacoustics response as well as the flow profile of the shear layer. The similar characteristics amongst the $O_{h/L}$ and $S_{h/L}$ cavities are attributed to the equivalent cavity depth, length, and admission ratio, thereby demonstrating the increased dependence of the aeroacoustics response on the depth and width of shallow cavities.

5.2 Chapter Summary

Flow visualizations are presented in this section for all the cavity cases explored in this study. The phase locked-measurements for the $R_{h/L}$ cavities provide valuable insight into the flow modulation of the shear layer and stream-wise vortex location as the acoustic resonance becomes stronger. A saturation in the velocity fluctuations of the vortex core is observed for the flow velocity corresponding to the strongest resonance. The flow cycle during the mode switching observed during the aeroacoustics response for this case reveals a similar switching between the dominant hydrodynamic mode. It can be seen that the coherence of the hydrodynamic mode can not be established, as both coincidence regions are equally favourable in exciting an acoustic mode at the same flow velocities. Velocity fluctuations for the $R_{0.5}$ cavity, outside of resonance conditions, shows the lack of spanwise coherence due to the absence of strong acoustic modulation. The shear layer in this case is easily affected by any

possible obstruction upstream of the cavity. This also reinforces the notion that the acoustic modulation greatly affects the organization of the shear layer topology. For the cylindrical cavities, the first three hydrodynamic modes are observed, where the size of the vortex cores increase with each lower order hydrodynamic mode, and the velocity fluctuations increase as the resonance grows stronger. The most notable feature of the cylindrical cavities are the crescent-like shapes induced by the circular cavity opening. This spanwise curvature appears to straighten due to the enhanced modulation of the shear layer. Though not as pronounced as the cylindrical cases, three-dimensional characteristics are also observed for the $S_{1.5}$ cavity, where increasing resonance amplitudes organize the shear layer and reduce the effects of these three-dimensional characteristics. The shallow cylindrical cavity, in agreement with literature, exhibits a highly asymmetric flow structure about the stream-wise direction. This flow asymmetry is caused by an interference of the recirculation region in the cavity due to the reduced cavity depth, explaining the significantly lower Strouhal numbers for this case. Furthermore, the $S_{0.5}$ cavity, having the same aspect ratio of 0.5, portrayed a slightly less, yet still, asymmetric flow pattern over the cavity mouth. This resemblance in flow pattern amongst the shallow cylindrical and square cavities explains the low Strouhal number, which also appear in the aeroacoustics response of the $S_{0.5}$ cavity. It can therefore be seen that the spanwise dimensions of the cavity relative to the duct, presented as the admission ratio, greatly affects the velocity dependent tones due to the changes induced in the flow dynamics of the shear layer.

Chapter 6

Conclusions

6.1 Summary and Conclusions

The flow-excited acoustic resonance, as well as, the hydrodynamic modes of various cavity geometries are investigated in this thesis. A summary of the main findings is provided in this section.

The results presented in this paper provide a comprehensive summary of the aeroacoustics response, as well as the shear layer dynamics for various cavities exposed to Mach numbers of up to 0.4. The cavities were mounted to the duct of an open-loop wind tunnel to include the potential effects of a cavity enclosure. The aeroaocustics response of the cylindrical cavities presented clear excitation of the $1/4\lambda$ acoustic depth mode, with exception to the $\emptyset_{0.5}$ cavity, which excited the $1/2\lambda$ acoustic mode of the cavity-duct configuration due to the larger admission ratio. The larger admission ratio introduced an improved interaction between the cavity and the duct, thereby hindering the formation of a trapped acoustic mode within the cavity, and promoting a standing acoustic cross-mode consisting of the cavity depth and duct height. The hydrodynamic modes for the cylindrical cavities with $h/L \geq 1$ present

Strouhal numbers in good agreement with reported literature, and further demonstrate the relative independence of the Strouhal number on aspect ratios larger than unity. More notably, the shallow cylindrical cavities showed evidence of low velocity-dependent tones at $St \sim 0.16$ and 0.25 attributed to the asymmetric flow in the cavity. However, characterizing the hydrodynamic modes for aspect ratios less than unity is not as straightforward. Documented literature for various cavity geometries with $h/L \leq 1$ exhibit significant dependence on the cavity depth, severely affecting the velocity dependent tones. This discrepancy is owed to the change in flow-dynamics of the flow recirculation in the cavity when the depth becomes smaller than the impingement length. These cylindrical cases clearly demonstrate the change in fluid and acoustic behaviour of shallow cylindrical cavities, as well as the influence of reflective boundaries on the sound production and ability to excite alternative acoustic standing waves.

The pressure distribution within the cavity-duct configuration is also presented for increasing flow velocities. A clear trend is seen as the velocity increases, where the wavelength of the standing acoustic mode becomes further compressed as the flow velocity increases. This compression occurs as the flow velocity increases within the lock-in range and the resonance becomes stronger. Resultantly, the compression of the acoustic mode becomes saturated when the acoustic amplitudes are at a maximum, where no further change in the wavelength is observed. This explains the added stiffness effects reported for strong resonance conditions.

Further scrutiny of the shear layer impingement measurements reveal that the frequency of the impingement, strictly for the current sensor locations, is not affected by the impingement location. Effectively, the shear layer is considered to develop a three-dimensional flow topology, and as a result, the curvature of this shear layer ensures what appears to be a simultaneous impingement of the shear layer. This is

further substantiated by the difference in amplitude between the aspect ratio of 1.5 and 1 for the cylindrical cavities when comparing the impingement measurements. It is clear from the spectral data that a large difference in acoustic amplitude exists between the sensor in the centre of the downstream edge and the other two lateral sensors. This difference is credited to an unaffected flow recirculation at the cavity mouth, such that the impingement near the centre of the shear layer occurs above or below the downstream edge. This feature disappears when reducing the cavity depth to $h/L \leq 1$.

The Strouhal numbers for two-dimensional rectangular cavities are not affected with changes in the aspect ratio for these cases, and values for the hydrodynamic modes conform with reported data. Two-dimensional rectangular cavities are understood to excite acoustic depth modes within the cavity when the depth of the cavity is much larger than the impingement length. Though the $R_{1.5}$ cavity is considered a deep cavity, the reflection from the boundaries promote an acoustic depth mode between the cavity depth and duct height. This same acoustic mode shape is excited in the shallow $R_{0.5}$ cavity, however, the frequency of this mode for the deeper cavity is a function of the cavity depth and duct height, whilst that for the shallow cavity is a function of the mean height of the cavity and duct. Furthermore, a mode-switching is present $R_{1.5}$ cavity due to the favourable excitation of the fundamental and the higher order acoustic modes for this particular geometry. Square cavities have displayed similarities amongst the two-dimensional rectangular and the cylindrical cavities. The acoustic behaviour of the $S_{h/L}$ cavities exhibit similar acoustic mode shapes, as well as similar frequencies for the resonance in comparison to the same aspect ratios for the $O_{h/L}$ cavities. This is due to the matching geometric parameters, *i.e.* aspect and admission ratio, yet the inherent differences in cavity shapes produces far lower acoustic amplitudes for the square cavity. Additionally, a low velocity dependant

tone for the $S_{0.5}$ case resembles those seen in the shallow cylindrical cavities. The presence of such a hydrodynamic mode in the shallow square cavity suggests a similar interference of the recirculation region, as seen in cylindrical cavities. This reinforces the notion that the asymmetry reported in shallow cylindrical cavities, is in fact a dominant feature due to the circular shape of the cavity mouth, however, flow asymmetry exists in other cavity shapes consisting of a finite spanwise width, though the amount of flow asymmetry may differ.

The PIV measurements for the deeper cylindrical cavity showed highly three-dimensional shear layer topology for the first three hydrodynamic modes. The curvature decreases at increasing resonance amplitudes due to the modulation of the shear layer. On the contrary, the shallow cylindrical cavity exhibited strong asymmetry caused by the interference of the recirculation region, explaining the very low Strouhal values. The deep two-dimensional cavity revealed highly coherent vortices in the spanwise direction, as well as an interesting mode-switching between the second and first hydrodynamic mode. This mode-switch is associated with m_1 and m_2 exciting the fundamental and higher order acoustic modes, respectively. The shallow $R_{0.5}$ cavity, exemplified the reduction in the spanwise coherence of the vortices as a result of weak acoustic resonance. From an acoustics perspective, the deeper square cavity resembled the cylindrical cavity with regard to the excited acoustic modes, however the flow behaviour of the square cavity is not as three-dimensional. Nevertheless, the finite edge of the square cavity formed a quasi two-dimensional profile in the vortex wake. The shallow square cavity demonstrated similarities in the aerouacoustics response and flow patterns of the shallow cylindrical cavity, where the floor of the shallow cavity disrupts the recirculation zone, and an asymmetric vortex cone is seen escaping the cavity mouth. The results reported in this thesis have shown the influence of confinement parameters on the aeroacoustics response of various cav-

ity shapes subject to confined turbulent flow. Furthermore, PIV measurements have presented a further understanding of the corresponding shear layer dynamics during flow-excited acoustic resonance, as to support the observations in the aeroacoustics response.

6.2 Major Contributions

The research presented in this thesis provides a thorough summary of the flow-acoustic coupling in ducted cavities. A series of numerical and experimental investigations were performed as to extend the existing knowledge in literature by making the following contributions:

1. The influence of the cavity aspect ratio, h/L, and admission, w/W, on the aeroacoustics response of ducted cylindrical cavities was thoroughly investigated. Results revealed that the confinement of a duct promotes the reflection of acoustic waves radiating from the cavity.

    (a) Reducing the aspect ratio or increasing the admission ratio hinders the entrapment of the cavity acoustic depth mode. This improves the interaction between the cavity and duct, influencing the resulting acoustic mode shape.

    (b) Aspect ratio significantly affects Strouhal periodicities in shallow cylindrical cavities, causing lower-than-expected values due to changes in flow dynamics. These deviations must be considered for flow-induced vibrations and acoustics in shallow cylindrical cavities.

2. The influence of the cavity shape is further detailed by investigating two-dimensional rectangular, as well as square cavities, with similar aspect and

admission ratios to the cylindrical cavities.

   (a) The deep two-dimensional rectangular cavity demonstrated mode-switching behaviour where the fundamental and higher order acoustic mode are intermittently excited by the first and second hydrodynamic modes, respectively.

   (b) From an acoustic standpoint, square cavities behave much like cylindrical cavities, revealing similar acoustic behaviour for the deep aspect ratio, and lower Strouhal numbers in the shallow case.

3. Particle Image Velocimetry (PIV) measurements of the shear layer both, inside and outside, the resonance excitation region, illustrate novel insight on the shear layer topology for the studied cavities.

   (a) Deep cylindrical cavities demonstrated highly three-dimensional flow topology, seen as a crescent-like shape, flowing over the cavity mouth. Shallow cylindrical cavities demonstrate strong flow asymmetry due to obstruction of the recirculation region in the cavity.

   (b) The shallow square cavity revealed asymmetric flow behaviour, much like the cylindrical cavity, emphasizing the spanwise effects of the cavity shape on the shear layer topology.

6.3 Recommendations for Future Investigations

While the research presented here is aimed at exploring a wide range of cavity shapes and geometric parameters, as to expand the current state of knowledge, it also provides a solid foundation to carry out future investigations. On account of this, the following is recommended:

1. Multiple shallow cavities should be investigated, since the flow asymmetry is extremely sensitive to aspect ratios less than one. This should be investigated by means of acoustic pressure measurements, as the existing literature regarding shallow cavities mainly consists of static pressure measurements on the cavity walls.

2. In light of this, the flow patterns associated with the aeroacoustics response provide a great deal of information regarding the coupled phenomena. Therefore, it is recommended to manufacture cavity sections made completely with acrylic and maximize the field of view, in order to provide flexibility for the positioning of the laser sheet during PIV measurements.

3. The rectangular confinement investigated in this thesis is used to explore the effects of reflective boundaries on cavity resonance. This confinement geometry is rather simple due to scarcity of literature for these configurations. However, in view of the complexity of the shear layer and acoustic behaviour, it would be of interest to investigate similar cavities mounted to cylindrical ducts, where the connection between cavity and duct present an elliptical shape. This would subsequently improve the applicability of the results to industrial applications such as pipeline systems.

Bibliography

[1] Abdelmwgoud, M., and Mohany, A. Control of the self-sustained shear layer oscillations over rectangular cavities using high-frequency vortex generators. *Physics of Fluids 33* (2021), 045115.

[2] Abdelmwgoud, M., Shaaban, M., and Mohany, A. Flow dynamics and azimuthal behavior of the self-excited acoustic modes in axisymmetric shallow cavities. *Physics of Fluids 32* (2020), 115109.

[3] Abdelmwgoud, M., Shaaban, M., and Mohany, A. Shear layer synchronization of aerodynamically isolated opposite cavities due to acoustic resonance excitation. *Physics of Fluids 33* (2021), 055112.

[4] Ahuja, K., and Mendoza, J. Effects of cavity dimensions, boundary layer, and temperature in cavity noise with emphasis on benchmark data to validate computational aeroacoustic codes. *NASA Contractor Report 4653* (1995).

[5] Aly, K., and Ziada, S. Flow-excited resonance of trapped modes of ducted shallow cavities. *Journal of Fluids and Structures 26(1)* (2010), 92–120.

[6] Aly, K., and Ziada, S. Review of flow-excited resonance of acoustic trapped modes in ducted shallow cavities. *Journal of Pressure Vessel Technology 138* (2016), 040803.

[7] Alziadeh, M., and Mohany, A. Vorticity shedding and acoustic resonance excitation of two tandem spirally finned cylinders in cross-flow. *Journal of Pressure Vessel Technology 143(2)* (2021), 021405.

[8] Alziadeh, M., and Mohany, A. Vortex shedding characteristics and aerodynamic forces of a finned cylinder in cross-flow. *Physics of Fluids 34(9)* (2022), 095110.

[9] Alziadeh, M., and Mohany, A. Flow structure and aerodynamic forces of finned cylinders during flow-induced acoustic resonance. *Journal of Fluids and Structures 119* (2023), 103887.

[10] Anderson, J. The effect of an air flow on a single side branch helmholtz resonator in a circular duct. *Journal of Sound and Vibration 52(3)* (1977), 423–431.

[11] Arafa, N., and Mohany, A. Aeroacoustic response of a single cylinder with straight circular fins in cross-flow. *Journal of Pressure Vessel Technology 137(5)* (2015), 051301.

[12] Arafa, N., Tariq, A., Mohany, A., and Hassan, M. Effect of cylinder location inside a rectangular duct on the excitation mechanism of acoustic resonance. *Journal of the Canadian Acoustical Association 42(1)* (2014), 33–40.

[13] Blevins, R., and Bressler, M. Experiments on acoustic resonance in heat exchanger tube bundles. *Journal of Sound and Vibration 164* (1993), 503–533.

[14] Bliss, D., and Hayden, R. Landing gear and cavity noise prediction. *NASA Contractor Report* (1976), CR–2714.

[15] Block, P. Noise response of cavities of varying dimensions at subsonic speeds. *NASA, Tech. Note D-8351* (1976).

[16] Bruggeman, J. C., Hirschberg, A., van Donge, M. E. H., and Wijnands, A. P. J. Self-sustained aero-acoustic pulsations in gas transport systems: experimental study of the influence of closed side branches. *Journal of Sound and Vibration 150(3)* (1991), 371–393.

[17] Cengel, Y. Shear layer. *Fluid mechanics Tata McGraw-Hill Education* (2010).

[18] Chatellier, L., Laumonier, J., and Gervais, Y. Theoretical and experimental investigations of low mach number turbulent cavity flows. *Experiments in Fluids 36* (2004), 728–740.

[19] Chicheportiche, D., and Gloerfelt, X. Direct noise computation of the flow over cylindrical cavities. *16th AIAA/CEAS Aeroacoustics Conference 2010-3775* (2010).

[20] Comte, P., Silvestrini, J., and Bègou, P. Streamwise vortices in large-eddy simulations of mixing layers. *European Journal of Mechanics - B/Fluids 17(4)* (1998), 615–637.

[21] Czech, M., Crouch, J., Stoker, R., Strelets, M., and Garbaruk, A. Cavity noise generation for circular and rectangular vent holes. *27th AIAA Aeroacoustics Conference 2508* (2006), 61–84.

[22] Dalmont, J., Nederveen, C., and Joy, N. Radiation impedance of tubes with different flanges numerical and experimental investigations. *Journal of Sound and Vibration 244* (2001), 505–534.

[23] Deboo, G., Ramsden, K., Gesior, R., and Strub, B. Identification of quad cities main steam line acoustic sources and vibration reduction. *ASME Pressure Vessels and Piping Division Conference 26658* (2007).

[24] Dowling, A. P., and Mahmoudi, Y. Combustion noise. *Proceedings of the Combustion Institute 35(1)* (2015), 65–100.

[25] Duan, Y., Koch, W., Linto, C., and McIver, M. Complex resonances and trapped modes in ducted domains. *Journal of Fluid Mechanics 571* (2007), 119–147.

[26] Dybenko, J., and Savory, E. An experimental investigation of turbulent boundary layer flow over surface-mounted circular cavities. *Journal of Aerospace Engineering 222* (2007), 109–125.

[27] East, L. Aerodynamically induced resonance in rectangular cavities. *Journal of Sound and Vibration 3* (1966), 277–287.

[28] El Hassan, M. Aero-acoustic coupling inside large deep cavities at low-subsonic speeds. *Journal of Fluids Engineering 131* (2008), 011204.

[29] El Hassan, M., Labraga, L., and Keirsbulck. Aero-acoustic oscillations inside large deep cavities. *16th Australian Fluid Mechanics Conference, Australia* (2007).

[30] Elder, S., Farabee, T., and DeMetz, F. Mechanisms of flow-excited cavity tones at low mach number. *Journal of the Acoustical Society of America 72* (1982), 532–549.

[31] Elhelaly, A., Hassan, M., Mohany, A., and Eid Moussa, S. Effect of the flow approach angle on the dynamics of loosely-supported tube arrays. *Nuclear Engineering and Design 368* (2020), 110802.

[32] Gaudet, L., and Winter, K. Measurements of the drag of some characteristic aircraft excrescences immersed in turbulent boundary layers. *Royal Aircraft Establishment Technical Report. Aero 1538* (1973).

[33] GENE. Bwr steam dryer integrity. *GE Nuclear Energy, San Jose, CA Services Information Letter No. 644* (2004).

[34] George, A. R. Automobile aerodynamics. *12th Aeroacoustic Conference 1067* (1989).

[35] Gloerfelt, X., Bogey, C., and Bailly, C. Numerical investigation of the coexistence of multiple tones in flow-induced cavity noise. *AIAA Aeroacoustics Conference* (2003), 3234.

[36] Graf, H., and Ziada, S. Flow induced acoustic resonance of closed side branches: an experimental determination of the excitation source. *Proceedings of the Third International Symposium on Flow-Induced Vibration and Noise 7* (1992), 63–80.

[37] Graf, H., and Ziada, S. Excitation source of a side-branch shear layer. *Journal of Sound and Vibration 329* (2010), 2825–2842.

[38] Grottadaurea, M., and Rona, M. Noise sources from a cylindrical cavity. *28th AIAA Aeroacoustics Conference 3723* (2007).

[39] Haigermoser, C., Scarano, F., and Onorato, M. Investigation of the flow in a circular cavity using stereo and tomographic particle image velocimetry. *Experiments in Fluids 46* (2009), 517–526.

[40] Hanna, M., and Mohany, A. The aeroacoustics response of cylindrical cavities in confined flow. *12th International Conference of Flow-Induced Vibration 979-10-699-9682-3* (2022), FSI8: 287–294.

[41] Heller, H., and Bliss, D. The physical mechanism of flow-induced pressure fluctuations in cavities and concepts for their suppression. *2nd Aeroacoustics Conference 491* (1975).

[42] Heller, H., and Dobrzynski, W. Sound radiation from aircraft wheel-well/landing-gear configurations. *Journal of Aircraft 14(8)* (1997), 768–774.

[43] Heller, H., Holmes, D., and Covert, E. Flow-induced pressure oscillations in shallow cavities. *Journal of Sound and Vibration 18* (1971), 545–553.

[44] Hirschberg, L., Hulshoff, S. J., Collinet, J., Schram, C., and Schuller, T. Influence of nozzle cavity on indirect vortex and entropy sound production. *American Institute of Aeronautics and Astronautic 57(7)* (2019).

[45] Hiwada, M., Kwamura, T., Mabuchi, I., and Kumada, M. Some characteristics of flow pattern and heat transfer past circular cylindrical cavity. *Bulletin of the JSME 26* (1983), 220.

[46] Howe, M. The dissipation of sound at an edge. *Journal of Sound and Vibration 70* (1980), 407–411.

[47] Howe, M. Edge, cavity and aperture tones at very low mach numbers. *Journal of Fluid Mechanics 330* (1997), 61–84.

[48] Howe, M. Theory of vortex sound. *Cambridge University Press* (2003).

[49] Islam, M., Shaaban, M., and Mohany, A. Vortex dynamics and acoustic sources in the wake of finned cylinders during resonance excitation. *Physics of Fluids 32* (2020), 075117.

[50] Kook, H., and Mongeau, L. Analysis of the periodic pressure fluctuations induced by flow over a cavity. *Journal of Sound and Vibration 251* (2002), 823–846.

[51] Kook, H., Mongeau, L., Brown, D., and Zorea, S. Analysis of the interior pressure oscillations induced by flow over vehicle openings. *Noise Control Engineering Journal 45* (1997), 223–234.

[52] Krishnamurty, K. Acoustic radiation from two-dimensional rectangular cutouts in aerodynamic surfaces. *NACA Technical Note No 3487* (1955).

[53] Lato, T., and Mohany, A. Passive damping of pressure pulsations in pipelines using herschel-quincke tubes. *Journal of Sound and Vibration 448* (2019), 160–177.

[54] Ma, R., Slaboch, P., and Morris, S. Fluid mechanics of the flow-excited helmholtz resonator. *Journal of Fluid Mechanics 623* (2009), 1–26.

[55] Marsden, O., Baily, C., Bogey, C., and Jondeau, E. Investigation of flow features and acoustic radiation of a round cavity. *Journal of Sound and Vibration 331* (2012), 3521–3543.

[56] Marsden, O., Bogey, C., and Baily, C. Investigation of flow features around shallow round cavities subject to subsonic grazing flow. *Physics of Fluids 24* (2012), 125107.

[57] Marsden, O., Jondeau, E., Souchotte, P., Bogey, C., Baily, C., and Juvé, D. Investigation of flow features and acoustic radiation of a round cavity. *AIAA Aeroacoustics Conference* (2008), 2851.

[58] McCarthy, P., and Ekmekci, A. Noise generation and flow features of shallow cylindrical cavities subject to grazing flow. *9th Flow Induced Vibration Conference 157* (2018).

[59] Mery, F., Mincu, D., Casalis, G., and A, S. Noise generation analysis of a cylindrical cavity by les and global instability. *15th AIAA/CEAS Aeroacoustics Conference 2009-3205* (2009).

[60] Mincu, D., Mary, I., Redonnet, S., Manoha, E., and Larcheveque, L. Numerical simulations of the sound generation by flow over surface mounted cylindrical cavities including wind tunnel installation effects. *30th AIAA Aeroacoustics Conference 3314* (2009).

[61] Mohany, A. Flow-sound interaction mechanisms of a single and two tandem cylinders in cross-flow. *ProQuest* (2007).

[62] Mohany, A., Arthurs, D., Bolduc, M., Hassan, M., and Ziada, S. Numerical and experimental investigation of flow-acoustic resonance of side-by-side cylinders in a duct. *Journal of Fluids and Structures 48* (2014), 316–331.

[63] Mohany, A., and Ziada, S. Flow-excited acoustic resonance of two tandem cylinders in cross-flow. *Journal of Fluids and Structures 21* (2005), 103–119.

[64] Nakiboğlu, G., Manders, H., and Hirschberg, A. Aeroacoustic power generated by a compact axisymmetric cavity: prediction of self-sustained oscillation and influence of the depth. *Journal of Fluid Mechanics 703* (2012), 163–191.

[65] Neri, E., Kennedy, J., and Bennett, G. J. Bay cavity noise for full-scale nose landing gear: a comparison between experimental and numerical results. *Aerospace Science and Technology 72* (2018), 278–291.

[66] Nomura, Y., Yamamura, I., and Inawashiro, S. On the acoustic radiation from a flanged circular pipe. *Journal of the Physical Society of Japan 15* (1960), 510–517.

[67] Norris, A., and I.C, S. Acoustic radiation from a circular pipe with an infinite flange. *Journal of Sound and Vibration 135* (1989), 85–93.

[68] Omer, A., Arafa, N., Mohany, A., and Hassan, M. The effect of upstream edge geometry on the acoustic resonance excitation in shallow rectangular cavities. *International Journal of Aeroacoustics 15* (2015), 253–275.

[69] Omer, A., Mohany, A., and Hassan, M. Effect of impingement edge geometry on the acoustic resonance excitation and strouhal numbers in a ducted shallow cavity. *Wind and Structures 23(2)* (2016), 91–107.

[70] Oshkai, P., and Yan, T. Experimental investigation of coaxial side branch resonators. *Journal of Fluids and Structures 24* (2008), 589–603.

[71] Parthasarathy, S., Cho, Y., and Back, L. Sound generation by flow over relatively deep cylindrical cavities. *Journal of the Acoustical Society of America 78* (1985), 1785.

[72] Plumblee, H., Gibson, J., and Lassiter, L. A theoretical and experimental investigation of the acoustic response of cavities in aerodynamic flow. *Wright-Patterson Air Force Base, Dayton, Ohio Tech. Rep. WADD-TR-61-75* (1962).

[73] Powell, A. Theory of vortex sound. *Journal of the Acoustical Society of America 36* (1964), 177–195.

[74] Rashwan, S., Mohany, A., and Dincer, I. Investigation of self-induced thermoacoustic instabilities in gas turbine combustors. *Energy 190* (2020), 116362.

[75] Rayleigh, B. Theory of sound, 2nd ed. pp.307.

[76] Rockwell, D., and Knisely, C. Vortex-edge interaction: Mechanisms for generating low frequency components. *Physics of Fluids 23(2)* (1979), 239–240.

[77] Rockwell, D., and Knisely, C. Observations of the three-dimensional nature of instable flow past a cavity. *Physics of Fluids 23(3)* (1980), 425–431.

[78] Rockwell, D., Lin, J.-C., Oshkai, P., Reiss, M., and Pollack, M. Shallow cavity flow tone experiments: onset of locked-on states. *Journal of Fluids and Structures 17* (2002), 381–414.

[79] Rockwell, D., and Naudascher, E. Review: self-sustaining oscillations of flow past cavities. *ASME Journal of Fluids Engineering 100* (1978), 152–165.

[80] Roshko, A. Structure of turbulent shear flows: a new look. *AIAA Journal 14(10)* (1955), 1349.

[81] Rossiter, J. Wind tunnel experiments on the flow over rectangular cavities at subsonic and transonic speeds. *Royal Aircraft Establishment, Farnborough, Ministry of Aviation Technical Report No 3438* (1964).

[82] Rossiter, J., and Kurn, A. Wind tunnel measurements of the unsteady pressures in and behind a bomb bay. *U.D.C. No. A.I.(42) C.P. Np. 728* (1965).

[83] Sadek, O., Shaaban, M., and Mohany, A. Suppression of acoustic resonance in piping system using passive control devices. *Canadian Acoustics - Acoustique Canadienne 42(3)* (2014), 58–59.

[84] Sarohia, V. Experimental investigation of oscillations in flows over shallow cavities. *AIAA Journal 15* (1977), 984–991.

[85] Scarano, F., and Riethmuller, M. Advances in iterative multigrid piv image processing. *Experiments in fluids 29* (2000), S51–S60.

[86] Sciacchitano, A., and Wieneke, B. Piv uncertainty propagation. *Measurement Science and Technology 27* (2016), 084006.

[87] Shaaban, M., and Mohany, A. Parametric investigation of the flow-excited acoustic resonance from multiple in-line cylinders in cross-flow. *Pressure Vessels and Piping Conference PVP2015* (2015), 45650.

[88] Shaaban, M., and Mohany, A. Passive control of flow-excited acoustic resonance in rectangular cavities using upstream mounted blocks. *Experiments in Fluids 56* (2015), 72.

[89] Shaaban, M., and Mohany, A. Phase-resolved piv measurements of flow over three unevenly spaced cylinders and its coupling with acoustic resonance. *Experiments in Fluids 60* (2019), 71.

[90] Shaw, L., Clark, R., and Talmadge, D. Generic weapons bay acoustic environment. *25th AIAA Aerospace Sciences Meeting 25(2)* (1988), 147–153.

[91] Stegen, G., and Karamcheti, K. Multiple tone operation of edgetones. *Journal of Sound and Vibration 12(3)* (1970), 281–284.

[92] Sun, Y., Liu, Q., Cattafesta, L., Ukeiley, L., and Taira, K. Effects of sidewalls and leading-edge blowing on flows over long rectangular cavities. *American Institute of Aeronautics and Astronautics 57(1)* (2018), 057413.

[93] Tam, C. The acoustic modes of a two-dimensional rectangular cavity. *Journal of Sound and Vibration 49* (1976), 353–364.

[94] Tonon, D., Hirschberg, A., Golliard, J., and Ziada, S. Aeroacoustics of pipe systems with closed branches. *Aeroacoustics 10* (2011), 201–276.

[95] US Nuclear Regulatory Commission, Washington, D. Failure of steam dryer cover plate after a recent power uprate. *NRC Information Notice No. 2002-26* (2002).

[96] US Nuclear Regulatory Commission, Washington, D. Additional flow-induced vibration failures after a recent power uprate. *NRC Information Notice No. 2002-26, SUPPLEMENT 2* (2004).

[97] Verdugo, F., Guitton, A., and Camussi, R. Experimental investigation of a cylindrical cavity in a low mach number flow. *Journal of Fluids and Structures 28* (2011), 1–19.

[98] Wang, P., Deng, Y., and Liu, Y. Vortex-excited acoustic resonance in channel with coaxial side-branches: Vortex dynamics and aeroacoustic energy transfer. *Physics of Fluids 30* (2018), 125104.

[99] Wang, X., Yang, D., Zhou, F., Wu, J., and Lu, B. Suppression of the cavity oscillation using high-speed mass injection. *International Journal of Modern Physics 2040098* (2020), 5.

[100] Westerweel, J., and Scarano, F. Universal outlier detection for piv data. *Experiments in fluids 39* (2005), 1096–1100.

[101] Yamouni, S., Sipp, D., and Jacquin, L. Interaction between feedback aeroacoustic and acoustic resonance mechanisms in a cavity flow: a global stability analysis. *Journal of Fluid Mechanics 717* (2013), 134–165.

[102] Ziada, S. Flow-excited acoustic resonance in industry. *Journal of Pressure Vessel Technology 132(1)* (2010), 015001.

[103] Ziada, S., Ng, H., and Blake, C. Flow excited resonance of a confined shallow cavity in low mach number flow and its control. *Journal of Fluids and Structures 18* (2003), 79–92.

[104] Ziada, S., and Shine, S. Strouhal numbers of flow-excited acoustic resonance of closed side branches. *Journal of Fluids and Structures 13* (1999), 127–142.

Appendix A

Uncertainty Analysis

A.1 Particle Image Velocimetry (PIV)

In this section, the uncertainty of the statistical quantities for the PIV measurements is discussed for off-resonance conditions at $U_\infty = 61\ m/s$ on the $O_{0.5}$ cavity. The images captured in the PIV measurements are statistically independent, therefore one can obtain the uncertainty of statistical quantities by following the method outlined by Sciacchitano and Wienke [86]. The uncertainty of the time-averaged velocity components with a 95% confidence interval can be computed as followed;

Uncertainty of mean streamwise velocity component:

$$\epsilon_{\bar{u}} = \frac{\sigma_u}{\sqrt{N}} \tag{A.1}$$

Uncertainty of mean spanwise velocity component:

$$\epsilon_{\bar{v}} = \frac{\sigma_v}{\sqrt{N}} \tag{A.2}$$

σ_u and σ_v represent the standard deviation of the streamwise (u) and spanwise (v) velocity components, respectively. N is the number of statistically independent pairs of images captured outside of resonance conditions ($N = 2000$).

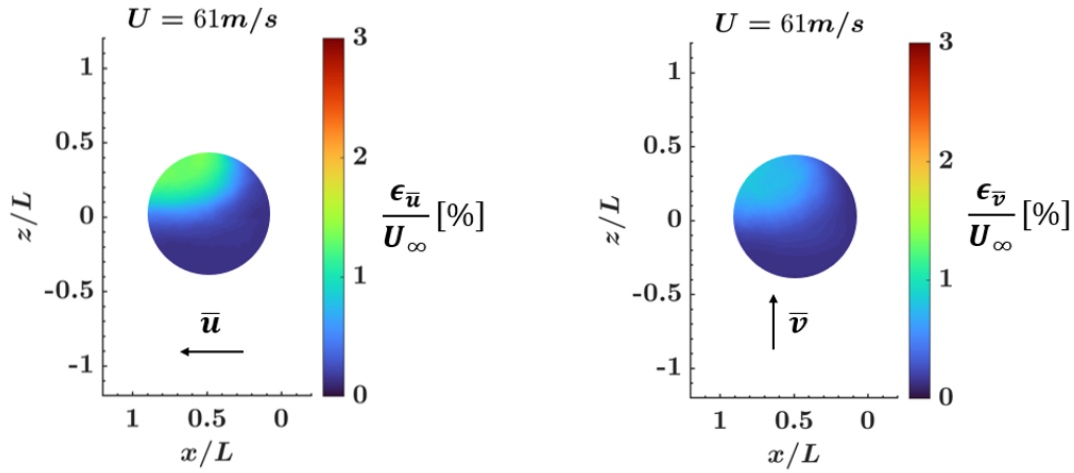

Figure A.1: Uncertainty of the time-averaged a) streamwise and b) spanwise velocity for the $O_{0.5}$ cavity. Values are normalized by the free-stream flow velocity and shown as a percentage.

As seen in Fig. A.1, the maximum uncertainty of the time-averaged velocity components do not exceed 3% with a 95% confidence interval.